Coating Mechanical and Acoustical Design Considerations for Resistance to Solid and Liquid Particle Impact

By:

Chanon Iamvasant

A dissertation submitted in fulfilment of the requirements for the

degree of

Doctor of Philosophy

The University Of Sheffield.

Department of Materials Science and Engineering

May 2017

Abstract

The erosion of components subjected to water droplet impact has been documented in various applications e.g. aircraft and wet-steam turbine blades. In wet-steam turbine systems, erosion of the of leading edge turbine blades causes significant loss of efficiency. Despite the efforts that have been put into this field over the past 50 years, no one has solved the problem of water droplet erosion. This may be attributed to the different damage phenomena; extremely high contact pressure; stress wave propagation; jetting and excessive heating etc. that occur in high-speed water droplet erosion. The main purpose of this thesis work was to attempt to link existing (but fragmented) knowledge of different aspects of water droplet erosion and the requirements to construct a protective coating to resist it. Discoveries from critical literature reviews were that the impact energy may be viewed as mechanical dissipation of stresses/strains or acoustic attenuation of stress waves. Therefore, architectural designs of protective WDE coating structures must try to satisfy both of these considerations.

To provide some validation of both the mechanical (stresses/strains) and acoustical (stress waves) considerations, titanium-based monolithic and multilayer PVD coatings will be investigated and characterization techniques (i.e. nano-indentation, x-ray diffractometer (XRD, Optical Microscopy (OM) Scanning electron microscopy (SEM), Transmission electron microscopy (TEM), Stylus profilometry) will be performed. Selected (both monolithic and multilayer) coatings will be subjected to both particulate (ball-on-plate) impact testing and water droplet erosion (WDE) testing.

This thesis illustrates the versatility of the triode ion-plating PVD technique and its feasibility to produce thick (Ti, Ti(N) and TiN) monolithic coatings and (TiN/Ti, TiN/Ti(N)) multilayer coatings with reliable controllability in terms of chemical composition and designate i

layer thickness. According to the results of this work, there is a definite distinction between the coating requirements for solid particle impact tests and liquid particle water droplet erosion, due to the differences in the way that the impact energy is delivered (i.e. strain rate, duration of the impact impulse, etc.) However, the results are inconclusive as to whether multilayer or monolithic coatings perform better in water droplet erosion.

Finally, the information gathered experimentally was analyzed (with existing proposed models and theories) and interpreted to propose a coating architecture which will be superior in water droplet erosion performance.

Acknowledgements

I would like to thank and express my appreciation to my supervisor Dr. Adrian Leyland for his encouragement, guidance, constructive comments and support from the initial to the final stages of my PhD study. I am thankful to Prof Allan Matthews for giving me the opportunity to study within his group.

I would like to thank Dr. Andrew Gant and Dr. Mark Gee for providing of Water Droplet Erosion (WDE) testing.

I would like to express my grateful thanks to a number of colleagues at The University of Sheffield, for their assistance in the preparation of this thesis:

Dr. Xingguang Liu, Mr. Tao Xiao and Dr. John Kavanagh for their help and assistance in both experimental procedures and data analysis.

Mr.Laurynas Lukosevicius, Mr. Gorkem Yumasek, Mr. Husein D Meshreghi, Mr. Liu Lian, Mr. Jack Cooper, Mr. Ming Sun, Mr. Chang Liu, Mr. Andrius Subacius, Mr. Alan Martin for their help, discussion and the joyful time we had together.

Special and deep appreciation to my parents, sister and other family members who although living in Thailand have always sent me their encouragement, care and support. And to my girlfriend, Joann Wan, who has always been by my side, accompanying me through every hard or good day.

Table of Contents

Chapter 1 Introduction

For the past century, there has been extensive research in a variety of erosion applications, including particulate erosion, liquid cavitation erosion and water droplet erosion. Therefore, there is a sustained interest in applying protective coatings and/or treatments to prolong the life-time of the components in erosive applications. However, out of the different types of erosion, water droplet erosion has received the least attention and interest. This is probably down to the complex responses involved when a (compressible) water droplet and solid material; including lateral (supersonic) jetting of the collapsing droplet, formation of cavitation inside the droplet, high-strain rates etc. Therefore, this PhD study focuses primarily on identifying the key mechanical and acoustical aspects of the water droplet erosion phenomenon and using the knowledge acquired to propose a solution to the problem, by means of using a protective coating of specific architectural design.

Among many other potential protective erosion-coating candidates, ceramic-ceramic and ceramic-metal multilayer coatings produced by Physical Vapour Deposition (PVD) have been extensively investigated for particulate erosion applications. One of the most widely reported PVD multilayers is the TiN/Ti ceramic-metal system, where alternating layers of hard/soft (or in this particular case also stiff/compliant) material can impart satisfactory particulate abrasion and erosion performance. Whilst for example, duplex nitriding + PVD ceramic coatings have only recently been explored for cavitation erosion resistance. Additionally, even though several coating models have also been proposed for water droplet erosion protection (including PVD multilayer architectures), little or no test validation of their durability has been performed. Furthermore, the way in which the impact energy is delivered to the (coated) substrate can be

very different for each of the three main erosion regimes; thus there may be no single 'optimal' coating architecture that can satisfy all requirements.

Firstly, we must understand how the intrinsic material properties arise; in materials science, one must be quite knowledgeable in the fields of physics and chemistry to understand the fundamentals of why materials exhibit the properties in the way they do. The atomic nature (i.e. atomic bonding length, coordination number, crystal structure) is core in justifying Hardness (strength), Elastic modulus and density of a material. A comparison of titanium (α-Ti) and titanium nitride (TiN) were chosen to illustrate the fundamentals of materials' properties because they were the materials used in this project.

Titanium, as the ninth most abundant element on the planet and the fourth most abundant structural metal was initially discovered in the 1790s. However, due to the lack of technological advancement, it was not purified until the early 20^{th} century. Since then, titanium and its alloy have been incorporated and utilised in a wide range of applications e.g. automotive, aerospace, marine and nuclear. Owing to its remarkable properties such as its relatively low density, high fracture toughness, corrosion resistance and biocompatibility compared with steels and other metal alloys.

Titanium metal has a much lower strength, elastic modulus and density than ceramic titanium nitride. This is due to numerous reasons; primarily, the structure of titanium is HCP whereas titanium nitride is BCC. In terms of atomic packing efficiency, normally a HCP structure has a packing percentage of 74% compared to 68% for a BCC structure. There's not much difference in the packing efficiency but in titanium nitride, nitrogen (which is a small

atom) sits in the interstitial sites of the BCC structure of titanium nitride, which gives rise to the higher density in titanium nitride compared with titanium.

In physics principles, the strength and elastic modulus of materials is associated with the bonding of atoms within the crystal structure. The atomic bonding, whether it is covalent, ionic or metallic, has different dissociative bond energy. The dissociative bond energy is usually inversely proportional to the bond length. Typically, bonding length in covalent is the shortest, followed by ionic and metallic. Therefore, in terms of strength, this means that the material strength usually follows the type of bonding it exhibits, from covalent>ionic>metallic bond. In titanium, the bonding is purely metallic and the coordination number is 12. Conversely in titanium nitride, there is a mixture of metallic and ionic bonding and the coordination number of the metal atoms is 8. Though the coordination number is much less in titanium nitride compared with titanium, the presence of ionic bonding in titanium nitride (between titanium and nitrogen atoms) gives rise to its high strength and elastic modulus.

1.1 Aims and Objectives

The first part of my PhD study will be concentrated in critically reviewing existing literature work on the subject of erosion (mainly at supersonic speeds) of impacting water droplets on a solid material. This will serve to identify the fundamental aspects of the response of a water droplet impacting onto a solid material surface. Furthermore, I will try to find possible ways to accommodate the mechanical (stresses/strains) and acoustical (stress waves) effects experienced by the solid material upon water droplet impact. Interestingly, the acoustical consideration, which has been extensively researched in the field of seismology, has yet to be applied in practice to water droplet erosion. Moreover, I will try to identify similarities (if any) or differences (in terms of the induced impact pressure, strain-rates, impulse duration, etc.) between water droplet erosion and particulate erosion.

Consequently, there are still no universal rules on choosing which materials or how to design a coating architecture in order to have the best erosion resistance. Many theories have been developed which look at how the properties of a material e.g. (Hardness, H, Young's Modulus, E, Poisson's ratio, v) can have an influence on erosion. Two distinct theoretical approaches, either mechanical or acoustical, have been identified in consideration of how to approach the problem of particulate/water droplet erosion. Variation in material properties appears to have similarities and differences that affect the outcome of the mechanical and/or acoustical consideration. Therefore, the next step in this PhD study was to bridge the gap of understanding of the two considerations together and try to recommend (monolithic and multilayer) coating designs which will be superior in water droplet erosion performance.

To validate some of the theories and (mechanical or acoustical) models on how to design a coating to resist erosion, in this PhD study, we examine different titanium-based monolithic

(including pure Ti, ‘nitrogen-doped’ Ti and sub-stoichiometric TiN) and multilayer (including TiN/Ti and TiN/Ti(N)) coatings of different architecture and/or composition. The coating deposition technique chosen is the electron-beam triode ion-plating method, which is renowned to produce coatings with superior properties with reasonable high deposition rate. The deposited coatings are subjected to mechanical properties testing and characterisation techniques such as Nano-indentation, X-Ray Diffraction (XRD) analysis, Transmission-Electron Microscopy (TEM) analysis etc. Also, selected coatings are tested under the ball-to-plate impact test (simulated solid particle erosion) and water droplet erosion testing. This will help to identify (if any) the similarity and difference in coating requirements between the two different types of impact wear regime.

1.2 Industrial Visit Report

For further insights on how coatings can improve the steam turbine blades service lifetime, I had the opportunity to visit PTT Asahi Chemical Company Limited (PTTAC) industrial plant, located in Thailand. PTTAC currently produces Acrylonitrile (AN) and Methyl Methacrylate (MMA) polymer precursors from the major feedstock of Propane. The industrial plant has its own small electricity power station, where it feeds electricity to be used in its own production line. However, the majority part of the electricity consumed is purchased directly from an out-source electricity power station.

During the industrial visit, I had the opportunity to gather information on problems associated with steam turbines. Generally, the materials used for the turbine blades are Fe-12Cr steel, 15/5 PH steel or 17/4 PH steel. The problem found was that eventually there will be a drop in the steam turbine efficiency; this was due to the high-energy water droplet impact onto turbine blades, which causes the ejection of material from the edge of the turbine blades. Furthermore, steam turbine blades operating in a corrosive environment would expected to have an even lower service lifetime. This coincides well with the reports and suggestions of the mechanism associated with the failure of a steam turbine; over 40% of turbine blade failures are associated with corrosion or fatigue. [1]

Eventually, the severe drop in efficiency would lead to the replacement of steam turbine blades. However, end-user companies such as PTTAC would like to avoid replacing (or reduce the frequency of) steam turbine blades because of the expenses involved and it would also halt the manufacturing production line.

Chapter 2 Literature Review

2.1 Brief Background to Water Droplet Erosion

2.2.1 Introduction

The erosion of components subjected to water droplet impact has been documented in various applications e.g. aircraft and wet-steam turbine blades – and, more recently, wind turbines for 'renewable' energy production. In wet-steam turbine systems, erosion of the leading of edge turbine blades causes significant loss of efficiency. During the early 20th century, Coles [2] suggested numerous mechanisms for the cause of erosion in wet-steam turbine blades e.g. oxidation, chemical corrosion and solid particle impact. However, he failed to recognize water droplet impact as a significant mechanism.

It was not until the 1920s that Engel [3] and Cook [4] acknowledged and experimentally studied the significance of water droplet erosion. They modelled the response of the water droplet to impact on a solid surface which, they concluded consists of 2 main stages:

1) The primary stage (Shown in Figure. 2.1): The initial impact to the solid surface causes the water droplet to be compressed. This consequently creates a high-pressure area in both the solid surface and the liquid known as the "shock envelope". The shock envelope is only intact whilst the edge of the contact area between the liquid and the solid surface moves supersonically with respect to the wave velocity of the liquid.
2) The secondary (Jetting) stage: Once the shock envelope collapses, extremely high velocity lateral water jets are formed.

Primary stage

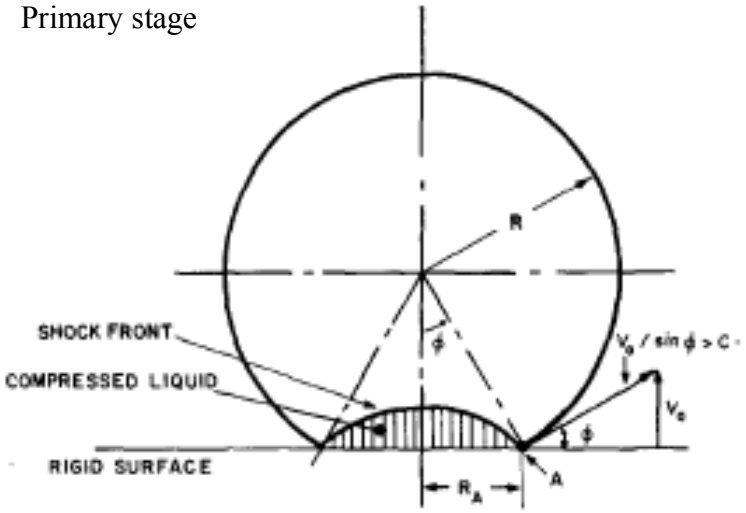

Secondary stage

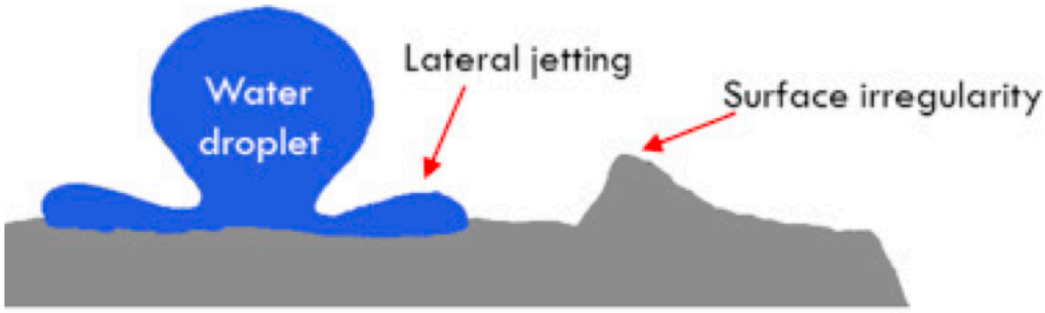

Figure. 2.1 The primary [5] and secondary [6] stages of liquid droplet impact

The pressure resulting from impact, known as the "water hammer pressure" was first modelled using a one-dimensional liquid-solid impact approach (given in equation.1). [7]

$P=\rho_1 C_1 V_1$ (1)

Where ρ_1 is the liquid density, $C_1$is the speed of sound in liquid and V_1 is the impact velocity of the liquid.

Heymann [8] proposed a more accurate value of the pressure generated, which also included the effect of shockwave formation (given in equation.2), however note that the pressure presented is independent of the droplet size.

$$P= \rho_1 C_1 V_1 \left[2+ (2k-1)\frac{V1}{C1}\right] (2)$$

Where k is the impacting liquid constant, in the case of water k = 2, ρ_1= 1000 kg/m^3 and C_1 = 1463 ms^{-1}.

Rochester and Brunton [9, 10] experimentally verified that, for impact velocities in the range of 10-140ms^{-1}, the pressure at the edge of the contact area was about 2.8 times higher compared with the water hammer pressure. Lesser [11] suggests that it could even reach up to 10 times the 'water hammer' pressure. He added that even though the pressure at the contact edge is of high magnitude; the duration is very short (a few nanoseconds). Therefore, the effects of this edge contact area pressure may be negligible (compared to the initial 'water hammer' pressure).

Bowden and Field [12] investigated the duration of an impulse of the water droplet; their calculations were based on the theory of propagating shockwaves through the water droplet (given in equation 3).

$$\Delta\tau = \frac{3rV}{2c_s^2} \quad (3)$$

Where r is the radius of the water droplet front curvature, V is the velocity of droplet impact, and Cs is the shock wave velocity in the liquid.

By using equation.3, I have calculated the duration of the impulse of the water droplet in relation to varying droplet size and impacting speed, which is shown in Figure. 2.2, where the

radius of the front curvature is approximated to be equal to the droplet radius. For a lower elastic modulus material, the duration of the impulse is longer, due to the contact angle at which jetting occurs being larger [13].

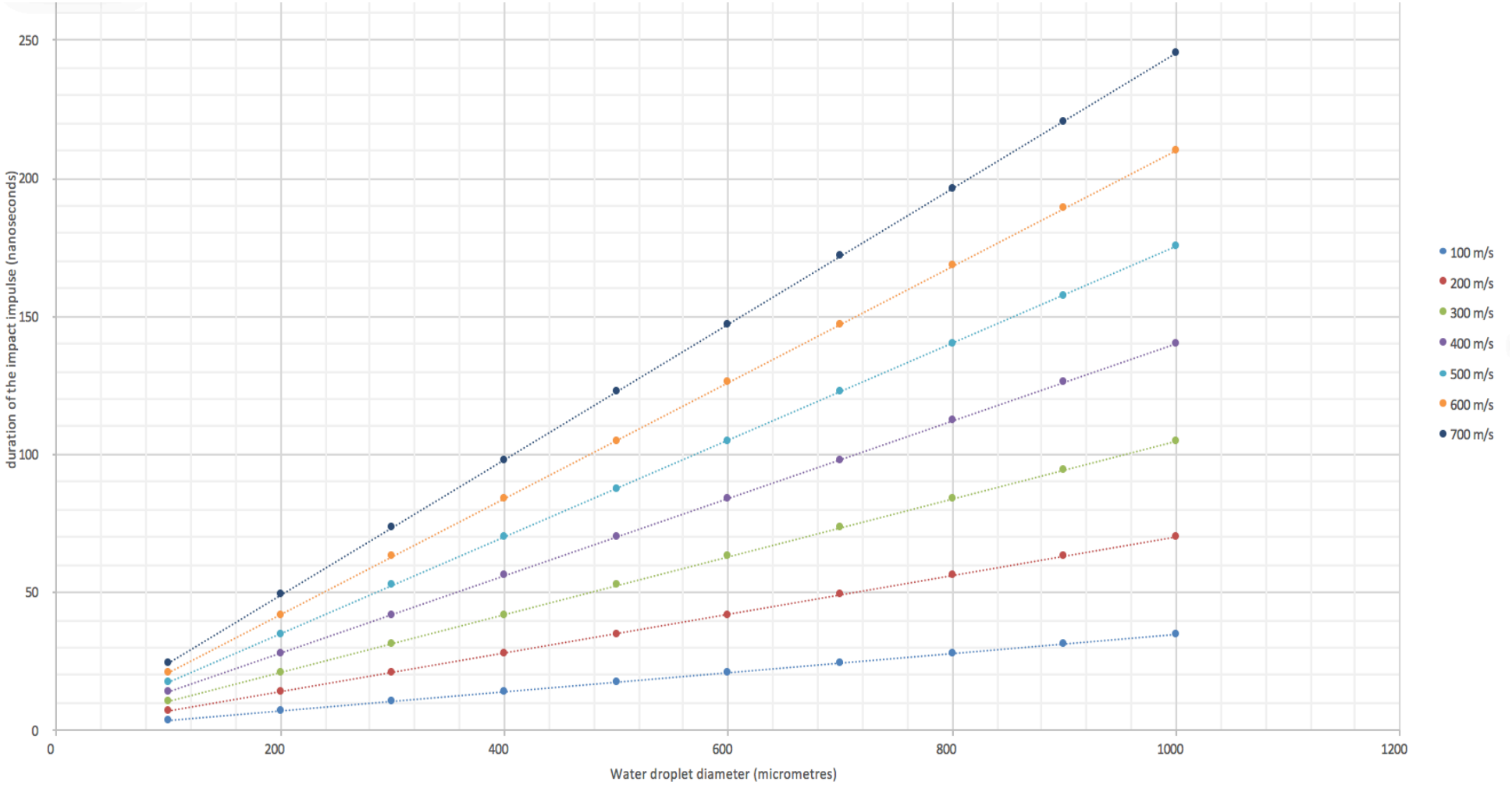

Figure. 2.2 Duration of the impulse with relation to droplet size and impact speed

It is clear that the duration of the impact pressure pulse is a function of the droplet size; smaller droplets would have a shorter impact pulse and vice versa. Suppose we have a droplet of 250 μm in radius and the speed of impact is 300 ms^{-1} and the shock wave velocity in water is 1463 ms^{-1}. For the values given, the duration of one impact pulse seems to be of a magnitude of 10^{-8} (i.e. ~10ns). Such loading times are extremely short compared to solid particle impact, which is reported to be in the order of 10^{-4} (i.e. ~100μs) [12] . In terms of loading, water droplet impact can therefore be classified as "dynamic" loading (where the mechanical behaviour of the impacted material may be highly 'non-equilibrium') and solid particle impact can be classified as "static" loading (where the timescales are sufficiently long that 'textbook' material property values remains applicable).

In terms of strain, we can conclude that materials subjected to water droplet erosion will experience exceptionally high strain rates, which mimics behaviour seen in explosive, shock loading. Typical shock impact pressures of 5-50 GPa usually induce strain rates in the magnitude of 10^{5}-10^{10} s^{-1} [14]. In theory, there is no material known that can accommodate plastically strain rate of this order of magnitude; one might expect therefore that any material (no matter how ductile under conventional mechanical loading) may deform in a brittle-failure fashion.

Water droplet sizes can range from very small (nanometres) to very large (centimetres), smaller droplets will cause the damaged volume to be small, and vice versa. In very small droplets, there may be an underlying effect (due to the small damaged area), which has not been considered in water droplet erosion. For instance, in other mechanical testing techniques such as micro-indentation, metals appear to be harder at lower indentation loads (smaller contact area), this is due to the fact that there is a size-related reduction in dislocation activity where there is

insufficient shear stress to activate all available slip planes in the crystal structure for dislocation movement.

Additionally, inside the “shock envelope”, cavitation bubbles may form near the water/solid interface (shown schematically in Figure. 2.3), which causes secondary damage (cavity collapse) [15-17]. When cavities collapse near the solid interface, a jet is produced which propagates across the cavity and impacts on the solid surface. Moreover, there have been suggestions that the number of cavities generated inside the shock envelope increase with increasing impact velocity.

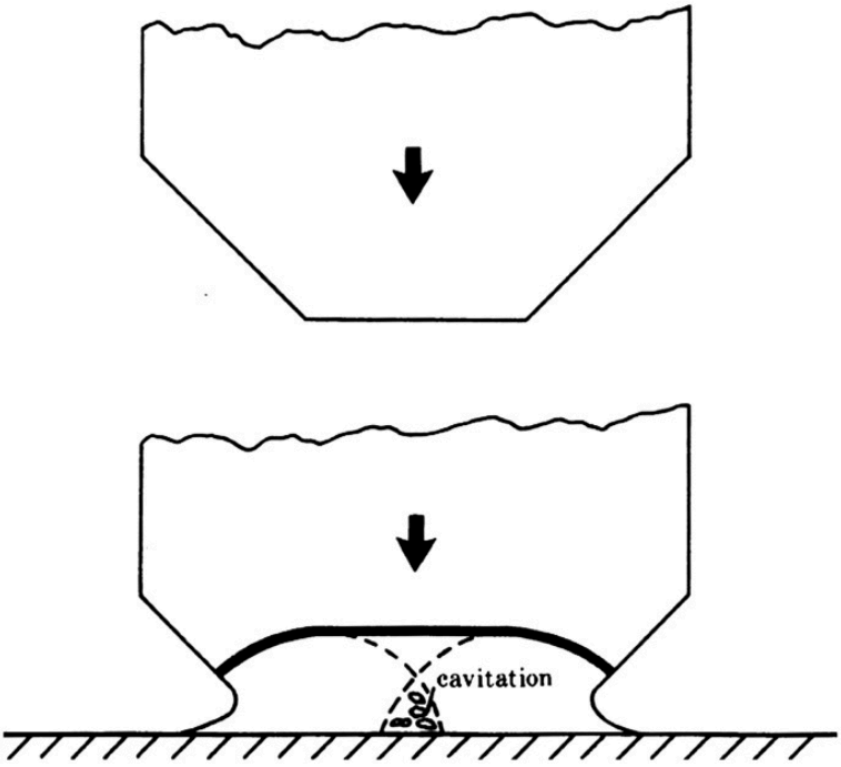

Figure. 2.3 Upon water droplet impact, when shockwaves intersect (dotted line), cavitation can be formed [17]

The high pressure inside the droplet then causes a high velocity lateral outflow of water, this is known as the “Jetting” effect. The jetting speeds of the liquid have been reported to be 2-3 times the initial impact speed [18], this causes the solid surface to be under immense tension which can create further damage to the surface as it interacts with existing surface flaws (e.g. surface asperities are shattered off) and promotes surface crack propagations. Ripple-like damage bands can be observed around the impact area (once jetting commences)[18].

2.2.2 Energy of the water droplet

Due to the high impact speed and very short impulse duration (order of nanoseconds) involved in water droplet erosion, I have attempt to relate the applied energy per droplet with varying droplet parameters i.e. water droplet size, mass and impacting speed. This leads to the adoption of a simple kinetic energy approach (shown in equation.4)

$$Kinetic\ Energy\ = \frac{1}{2} \cdot M \cdot V^2 \quad (4)$$

Where M is the mass of the water droplet and V is the impacting speed. My consideration assumes that the droplet shape is perfectly spherical (therefore the volume of the droplet can be considered as $\frac{4}{3}\pi r^3$ where r is the radius of the water droplet) and that the impacting water droplet has a density of 1000kgm^{-3}. Therefore, the mass of the droplet is calculated by the simple relationship of density and volume of the droplet (Mass = Volume x Density).

The kinetic energy of the water droplet with varying water droplet radius and impacting speed is shown in Figure. 2.4. At low impact speeds, increasing the radius of the droplet makes insignificant difference to the kinetic energy. Conversely, at high impact speed, the kinetic energy of the water droplet scales with increase in droplet radius. Theoretically, the kinetic energy can rise to infinity with increasing in droplet size and impacting speeds.

It would have been more beneficial to calculate the absorbed energy of the impacting droplet, however the considerations become immensely complex and may be impossible to compute.

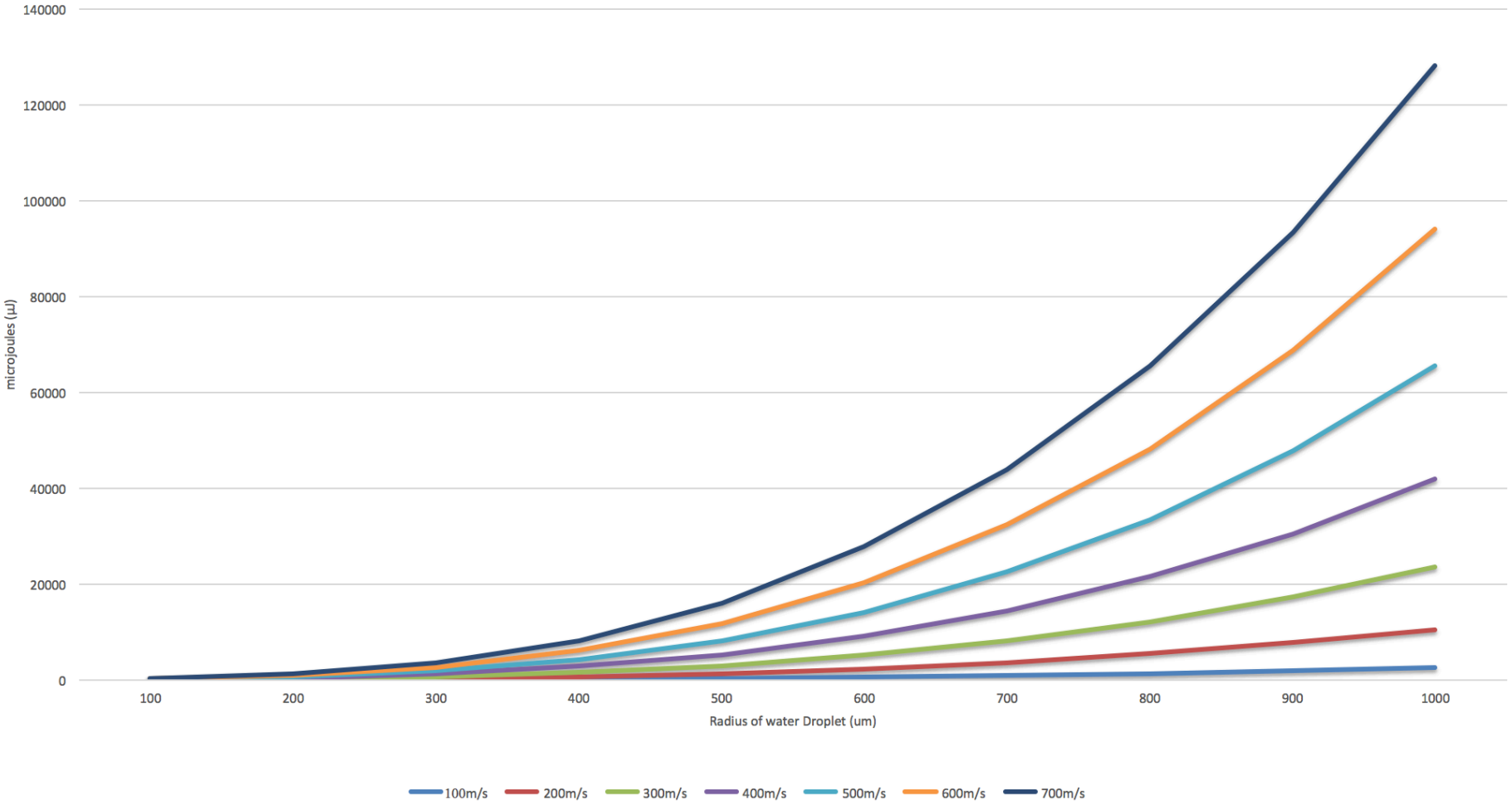

Figure. 2.4 My calculation of the kinetic energy of the water droplet with varying water droplet size and impact speed

Heymann [19] agreed that the energy balance in such systems is very complex. He suggested that the water droplet kinetic energy would be distributed into three portions:

1) Absorbed by the impacting target material
2) Lateral outflow (jetting)
3) In the form of stress waves inside the water droplet

Heymann [19] did not give quantitative percentages of the energy partitioning. He proposed that the amount of energy absorbed by the surface is not only a function of mass and the velocity of impact, but also the behaviour of the water droplet after impact, where the geometry of the droplet will change. However, he failed to recognise that for water droplets with high velocity, another essential portion of the kinetic energy would be converted to heat.

Despite to the unknown stress/strain volume/depth of the material from the impinging water droplet, the interaction volume/depth observably will change according to the material's mechanical properties; i.e. primarily Elastic modulus. Using the Hertzian contact stress to estimate the impact depth is somewhat inaccurate because there is an intrinsic assumption that the contact region will deform elastically. In practice, considering the "dynamic" loading nature of water droplet impact and the levels of compressive stress involved, the contact region would definitely be deforming plastically. This knowledge of the interaction depth remains key to choosing an optimum coating thickness and architecture to withstand water droplet erosion.

2.2.3 Stress wave propagation theory (acoustic considerations)

The theory of stress wave propagation has been extensively researched in the field of seismology. Nevertheless, it has not been extensively applied to solid particles/water droplets impinging onto a surface. Through my research I would like to attempt to bridge this gap of knowledge and apply this theory of stress wave propagation with materials subjected to impacting particles/water droplets.

However, I believe that stress wave propagation theory has a more significant role in explaining water droplet (rather than solid particle) impact; the reason being the vast difference in the impact impulse duration, with water droplet impact being in the order of nanoseconds and solid particle impact being in the order of microseconds. The longer impulse duration for the latter allows the stress waves to be attenuated within the solid particle (allowing stress waves to reflected and to propagate numerous times inside the solid before unloading). However, for water droplet impact, due to the short impulse duration and the phenomenon of collapsing of the "shock envelope", the stress wave can only propagate one time (upward and downward).

The different types of stress waves that are generated upon impact are longitudinal, shear and surface waves (shown schematically in Figure.2.5). Miller [20] suggested (based on an arbitrary assumption that Poisson's ratio of the solid is 0.25) that longitudinal and shear waves are the first to propagate through the impacted solid medium, followed by the surface wave. Surprisingly however, the surface wave carries the most energy (67.35%), followed by the shear (25.76%) and longitudinal (6.89%) wave [20, 21]. The fact that the surface waves carry the most energy may suggest that most of the heating effects (in the solid material) are generated through the attenuation of the surface waves.

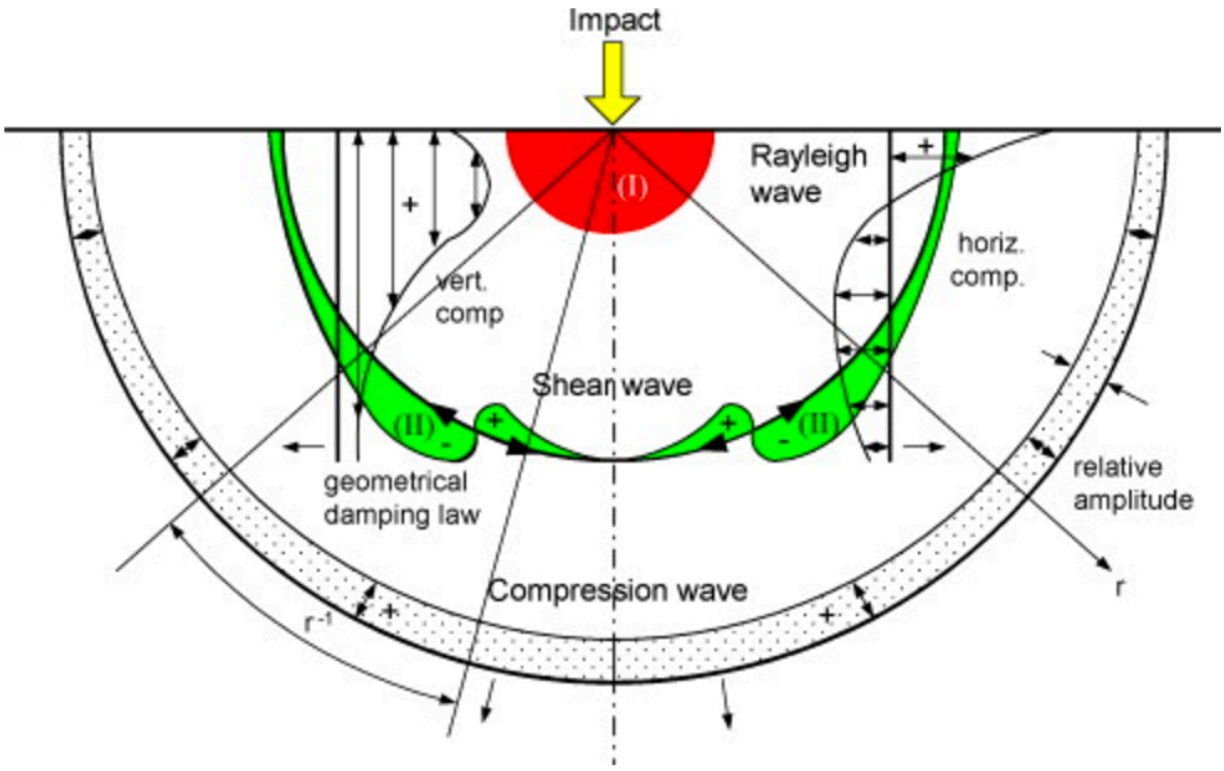

Figure. 2.5 The different types of stress waves that are generated upon impact [22]

Different types of wave travel in a solid at different velocities, the speed of the wave depending mainly on the material's mechanical properties; i.e. Elastic modulus, density and Poisson's ratio. The longitudinal wave travels the fastest and the surface wave travels the slowest (Summarised in table.2.1). On the other hand, in terms of the attenuation of stress waves in a solid, the surface wave is the hardest to attenuate.

Table. 2.1 Summary of the different types of waves speed

	Longitudinal waves	Transverse waves	Approximated Surface waves
Equation	$C_L = \sqrt{\frac{E}{\rho}}$ [7, 23]	$C_S = \sqrt{\frac{G}{\rho}}$ [7, 23]	$C_R = \frac{0.87+1.12v}{1+v}\sqrt{\frac{E}{2\rho(1+v)}}$ [24]

Where E is the elastic modulus of the material, v is the Poisson's ratio, ρ is the density and G is the shear modulus

Note that in isotropic solids, the shear modulus of a solid has relationship with the elastic modulus and Poisson's ratio (shown in equation.5)

$$E = 2G(1 + v) \quad (5)$$

Where E is the Elastic modulus of the material, G is the Shear modulus of the material and v is the Poisson's ratio of the material.

Another important parameter is the Acoustic Impedance of a material. The acoustic impedance may influence the material's ability to attenuate the induced stress waves; however, it is not fully understood. The acoustic impedance in a solid is given by equation.6. [7, 25]

$$Z = \rho C_L \quad (6)$$

Where Z is the acoustic impedance, ρ is the density and C_L is the longitudinal wave velocity of the solid. The longitudinal wave is used here for simplicity, since all the different wave speeds are physically connected by the properties of the chosen material.

From an acoustical vibration energy aspect, as a wave passes through planes of atoms, it will cause the atoms to vibrate as a means to transmit its energy. Therefore, materials with high

density will be able to transfer the wave energy rapidly (effectively to pass the vibrational energy to subsequent atoms more quickly due to the closer distance between atoms). Moreover, materials with higher wave velocity can also spread the energy faster. Hence from my point of view in this research, the acoustic impedance parameter directly relates to the materials' ability to attenuate/spread the stress waves.

As waves travel through the interface boundary of different media, acoustic impedance can be used to calculate the percentage of reflection and/or transmission of the waves (as shown in equation.7)

$$W_R = \left(\frac{Z_2 - Z_1}{Z_2 + Z_1}\right)^2 \quad (7)$$

Where W_R is the reflected wave percentage, Z_1 is the Acoustic Impedance of the first medium and Z_2 is the acoustic impedance of the second medium [23].

When it comes to designing a coating to resist water droplet erosion, these parameters can help to decide which materials are most desirable. The material's Elastic modulus and density play a major role in determining the characteristics of the waves. Higher wave speeds are normally associated with material that has a high Elastic modulus and low density.

Reflection and/or interference of the waves (stress) in the solid can catastrophically damage the material [26, 27]. To eliminate this aspect, Springer [28] proposed that the reflection of longitudinal waves within the body maybe negligible if the coating thickness satisfies equation.8 . The argument is related to the impulse duration of the water droplet impact, t_L, (given in equation.9) and the time duration required for the wave to travel through the coating thickness, t_S, (given in equation.10).

$$h_s > 2d_L\left(\frac{C_{Solid}}{C_{Liquid}}\right) \quad (8)$$

$$t_L = \frac{2d_L}{C_{Liquid}} \quad (9)$$

$$t_s = \frac{h_s}{C_{solid}} \quad (10)$$

Where h_s is the thickness of the solid, d_L is the liquid droplet diameter, C_{solid} is the velocity of the wave in the solid and C_{Liquid} is the velocity of the wave in the liquid droplet.

Basing this calculation on equation.8, suppose we take α-HCP titanium as a coating material, with C_{solid} being 5050 ms^{-1} and we have a droplet size of 500 μm in diameter and the liquid droplet (C_{Liquid}) is 1463 ms^{-1}. The minimum coating thickness must be more than 3.4 millimetres for the reflection of the waves to be imperceptible. Therefore, it's safe to say that for a thin film coating system, being either monolithic or multilayer, the effects of waves reflection and interference cannot be disregarded.

2.2.4 Maximum Penetration Depth (acoustic considerations)

Consider an impacting particle/water droplet from a purely surface wave propagation standpoint. It carries the most energy and is the hardest to attenuate amongst the different types of stress wave. In multiple particle impacts (i.e. real life applications) the stress waves will possess a wide range of frequency, amplitude, and wavelength - depending on the impact speed and particle/water droplet size/shape.

By using a simple relationship between the frequency and wavelength, the maximum interaction depth of the wave can be estimated, based on an assumption that the maximum penetration depth of the surface wave is equal to its wavelength. As the frequency of a wave is inversely proportional to the wavelength (given a fixed stress wave velocity; shown in table.2.2, higher frequency waves will therefore have shorter wavelength, and vice versa.

Note that the range of frequencies proposed is based on the fact that for waves with higher frequency (>200MHz), a polycrystalline material will rapidly attenuate the stress waves [29]. And at lower frequency (< 0.1MHz) i.e. penetration depth of 50mm, is exceeding the thickness limit of coating deposition. There appears to be no detailed or systematic literature review on this subject. Therefore, it would be useful to know the most frequently occurring frequency range in real-life water droplet erosion conditions. If the frequency range is known, this may resolve the question of the optimum coating thickness for water droplet erosion purposes.

Table. 2.2. Shows how frequency varies with wavelength, taking the speed of the surface wave as 5000 ms^{-1} (Approximation of titanium nitride surface wave velocity).

Frequency (MHz)	**Maximum interaction depth (µm)**
0.1	50000
0.3	16667
0.5	10000
0.8	6250
1	5000
5	1000
10	500
30	166
50	100
80	63
100	50
150	33
200	25

Mahdipoor et.al [30] investigated the water droplet erosion of different gas nitriding treated Ti6Al4V samples and revealed that the damage depth in the advanced stages of erosion(of different gas nitride treated Ti6Al4V samples) was found commonly to occur at 300-400μm depth. Taking 300-400μm as the approximate depth where the damage is initiated (i.e. sub-surface crack initiation), referring to table. 2.2, this may suggest that the most damaging frequency range of surface waves is between 10 and 30 MHz.

From Table. 2.3, there is an indication that a coating that has thickness in the nanometre (100 nm) range would not be suitable for water droplet erosion purposes, due to the negligible interaction percentage (less than 0.4%) with surface waves of the ranges of frequencies in which significant acoustic interaction can occur. However, for a coating 10 μm thick, the interaction percentage between the coating and the surface wave could be more significant (up to 40%) and for a coating that is 50μm thick, the interaction percentage could be up to 100% for the range of frequencies indicated.

As the purpose of the coating is to protect the substrate, ideally a 100% coating interaction percentage with the surface waves is desired for all relevant frequencies. Therefore, increasing the thickness of the coating seems to be the only way to increase the shock wave interaction percentage. However, in practice, depositing thick coatings with the desirable properties seems to be a challenge due to various issue i.e. residual stress, adhesion. For thin coatings (100nm), low interaction percentage, I speculate that the coating may be ineffective, since the propagating surface wave (which carries most of the transferred impact energy) will be concentrated mostly in substrate material.

Table. 2.3 Compares coatings with different thicknesses and the coating interaction percentage with the surface wave.

Frequency (MHz)	**Wavelength/ Penetration depth (µm)**	**Interaction percentage of a 100 nm coating**	**Interaction percentage of a 10µm coating**	**Interaction percentage of a 50µm coating**
0.1	50000	0.0002%	0.02%	0.10%
0.3	16667	0.0006%	0.06%	0.30%
0.5	10000	0.0010%	0.10%	0.50%
0.8	6250	0.0016%	0.16%	0.80%
1	5000	0.0020%	0.20%	1%
5	1000	0.0100%	1.00%	5%
10	500	0.0200%	2.00%	10%
30	166	0.0602%	6.02%	30.12%
50	100	0.1000%	10.00%	50.00%
80	63	0.1587%	15.87%	79.37%
100	50	0.2000%	20.00%	100%
150	33	0.3030%	30.30%	100%
200	25	0.4000%	40.00%	100%

The energy associated with a wave is another important factor, where the energy of a wave is related to the frequency and the amplitude. As frequency can be defined as “the number of waves passing through each second”, measured in Hertz. Therefore, if the amplitude of the waves stays the same, higher frequency waves will transmit more energy per second.

There appears to be no literature review on this subject matter. In reality, there could be a wide range of amplitude and frequency depending on the velocity of the impacting water droplet. For that reason, again I could not stress enough the importance of knowing the most likely occurring frequency range in materials subjected to water droplet erosion.

My calculations suggest that the waves in the low frequency range may be the most damaging, since most of the energy carried will be dissipated in the substrate material. Validating this whole theory appears to be challenging, since implementing equipment to measure the frequency in water droplet erosion test machine seems to be difficult and technology in the field has not caught up with this prospect. Instead, another simpler alternative may be to measure the frequency of the water droplet impact using a single-shot liquid impact apparatus. However, the investigation in this matter is not possible in this PhD work because of the lack of equipment in the laboratory.

2.2.5 Water Droplet Erosion Zone

The time-dependency on the rate of water droplet erosion and distinct "zone" of erosion has been clearly established. Similar to other types of erosion, the performance of a material is usually measured by the mass loss against exposure time; Water droplet erosion has four distinct zones (Shown in Figure. 2.6):

1) Incubation period: the period where no mass loss occurs. However, the surface may become randomly covered by shallow depressions (increase in surface roughness) caused by the collapsing of cavitation bubbles formed within the "shock envelope" [17] or from the compressive stress induced by the impacting liquid droplet; which causes the solid to yield [31].
2) Acceleration period: where mass loss starts occur and then proceeds at a constant rate: mass loss is due to material being removed from the pits and crack intersections formed during the incubation period.
3) Deceleration Period: Mass loss occurs at a progressively lower rate than in the previous stage: This reduction in erosion rate is believed to be due to the water retained in pits and cracks, providing shielding of the surface from direct impact damage [32].
4) Steady-state Period: The Erosion rate remains steady throughout its exposure time.

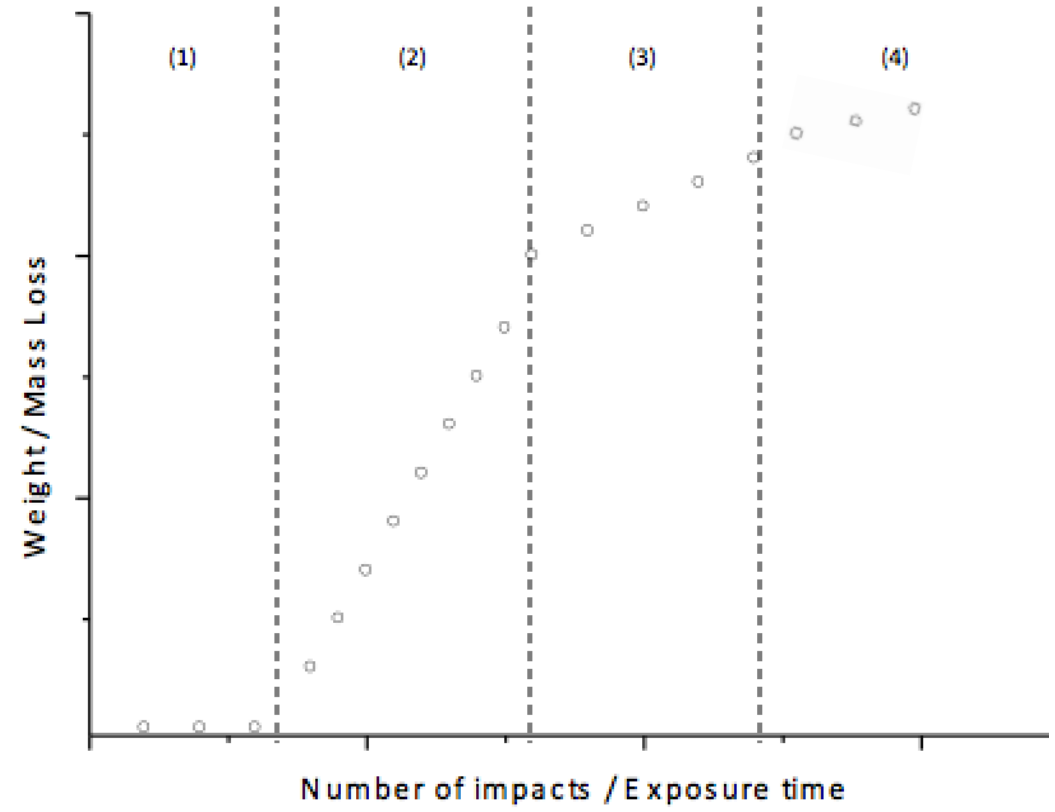

Figure. 2.6 Schematic representation of the different water droplet erosion zones, Adapted from Heymann [32] and Springer [7]

2.2.6 Effect of the impact angle on water droplet erosion (WDE)

Earlier studies on solid particle erosion revealed that the incident angle at which the impacting particles arrive at the material surface has a significant effect on the erosive wear (shown in Figure. 2.7). Schmitt et al. [33] and Hoff et al. [34] claimed that the incident angle also plays a role in the erosive wear of water droplet erosion. Ahmad et al. [35] experimentally verified that for, a martensitic stainless steel (X20Cr13), the maximum rate of erosion occurs at a water droplet impact angle of 90^{o} (shown in Figure. 2.8) i.e. actually similar (brittle) erosion behaviour to glass (for particulate erosion).

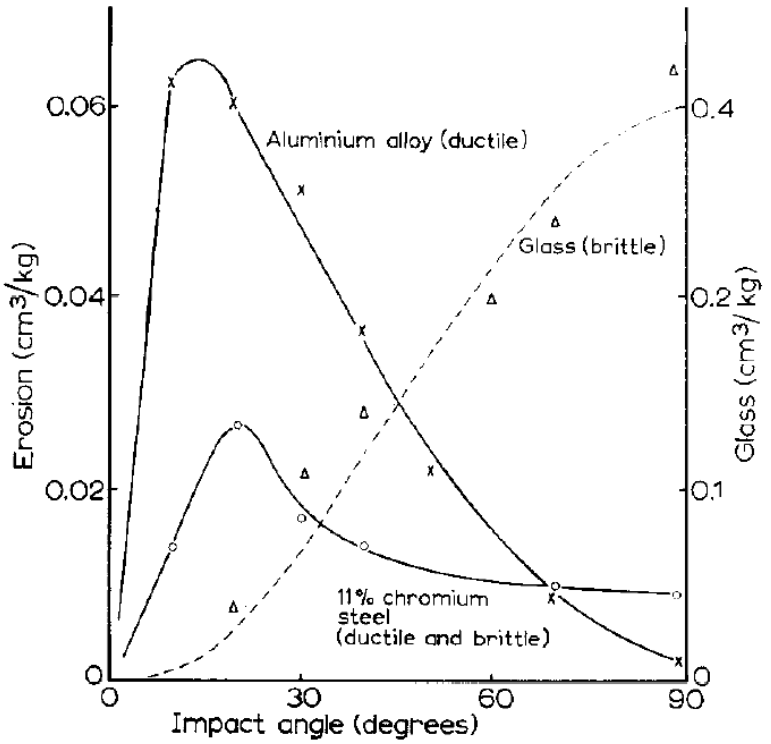

Figure. 2.7 Typical particle erosion wear response to different impact angles for brittle and ductile materials [27]

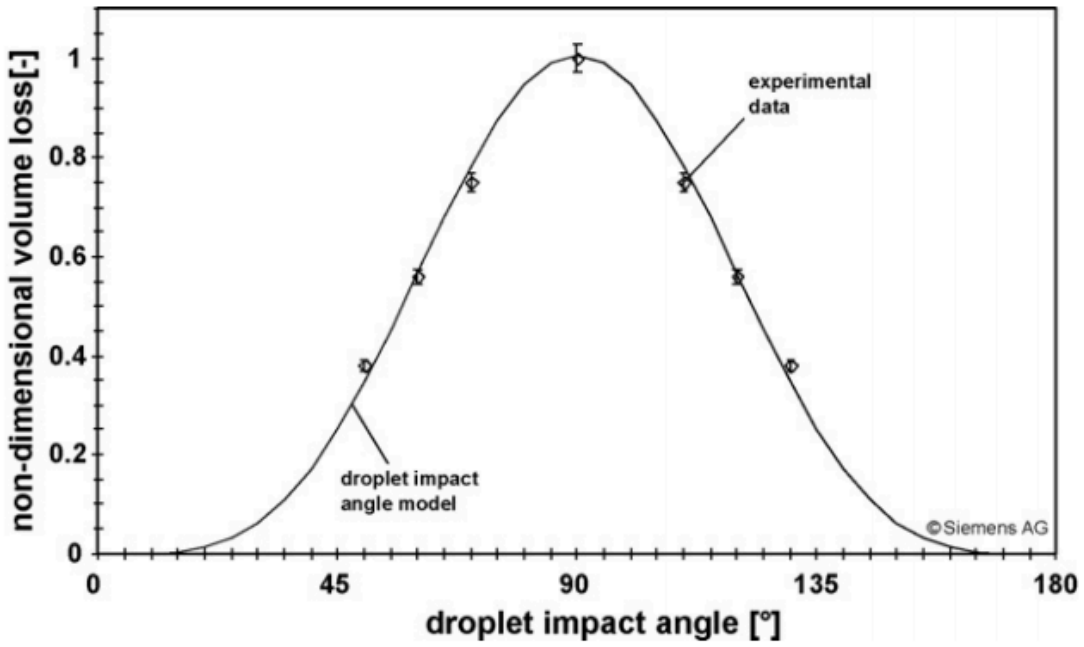

Figure. 2.8 Normalized volume loss of martensitic stainless steel X20Cr13 as a function of droplet impact angle. [35]

2.2.7 Water Droplet Pit Depth

Engel [36] appears to be the only person who has tried to suggest an equation (see below equation.11) to determine the pit depth of a water droplet impacting onto a stationary flat solid plate. The pit depth was found to be a function of impact velocity, droplet diameter and the properties of both entities (water droplet and solid plate) – the properties various properties are discussed in equation 11. Note that the liquid jetting phenomenon is not taken in consideration.

$$\delta' = \frac{7.2 d z_l}{C_s(z_l+z_s)}[\text{V-V}_\text{t}] \quad (11)$$

Where δ' is the pit depth, d is the water droplet diameter, C_s is the speed of sound in the solid plate, z_l is the acoustic impedance of the liquid and z_s is the acoustic impedance of the solid, V is the impacting velocity of the water droplet, and V_t is the threshold velocity for pitting damage initiation (shown in equation.12 below).

$$V_t = \frac{19K'(z_l+z_s)}{(\rho_l C_s z_l^3)^{1/2}} \quad (12)$$

Where K' is the dynamic compressive yield strength of the material. However, the available literature data for the dynamic compressive yield strength of materials is very limited.

From Engel's proposal, the pit depth is inversely proportional to the speed of sound in the solid and the impedance of the solid material subjected to impact. Moreover, Engel concluded that, for any given velocity and size of the impacting body, the physical nature of the impinging material (being solid or liquid), also plays an important role on the critical threshold velocity (shown in Figure. 2.9); of which below this critical threshold velocity no pitting damage, will be observed.

The practicality of this equation lies on the availability of the data of dynamic compressive yield strength of the material being subjected to impact. No literature data were found for the material of titanium or titanium nitride. If the data was available, one must take caution on using the values, since the dynamic compressive yield strength of a material value would vary, depending on the strain-rate applied.

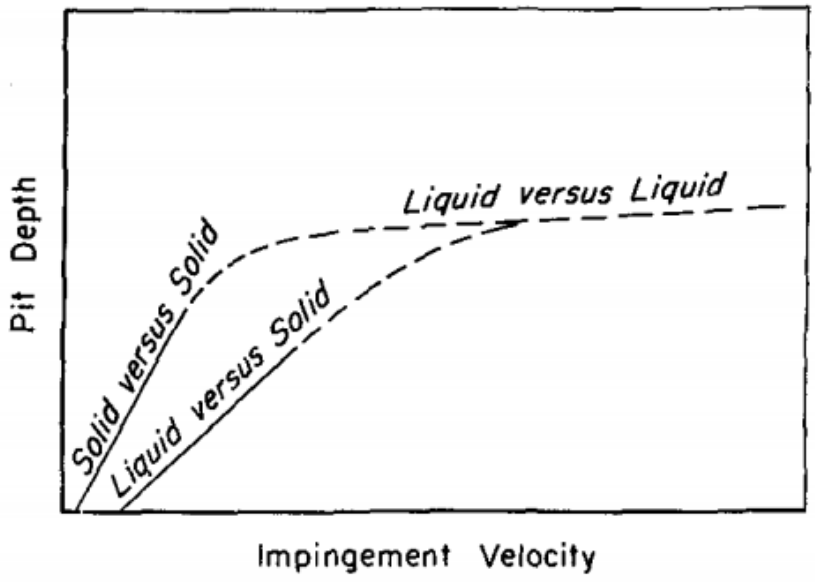

Figure. 2.9 Schematic of the relation between of the projectile physical nature and the damage pit depth and impacting velocity [36].

2.2 Brief history and development of ion-plating processes

Amongst the variety of thin film coating deposition techniques in a vacuum environment, the triode ion-plating deposition technique is renowned for producing coatings with superior properties with reasonably high deposition rates. High deposition rate techniques are desirable for producing erosion-protective coatings because thick coatings are desired. Furthermore, as triode ion-plating technique will be chosen as the technique to produce coatings in this PhD study, I would like to review the fundamental aspects of this technique.

The term 'Ion Plating' is described by Mattox [37, 38] as "An atomistic vacuum coating process in which the substrate surface is sputter-cleaned and maintained clean until the depositing film material covers the surface. The depositing film is then continuously or periodically bombarded by energetic atomized inert or reactive particles during film growth". His earlier work in the 1970s was on metallic thin film deposition, using a simple DC diode plasma configuration [39] where typical process parameters were 2 to 5 kV DC substrate negative bias, $1.5 – 6 \times 10^{-2}$mbar chamber gas pressure and a (rather low) substrate current density of ~0.5mA/cm^2; i.e. 5 to 10 times less current density than modern plasma-assisted PVD ceramic coating deposition systems.

Although it is difficult to evaporate a compound material from a source to get the right stoichiometry and composition in the deposited film (due to differences in vapour pressure of constituent elements), Bunshah [39] pioneered the production of ceramic coatings by Physical Vapour deposition (PVD), with the introduction of 'reactive' gases such as nitrogen, oxygen and carbon while the (metallic) source material is evaporated. His Bias Activated Reactive Evaporation (BARE) process configuration broadened the range of coatings that could be deposited and expanded the prospect of producing ceramic coatings with astonishing properties.

In order to put this concept into industrial use, the deposition technique needed to be improved because of low deposition rates at the (much higher) substrate current densities required; i.e. ~5 mA/cm^2. Moreover, people were struggling to maintain the required plasma intensity at lower chamber pressure (less than $1x10^{-2}$mbar) required to produce phase-pure ceramic thin films.

Baum [40] was probably one of the first to recognise the benefit of an addition electrode (as a source of electron emission to an ion-plating system), to enhance the degree of ionisation – and thus increase plasma current density at the substrate. The work of Matthews [41] further elaborated on this idea in order to develop a practical industrial 'triode' ion-plating system.

The major benefit of the additional thermionic electron source is due to the high-energy electron impact ionisation of the reactive gases involved; eg. Nitrogen (as well as to the Argon carrier gas and metal ion evaporant species). This will enhance the discharge and allows it to be sustained at lower pressure (in comparison to a diode vacuum plasma system).

Additionally, this increases the ionisation efficiency of the system, in terms of the total number of ionised gas species; degree of ionisation for a diode system is <0.01% while generally for a triode process is >1% [42]. This enables the workpiece bias to be operated at a lower negative voltage, which is known to have beneficial effects on the coating deposited.

To fully understand (and control and optimise) the benefits of enhanced plasma discharge triode ion-plating systems requires detailed knowledge of the impacting ion and neutral energy distributions at the workpiece surface. Davis and Vanderslice [43] proposed that the ion energy distribution of such systems depends on the ratio of the parameters L (the cathode sheath thickness) and λ (mean free path for charge collision exchange).

The critical parameter L can be determined by the free-fall version of the Child-Langmuir equation [44] (shown in equation.13)

$$L = \frac{2}{3}\left(\frac{\varepsilon_0}{J}\right)^{\frac{1}{2}}\left(\frac{2q}{M}\right)^{\frac{1}{4}}V_c^{\frac{3}{4}} \quad (13)$$

Where ε_0 is the permittivity of free space, J is the cathode (substrate) current density, q is the ionic charge, M is the ion mass, and V_c is the voltage across the cathode sheath.

Rickards [45] elaborated on the Davis &Vanderslice model and adapted it to accommodate the non-linear field distribution exhibited in practical discharge circumstances. The model (shown in equation.14) predicts the ion energy distribution for a discharge situation if the parameters of L and λ are known.

$$\frac{dN}{DE} = \frac{N_o}{m}\frac{L}{\lambda}(1-E)^{(1-m)-1}\exp\left[-\frac{L}{\lambda}+\frac{L}{\lambda}(1-E)^{\frac{1}{m}}\right] \quad (14)$$

Where E defines the relative fraction of ion energy that lies between zero and unity (Unity defines maximum energy, justified by collision-less ions travelling across the cathode sheath thickness), N_0 is the number of ions entering the cathode sheath from the negative glow region, and m is a constant which takes the value of $\frac{4}{3}$ for the abnormal glow discharge regime commonly found in plasma assisted PVD processes.

The significant ratio of L/λ determines the energies of the ions travelling across the cathode sheath. If the ratio of L/λ is large, the ions undergo many collision exchanges and ions will arrive at the workpiece surface with fractional energy of the theoretical maximum defined by the substrate negative bias. If the ratio of L/λ is small, the ions undergo fewer collision exchanges and the ions will arrive at the workpiece surface with maximum energy.

The benefit of a triode ion-plating system compared with a diode ion-plating system is such that workpiece current density can be increased by controlling the power on the additional electron emission electrode without needing to increase the workpiece bias (increasing L) or increasing the ionised gas pressure (lowering λ).

Previous work by Fancey and Matthews [42, 46] showed that L/λ will fall in the range of 10-15 in an argon diode system, where <0.1% of the ions will be carrying maximum energy (i.e. most of the energy is carried by energetic neutrals which were once ions, before they experienced charge exchange collision). However, the L/λ ratio for a triode system can be as low as 0.5 and as much as 99% of the ions will carry maximum energy.

2.3 Review of PVD coatings for WDE protection

In this section, I attempt to critically review existing (both mechanical and acoustical) models and theories that have been put forward by researchers on how to design a coating to resist all types of erosion. This will then enable me to summarise and put forward a coating design which will be superior in resisting water droplet erosion (WDE).

2.3.1 Mechanical model

2.3.1.1 Monolithic coatings

There are three classes of materials that can be used for a coating system: ceramics, metals and polymers. Each class of materials have very different properties; e.g. mechanical, electrical, optical and acoustical. Material selection for the coating must be in accordance to the application criteria.

Many classical wear theories state that the most influential property for wear resistance of a material is the hardness (H), despite the fact that several studies have shown that elastic modulus (E) may play an equally (if not more) significant role in different types of wear behaviour [47]. Therefore, the relationship between hardness and elastic modulus should be considered in determining the potential WDE resistance of any coating.

In material deformations, many researchers often confuse (or do not accurately discriminate between) the terms which define “Elastic” and “Plastic” energy input. The ability to absorb elastic energy of a material before initiation of permanent deformation (yield strength) is known as ‘Resilience’. On the other hand, the toughness of a material is more closely related to the total energy (Elastic + Plastic) required to reach the point of fracture [48].

Recent studies showed that high H/E ratio provides a good correlation to the resilience of a material. However, in studying cavitation erosion, Smart [49] indicated that a better indicator for toughness may be a high H^2/E ratio, since it accounts for both elastic and plastic work of deformation (to a material's ultimate tensile stress). The importance of reducing the Elastic Modulus of the coating is usually neglected because textbooks refer always to the Archard equation [50] when considering wear; researchers therefore often focus more on achieving high hardness, rather than attaining a low (or functionally graded) modulus [47].

In view of the fact that, in most applications, the substrate material is relatively soft and compliant (i.e. not just low Hardness, but also low Elastic modulus), choosing coating materials to match the elastic modulus of the substrate material may prove to be a superior approach in terms of improving the coating-substrate adhesion/interfacial toughness under loading [47, 51].

Polymer coatings [52] (of low Elastic modulus) have been extensively studied as materials to resist WDE on wind turbine blade leading edges, owing to the high impact toughness (i.e. low E and long plastic/viscoelastic strain to failure) which they exhibit. However, employing polymeric coatings in (for example) steam turbine blade applications is not technically feasible, since the available materials cannot survive the high temperatures involved.

With regards to the tensile stress generated during supersonic droplet impact in WDE, the maximum impact stresses generally exceed significantly the yield strength of the substrate material. In developing an ideal coating for resisting WDE, selecting a material with high hardness (stiffness) must be considered in combination with the need for a high degree of toughness and resilience (i.e. mechanically conflicting requirements, in a monolithic (bulk)

material). Hence a coating should be able to elastically deform and yet also resist crack initiation [47].

The crystal structure (HCP, BCC or FCC) of a coating (or substrate) material will also play a role in the failure mode of the material. Different crystal structures exhibit different numbers of available (but not necessarily active) slip systems under plastic yielding (number of slip systems: HCP<FCC<BCC), where dislocation can move. BCC structure would be pre-eminent in terms of plastic deformation, since dislocations can glide/move in more slip systems. HCP materials typically have no more than 4 available primary slip systems (when Von Mises' criterion says 5 are a minimum requirement for uniform plastic deformation; this is due to the ideal c/a ratio in the crystal of 1.633 being rarely achieved). Thus, materials with HCP structure are more likely to fail by brittle fracture than BCC/FCC where the failure mode is more conducive to ductile tearing.

For materials experiencing water droplet impact at supersonic speeds, it has previously been calculated that the impact pulse will be in the order of a few nanoseconds (previously shown in figure 2.2). There may not be enough time for any available slip system to accommodate dislocation movements (even for BCC structures) and this will lead the material to fail in a brittle fashion (see again Figure 2.8). In order to avoid brittle fracture, materials exhibiting low time-dependency deformation mechanism would be desirable; where twinning, giant faults (eg. shear bands) or diffusionless (eg. martensitic) phase transformations are the predominant deformation mechanisms [53-55].

The Dundurs' parameters are normally utilised for the selection of laminated composite materials for structural design purposes. In spite of this, the parameter may be adapted to aid a

coating system material's selection where adhesion/interfacial toughness is essential [56, 57]. The two parameters are "α and β", which are defined in Equations (15) and (16).

$$\alpha = \frac{\mu^*(k_1+1)-(k_2+1)}{\mu^*(k_1+1)+(k_2+1)} \quad (15)$$

$$\beta = \frac{\mu^*(k_1-1)-(k_2-1)}{\mu^*(k_1+1)+(k_2+1)} \quad (16)$$

Where μ* is the shear modulus ratio ($\frac{\mu_1}{\mu_2}$) and k_i is the Muskhelishwili's constant corresponding to the materials' Poisson's ratios (v) – i.e. $k_i = (3 - 4v_i)$ for plane strain (bulk material properties) and $k_i = (\frac{3-v_i}{1+v_i})$ for plane stress (i.e. thin plates or layers of a material; relevant to coatings). Furthermore, α can be further described in terms of the elastic moduli of the two materials (shown in equation.17)

$$\alpha = \frac{E_2^+ - E_1^+}{E_2^+ + E_1^+} \quad (17)$$

where E_1^+ is either $|E_i/(1 - v_i^2)|$ or $|E_i|$ (for plane strain or stress, respectively)

An attempt to link α and β to the design of coating-substrate systems has been made [58], interpretations can be made that if coating and substrate material have the same Poisson's ratio, minimising alpha and beta (i.e. matching the Elastic modulus of the materials) would improve the coating/substrate interfacial toughness. However, in effect neither the elastic modulus and/or Poisson's ratio of the materials would be similar (high hardness coatings generally will have high Elastic modulus and low Poisson's ratio, while substrate materials will have low elastic modulus and high Poisson's ratio). Another interpretation that can be deduced from α and β is that it

would be beneficial to functionally grade the coatings (with decreasing elastic modulus towards the coating/substrate interface) to match the substrates elastic modulus, thus minimising the α and β parameter values at the coating-substrate interface (i.e. to maximise interfacial toughness).

2.3.1.2 Multilayer coatings

A substantial limitation of monolithic coatings (especially high modulus ceramic coatings deposited by PVD) is that compressive residual stress in the coating tends to scale with increasing coating thickness. For elevated-temperature deposition techniques such as Plasma-assisted PVD, the residual stress arises in part from the thermal contraction mismatch between the coating and substrate upon cooling. Although desirable in resisting crack initiation, an excessively high level of residual compressive stress makes the coating more vulnerable (susceptible) to spallation and can lead to premature failure. Low-to-moderate levels of residual compressive stress in the coating may be more desirable in resisting transient tensile stresses under impact loading [59, 60]. A potential solution to this problem lies in multi-layered coating systems; this has been recognised by many researchers as a means to build thicker coatings (>20μm) with high structural integrity, to resist abrasion, erosion and impact wear [61-64].

Multilayers can be separated into two categories; isostructural and non-isostructural. Multilayers that fall into the isostructural category contain layered materials with the same crystal structure and dislocations slip systems, whereas non-isostructural multilayers exhibit layered materials with different crystal structure and dislocations slip systems. Generally speaking, dislocation movement from one layer to another in isostructural multilayers is more favourable than in non-isostructural. [65]

Koehler [66] was one of the first to explore how to strengthen a material via a layered system of two dissimilar materials. He suggested that the layered materials should be

isostructural, have a similar lattice parameter and have sharp layer interfaces – but different elastic properties. Additionally, the thickness of each layer should be low (<20nm) so that dislocations cannot be generated within the individual layers (and/or dislocation propagation from layer to layer is suppressed).

His key argument was thus focused on restricting dislocation movement within the structure. In order to achieve this, layers selected must exhibit as large a difference in shear modulus between them as possible. This means that large stress is required to drive a dislocation from material (A), which has a lower shear modulus, into material (B) of a higher shear modulus. Moreover, if the layers are thin enough, Frank-Read dislocation sources cannot multiply.

As researchers started to investigate Koehler's arguments regarding the "Superlattice Effect", one of the first to experimentally confirm Koehler's argument was Lehoczky [67]. He deposited Al/Cu multilayers of various layer thickness (ranging from 500-10nm for each layer) onto single crystal NaCl substrates, where he reported an increase of approximately three-fold in yield strength with decreasing bilayer thickness. This trend follows the Hall-Petch relationship, which relates the grain size to the hardness of a polycrystalline material. Therefore, in order to model the hardness of a multilayer composite/coating material, the grain size parameter is substituted by the layer period (Λ) [68, 69]. The adapted relationship between Hardness and bilayer thickness is given by the equation.18

$$H = H_o + k\Lambda^{-\frac{1}{2}} \quad (18)$$

Where H is the hardness of the material, Λ is the layer pair thickness and k is a constant of the hardening contribution due to the grain boundaries. According to the relationship, hardness should increase to infinity as the layer thickness diverges to zero.

On the contrary, Anderson and Li [70] calculated that, beyond a threshold layer thickness, decreasing the thickness further would be detrimental to the strength of the material (reverse Hall-Petch relationship), this is due to reduction of dislocation pile-up effects at low thicknesses.

The fact that Koehler implied in his argument that the layers should be as thin as possible so that Frank-Read dislocation source cannot operate, which act as a strengthening mechanism, and in combination with Hall-Petch inverse relationship of Hardness and thickness has led researchers to construct nano-metric thickness range PVD multilayer coatings for erosion resistance. However, Frank-Read dislocation sources are not the only dislocation mechanism, homogeneous nucleation is also permitted. Moreover, there have been suggestions that for high strain rate applications, Frank-Read sources are too slow to generate dislocations and therefore homogeneous nucleation, which can operate instantaneously, is the predominant process basis of dislocation generation. However, note that the stresses required to activate homogenous nucleation sources are much higher for Frank-Read sources [71-77].

Koehler's argument can be adapted and interpreted into building a multilayer via a combination of high and low elastic modulus materials. This type of multilayer may prove to be beneficial as a means to combine the properties of high 'resilience' and 'toughness'. Stiff (Hard/Brittle) layers will help to shield the substrate from high impact strains (so called "stress-shielding"), although such layers would be susceptible to brittle fracture due to the high bending stress under normal deflections. To aid in the reduction of the bending stress, a low elastic modulus (tough) interlayer may deflect and/or yield, allowing the high elastic modulus (resilient) layers to slide over each other (shown schematically in Figure. 2.10) [61, 78].

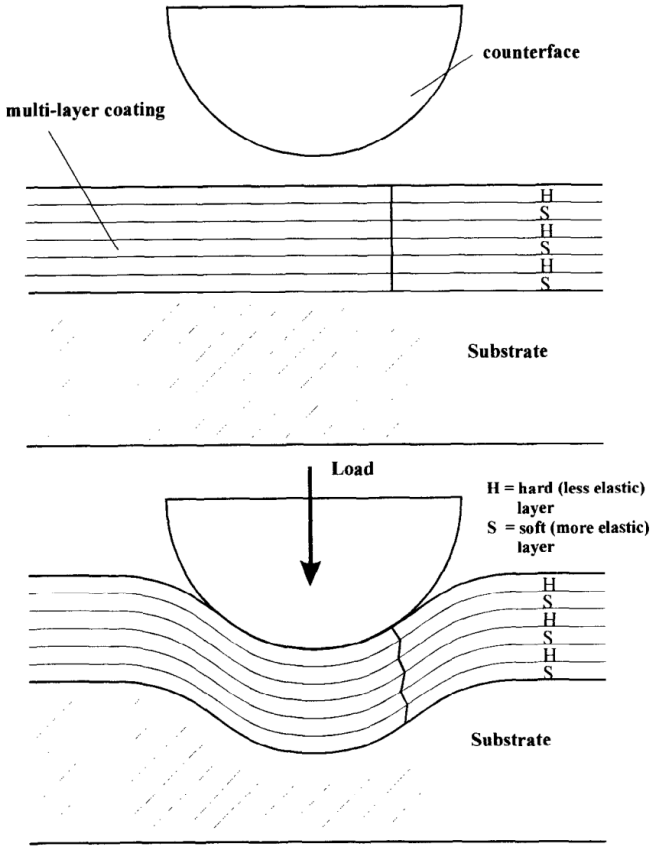

Figure. 2.10 illustrates how a multilayer structure with alternating stiff and compliant layers allows coatings to deformation without fracturing, the line through the film shows how shear in the more compliant (soft) layers allows the stiff (hard, but brittle) layers to slide over each other [78].

As promising as the "Superlattice effect" seems in theory, the drawback of this approach is that adhesion is sacrificed. From a purely elastic consideration, multilayer systems that adopt the "Superlattice effect" approach experience high elastic modulus (E) mismatch among the layers, making them predisposed to spallation and to fail long before their theoretical strength.

Holleck [62] reviewed the toughening mechanisms (summarised in Figure. 2.11) that a multilayer coating may exhibit. He stated that multilayer coatings exhibit stepped failure mechanisms, which gives evidence that the interfacial boundaries between the layers can act as sites for crack deflection and will be able to open/delaminate - to reduce stress concentration.

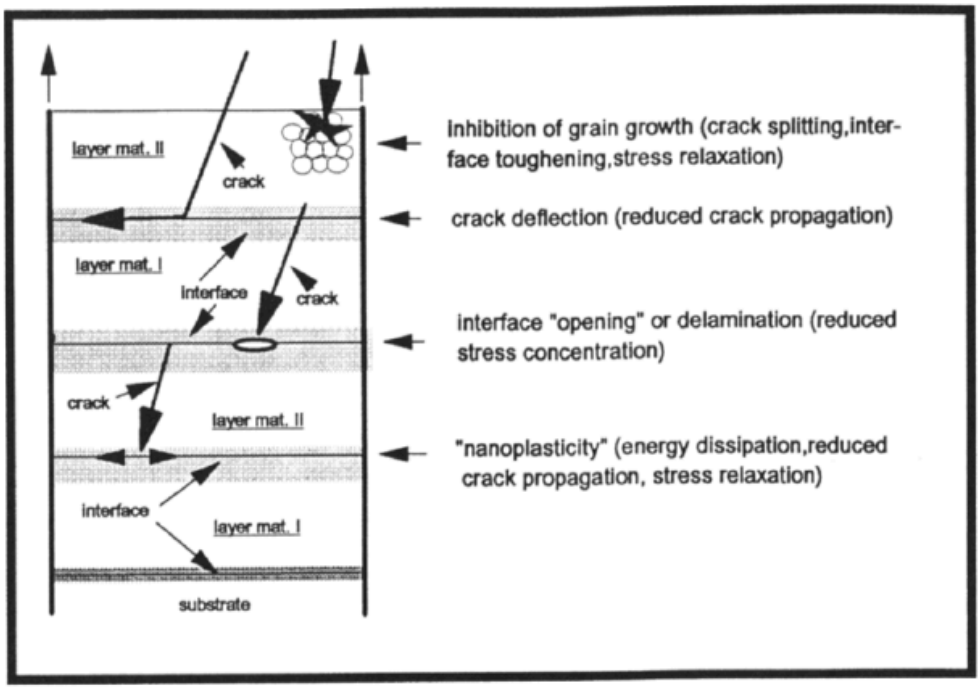

Figure. 2.11 Strengthening mechanisms in ceramic multilayer materials (schematic representation) [62]

Many attempts have been made model to and develop coatings for Solid Particle Erosion (SPE). Hassini [79] proposed that a multi-layered coating design with increasing elastic modulus from the surface to the coating/substrate interface would provide the best solution in reducing the impact tensile stress. Chai and Lawn [80, 81] proposed that, for high-energy impact, the first layer must be thick and of high hardness.

According to the Thornton structure zone model [82], physical vapour deposition (PVD) techniques usually promote coatings to have dense columnar structures, due to the low gas pressure and elevated working temperature involved. For multilayer systems, the columnar structure may be advantageous as a method to spread the loading to subsequent columns below them under normal loading. Moreover, when there is insufficient resilience and/or toughness, these columns can also 'pluck out', leaving the adjacent and perpendicular columns structures with the same integrity [83].

2.3.2 Acoustic model

The phenomenon of shock waves propagation through layered strata has been extensively reviewed in the field of seismology. Yet there is minimal investigation in the field of water droplet erosion (WDE). The principle of an acoustic model in WDE is to view the energy/momentum transfer of an impacting water droplet on the solid material surface as acoustic waves (rather than mechanical stresses/strains), which propagate through the solid medium at the speed of sound in that medium. Therefore, part of this PhD project involves attempts to review the possible ways to accommodate and alleviate these stress waves.

One possible approach to dissipate the droplet impact energy is by selecting a material with a high acoustic wave velocity to spread laterally the stress waves as fast as possible [84], where the stress wave velocity is strongly related to the material's Elastic modulus and density. Materials that concurrently exhibit high elastic modulus and low density possess the highest acoustic wave velocity.

The acoustic impedance of a material under interaction with a stress wave is yet to be fully understood. However, the product of acoustic wave velocity and density governs the

acoustic impedance of a material. Consequently, basic assumptions can be made that materials with higher acoustic impedance values would exhibit better ability in dispersion of stress waves in a material of uniform structure and composition.

Another approach may be by means of a multi-layered coating system. This can be conceived as alternating layers of materials with high and low acoustic impedance (Z), where the interface boundary is sharp. As a stress wave propagates through the (composite, layered) medium and reaches the interface boundaries of each layer, because of the mismatch in acoustic impedance, a significant fraction of the stress wave energy may be reflected (i.e. a reduced proportion of the energy is transmitted to subsequent layers). The model is proposed as a means to restrict a substantial proportion of the incoming normal impact energy to the top few layers of the coating system (and thus protect the substrate). Furthermore, partial transmission of waves will through layers of different media, will assist to attenuate them.

Nevertheless, there are flaws in this approach. The first being that this method mainly considers the longitudinal stress waves, which carries the least energy (6.89%) partitioned among the stress waves. Additionally, this approach may accentuate the phenomenon of constructive interference of longitudinal/lateral compression waves with the surface Rayleigh waves, which will promote areas of increased (and possibly tensile) stress-concentration in the surface (coating) and may lead to formation of cracks and gradual removal of material by cyclic fatigue under repeated impact.

The void of knowledge in the penetration depth of the stress waves, most importantly in surface waves (believed to carry nearly 70% of the energy partitioned), suppresses the ability to optimise the design of a coating to resist stress wave propagation. The penetration depth of the

surface wave is related to the frequency and wavelength, which in turn depends on the duration of the shock impact (which relates to the droplet impact velocity and size, the coating material properties, thicknesses etc.). Referring back to section 2.2.3, obviously, there are in principle infinite possibilities of penetration depth for the stress waves. The measurement of shockwave distributions from impacting water droplets in real-life application remains an unresolved challenge. However, if possible in the future, enlightenment in the most damaging and occurring range of frequencies/wavelength of the stress waves is potentially the key in optimisation coating design for WDE applications.

Furthermore, the total thickness and layering effect will be an important factor in the coatings' ability to attenuate the stress-waves [85]. It would be ideal to build a layered structure as thick as possible (millimetres range) to minimise the effect of stress wave reflection, but in practice it would be difficult and costly.

Lastly, with reference to table.2.2, the frequency of a surface wave that could interact with a coating having layers in the nanometre thickness range would have to be approaching the Terahertz range. Such high frequency waves are unlikely to be the ones causing the damage, since they will be quickly attenuated in a polycrystalline solid. Therefore, in terms of the thickness of the individual layer, I speculate that the threshold minmum thickness of the individual layer is of the order of ~500nm because, below this threshold limit, a multilayer will have no distinct laminar structure that is 'visible' to acoustic waves of a frequency likely to transmit sufficient energy to cause damage. Deprived of the sharp interface boundaries, the layered structure may prove to have no significant effect on the stress waves.

2.3.4 PVD coating design summary for WDE

The purpose of this chapter was to link existing mechanical/acoustical knowledge of water droplet erosion and the requirements on how to construct a protective coating to resist it. Emphasis has been given to the influence of the coating properties i.e. hardness; elastic modulus; density; Poisson's ratio in the ability to counteract different damage phenomena; extremely high contact pressure; stress wave propagation; lateral jetting of a collapsing droplet and excessive heating that occurs in high-speed water droplet erosion. These multiple factors make the design of the coating challenging. Despite the efforts that have been put into this field, no one has solved the practical problem of water droplet erosion.

There may be no single 'optimal' coating architecture that can satisfy all requirements for different types of erosion i.e. solid particle, liquid droplet, or cavitation (gas bubble) erosion. Contradictions exist within the different models proposed. Furthermore, the overarching lack of scientific justification by experimental validation calls into question the relevance of any of these models. Nonetheless, it is safe to say that, for solid particle erosion applications, the requirements might not be as challenging as water droplet erosion applications since impact impulse duration is in the order of tens to hundreds of microseconds (i.e. 3 to 4 orders of magnitude longer than in WDE).

In terms of the deformation failure mode being brittle or ductile, a ductile deformation failure mode (with high energy absorption capability) would be desirable. However, even the toughest (ductile) material may deform in a brittle manner in WDE applications [86]. This is because normally the plasticity characteristic of (in particular) crystalline materials is governed by the time-dependent deformation mechanism of dislocation glide through their available (and

active) slip systems. Thus when there is insufficient time to move dislocations/defects, these will act as stress concentrators and cracks would be initiated.

Materials' with predominantly time-independent deformation mechanisms, by means of twinning, giant faults (shear bands) and/or martensitic (diffusionless) phase transformations, may be most desirable. Projections can be made that such materials might still exhibit some measure of ductile deformation behaviour in such extreme high strain-rate conditions as WDE applications.

No literature has been found in terms of bridging the mechanical and acoustical aspects in designing coatings to resist water droplet erosion. The only agreement that could be made in the mechanical and acoustical aspect is the necessity to have a material with a high Poisson's ratio, since this gives better capability to distribute the acoustic stress waves and/or mechanical impact stresses/strains laterally. However, in practice, there is a relatively small deviation in the Poisson's ratio within individual material categories (i.e. metals, ceramics or polymers).

Both mechanical and acoustical aspects will play a vital role in the determination of coating performance. However, the 'gut' feeling is that acoustical aspects will play a more important role in coatings for water droplet erosion, whereas mechanical aspects will play a more important role in solid particle erosion. This is primarily due to differences in the impulse duration between solid particle and liquid droplet impact, being microseconds and nanoseconds respectively. Longer impulse duration in solid particle impact allows the stress waves to be attenuated in the impinging particles; therefore, the effect of stress waves may be diminished. There are links between the mechanical and acoustical models with the materials' properties

(primarily the elastic modulus), which can be applied in the design of monolithic and multilayer coating systems.

If one elects to design a monolithic coating system, there is a distinct divide in the approach taken to designing a coating, when taking either the route of mechanical or of acoustical aspects (summarised in table. 2.4). In my perspective, monolithic coatings do not offer versatility in control of the acoustic properties, where focus on optimisation of acoustical considerations will totally compromise the mechanical consideration and vice versa. As a result, the need to satisfy basic mechanical aspects will likely outweigh the acoustical aspects in the design of a monolithic coating system. The key in the monolithic coating may be to select a material with as high an H/E ratio (High hardness, low elastic modulus as possible); this is where the material would be resilient (long elastic region to failure) and hence, being compliant (when E is lowered and/or matched to the substrate), will enhance the toughness to assist in distribution of the impact stresses/strains over as larger a volume as possible. Electing to use a high H/E material of the correct elastic modulus will optimise the interfacial toughness, where commonly large mismatch in elastic modulus between the coating and substrate stimulates premature failure (through different preferred bending deflections under loading).

The only means to take to account of both mechanical and acoustical aspects in monolithic coatings seems to lie in developing functionally-graded coatings. Selected material properties such as elastic modulus might be modulated/graded throughout the coating thickness, where a coating could exhibit much higher elastic modulus near the surface compared to the coating/substrate interface. This would satisfy the mechanical aspects in terms of interfacial adhesion and satisfy the acoustical aspects in terms of improved attenuation of the stress waves

(as effectively stress waves will be passing thorough regions of continuously varying acoustic impedance).

Electing to employ a multilayer coating system (summarised in table. 2.5) might be a superior approach in satisfying both the mechanical and acoustical aspects, due to overlapping of beneficial effects when certain types of multilayer design architecture/characteristic are implemented.

Having layers with large elastic modulus mismatch between them will prohibit dislocation movement from one layer to another. The combination of high elastic modulus (usually resilience) and compliance (usually tough) could amalgamate the resilience and toughness of the specific layers. Combining resilience and toughness is desirable in the material, making it superior in resisting both elastic and plastic deformations in WDE. Layers with large elastic modulus mismatch would also be likely to have a large mismatch in acoustic impedance. This will help to shield the substrate from the impacting stresses/strains, since large mismatch in acoustic impedance between the layers will stimulate a higher proportion of the stress wave energy to be reflected (at the layer interface boundary), therefore energy will likely be dissipated towards the top few layers of the coating.

In regard to the thickness of the layers, there is a divided consensus between the mechanical and acoustical aspects in the choosing of an ideal layer thickness. The mechanical aspect points to nanometre layers; this is because of the inhibition in the multiplication of Frank-Read dislocation sources. However, the ductile interlayers should not be so thin that they restrict dislocation motion or pile up of dislocations at the layer boundary, thus stiffening the layer. This complies with the argument that minimum layer thickness should be of a micrometric (>0.5μm)

order, to provide the coating with a laminar structure to accommodate interactions with propagating stress waves in the structure.

Building a multilayer coating with a large number of layers will create more layer interfaces as a site for cracks to be deflected/bifurcated. Furthermore, layer interfaces may open/delaminate to reduce stress concentrations. An enhancement in the attenuation of stress waves is also likely to be achieved, as they are forced to propagate through more layers of different acoustic impedance.

Definitive conclusions cannot be made from the above discussions as to whether the ideal coating would be monolithic or multi-layered for a WDE application. Conversely, monolithic coatings may perform as well as a multilayer coating with the "right" architecture/design considerations (and vice versa). In consideration to mechanical/acoustical aspects, the experimental coating deposition and test validation thesis in this project will attempt to and test coating features and architectural designs which will in theory will be beneficial for resisting WDE.

Table. 2.4 Summary of the monolithic coating materials properties desirable for WDE resistance considerations and the effects of the mechanical and acoustic modelling criteria

Monolithic coating materials properties / other considerations	**Beneficial effect for mechanical model**	**Beneficial effect for acoustic model**
High elastic modulus	Shields substrate from impact strains (but is susceptible to brittle fracture) [87]	Supports stress waves "load spreading" aspect by the means of higher acoustic wave velocity [7]
Low elastic modulus	Allows impact strains to be distributed over a larger volume (reduces maximum impact stress) [88] and minimise the elastic modulus mismatch between the coating and substrate (better interfacial adhesion under loading) [51, 56]	N/A
High H/E ratio	Provide resilience (long elastic strain to failure) and toughness[47]	N/A
Low density	N/A	Supports stress wave "load spreading" aspect by increasing the acoustic speed of the stress waves in solid [7]
High Poisson's ratio	Helps to laterally distribute the stresses/strains laterally	Helps to laterally distribute the stress waves
Functionally grading or modulate layers with increasing elastic modulus towards the coating/substrate interface	Helps to minimise the tensile stresses experience by the substrate [79]	Assist in attenuation of the stress waves as it propagates through effective region in difference in acoustic impedance [85]

Table. 2.5 Summary of the multilayer coatings materials properties desirable for WDE resistance considerations and the effects of the mechanical and acoustical modelling criteria

Multi-layered materials properties / other considerations	**Beneficial effect for mechanical model**	**Beneficial effect for acoustic model**
High mismatch in elastic modulus between the layers (high mismatch in acoustic impedance)	Limits the dislocation movement from one layer to another [66] and to combine the properties of high 'resilience' and 'toughness' [61]	Reject proportion of the incoming impact energy toward the top few layers by stress wave reflection at the layer interface boundary [7]
Low mismatch in elastic modulus between layers (low mismatch in acoustic impedance)	To match the bending deflections of each layers (better interfacial adhesion) [51, 56]	N/A
Thin layers (nanometres)	Frank-Read dislocation source cannot operate [66]	N/A
Thick layers (>micrometres)	Provide better shielding of impact stresses to the substrate	To provide the coating with a laminar structure to accommodate interactions with propagating stress wave in the structure.
Larger Number of layers	Many layer interfaces sites for crack to be deflected and can opening up or delaminate to reduce stress concentration[62]	Assist in attenuation of the stress waves by propagating through different media [85]

2.3.5 Material selection rule for multilayer coatings to resist WDE

As stated previously, I strongly believe the best way to construct a multilayer system is through interlayering of a stiff (hard) material with a (compliant) ductile, soft material. The only cost-effective way to do this is probably via a layered ceramic-metal route. The ideal material properties for the hard and soft layers are shown in table.2.6, however, real-life material may not exhibit all these properties. The rule in choosing the materials for the hard/stiff or ductile/compliant layers must be in conjecture with the desired properties as discussed previously, to satisfy the combined mechanical and acoustical considerations.

Table 2.6 the ideal material properties for a multilayer system

Hard layer	ductile interlayer
• High Hardness • As low an Elastic Modulus as possible • Low Density • High Poisson's ratio • As high an Acoustic Impedance as possible	• Very low Elastic modulus, if possible • High Density • High Poisson's ratio • As low an Acoustic Impedance as possible

It should be borne in mind that, generally, low elastic modulus material will in turn exhibit low acoustic impedance; in order to raise the parameter of acoustic impedance, the material must therefore also exhibit low density. Thus the ideal material properties for the hard/stiff layer, must exhibit the combination of relatively high hardness, as low elastic

modulus as possible, whilst choosing also a low density, to not drop the material's acoustic impedance too much. Moreover, this propertiy combination will increase the H/E ratio which justifies the means to increase the elastic strain to failure and also have enough strength to resist crack initiation.

Fundamentally, I think that choosing materials for the soft layer maybe more or equally as important to the hard layer. In my opinion, the two material parameters that are most important in selecting the soft interlayering materials are elastic modulus and density. Very low elastic modulus and high density is desirable (however, most high density and low elastic modulus metals tends to be toxic; e.g. Lead, Tin), since very low elastic modulus can plastically yield (without cracking) under impacting deformation and reduces the maximum bending stress experienced by the hard, (and usually more stiff) layers; this will enhance the degree of toughness in the coating system.

Coupling the two ideal materials of hard layer and soft interlayer will create a multilayer which would be superior in satisfying both mechanical and acoustical considerations. Layers would have high acoustic impedance mismatch, to attenuate the compressive stress waves. Furthermore, this multilayer architecture complies with Koehler's argument of coupling layers with different shear modulus (which is related directly to elastic modulus by Poisson's ratio) to stop dislocations from driving across one layer to another. High Poisson's ratio is desired in both hard and soft layers; this is due to the fact that high Poisson's ratio material subjected to normal particle/water droplet impact will have a better capability to distribute laterally the induced impact strain.

Chapter 3 Experimental Procedure

3.1 Coating analysis techniques

3.1.1 X-ray diffraction (XRD) analysis

X-ray diffraction measurements of all PVD coating samples deposited in this work were performed using a Siemens D5000 diffractometer equipped with a Cu-Kα source (λ=0.1541nm). For thin film coatings, θ-θ (glancing angle) mode is preferred to conventional θ-2θ. This is primarily to avoid the substrate diffraction peak intensity dominating the diffraction pattern, making it easier to distinguish the thin film coating diffraction peaks. The θ-θ (glancing angle) mode uses a small incident angle, where the beam penetration depth will be low (to eliminate substrate diffraction patterns).

3.1.2 Optical Microscopy (OM)

A "Nikon Eclipse LV150" optical microscope was used to examine the surface wear of samples subjected to ball-on-plate impact testing or water droplet erosion. Magnification of 10x to 1000x were possible. However, the optical micrographs produced in this thesis were in the magnification range of 10x to 50x.

3.1.3 Stylus Profilometry

A "Veeco Dektak 150" stylus profilometer, as shown in Figure 3.1, was used to identify the surface profile of the wear crater volume after impact testing. The profilometer uses a 12.5 μm radius diamond stylus and moves laterally across the surface; for maximum accuracy the stylus needs to be set to move straight through the middle of the wear crater. The profilometer can map the shape, depth and roughness of the wear crater.

Nonetheless, there are limitations and errors which could occur in the profilometer. The errors could arise from the human judgment of where to place the stylus tip in order for it to move through the centre of the wear crater. Deviation of the scan line from the centre of the wear crater decreases the width and depth value obtained compared to the actual value. This would then result in the miscalculation of the crater wear volume. Moreover, the method used for calculating the crater wear volume uses assumes that the crater is hemi-spherical in shape. However, some craters shapes are asymmetrical. Taking these facts in to account, the calculation of the impact wear volume may be somewhat inaccurate.

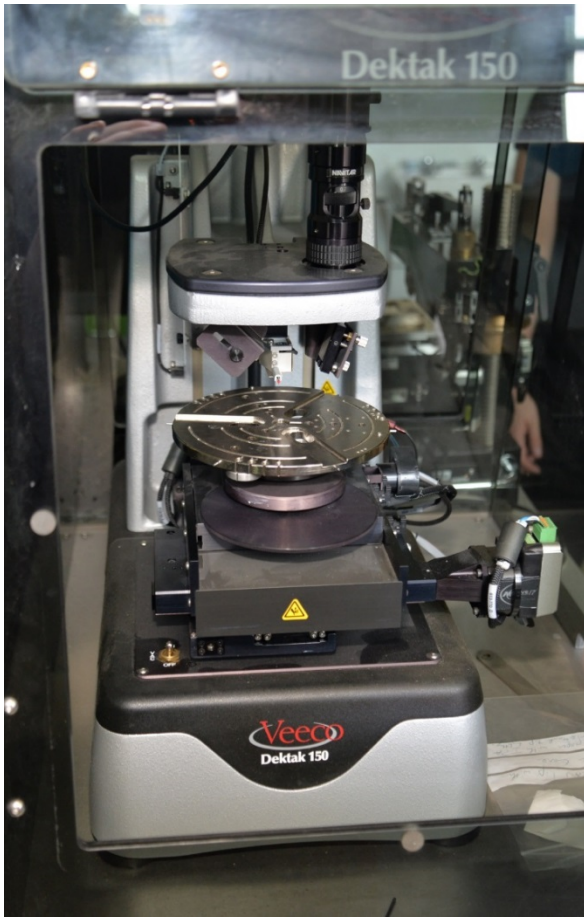

Figure. 3.1 ‘’Veeco Dektak 150’’profilometer

3.1.4 Scanning electron microscopy (SEM) and Energy Dispersive X-ray (EDX) analysis

This research utilised a Philips XL-30s field emission gun scanning electron microscope (FEG-SEM) to image various parts of the coating such as the thickness in cross-section and damaged surface morphology.

Quantitative Energy Dispersive X-ray (EDX) analyses was also performed by using the XL-30s FEG-SEM equipped with an Oxford Instruments EDX detector. To obtain accurate EDX analysis results of each elemental concentration present in the coatings, a cobalt sample of 99.99% purity was used as a source of calibration.

3.1.5 Nano indentation

A Hysitron Triboscope Nano-indenter was used to examine the coating hardness (H) and elastic modulus (E). To ensure the results are indisputable and reliable, 16 indentations were applied; this enables the extraction of average values of both H and E for each coating. The indentation load was chosen in conjunction with the Oliver and Pharr [89] rule which suggested that the maximum indentation depth should not exceed 1/10 of the coating thickness or substrate effect will occur.

3.1.6 Transmission Electron Microscopy (TEM) and Focussed Ion Beam (FIB)

` The Cross-sectional TEM analysis presented in this thesis was carried out using two pieces of equipment; a Philips EM420 (using a tungsten filament) and FEI Tecnai T20 (using a LaB_6 filament). The equipment was able to obtain bright field (BF) and, Dark Field (DF) images, with their corresponding Selected Area Electron Diffraction (SAED) patterns. Detailed sample preparation was needed before the TEM analysis could be performed. Selected samples were prepared using an FEI Quanta 200 3D SEM equipped with gallium Focused Ion Beam (FIB) to extract thin-foil samples for TEM analysis. These thin-foil samples in the dimension of 10μm x 4μm x 1 μm were obtained directly from the surface of

the coated sample. The foils were then lifted out of the sample, attached to a copper grid, and then subjected to ion milling, using the gallium focussed ion beam (FIB), to obtain a final thickness of less than 50nm.

The cross-sectional FIB analysis presented in this thesis was also carried out using the FEI Quanta 200 3D SEM equipped with gallium focused Ion Beam (FIB). In this method, a section of the sample from the surface is then removed or milled away using the FIB, to form a trench. The sample is then titled 45° where the resulting cross-section (trench) is imaged using the electron beam.

3.1.7 Ball-on-Plate Impact Testing

The impact test machine is designed to model the wear and fatigue of a material subjected to a high local compressive stress at its surface. Other well-known wear test methods such as pin-on-disc, scratch adhesion or abrasive wheel test do not satisfy the condition of repetitive static impact. Since the impact tester creates an impulsive strain on the surface of the material, it mimics the environment in which the thin hard-coated films are exposed for erosion and fatigue.

Knotek [90] first introduced the impact tester in 1992. The most common type of impact testing is a ball-on-plate machine. The machine uses a high hardness/elastic modulus indenter ball, normally tungsten carbide. The ball oscillates up-and-down, striking the coating/substrate at a constant force. The machine (shown in Figure.3.2) uses compressed air as a force for oscillation. To ensure that the impact force and frequency is constant a piezo-force transducer is inserted. The frequency of the impact is fixed at ~ 8Hertz.

Several different wear/failure mechanisms can be assessed depending on the loading conditions used. To assess the toughness and adhesion of the coating and substrate, low impact cycles and high loading are desired. This is due to the mode of deformation that

would be in the plastic region. However, to assess fatigue of the coating-substrate system, high impact cycles and low loading are preferred, this is to ensure the primary mode of deformation would be elastic.

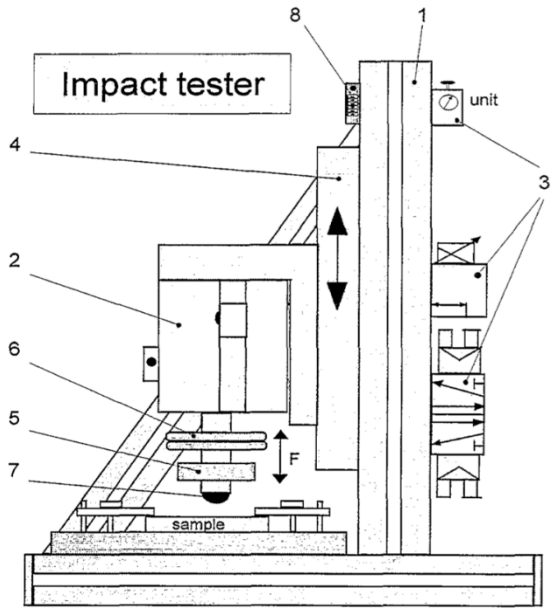

Figure. 3.2 Schematic of impact tester (1,aluminium frame with slots; 2,pneumatic cylinder with proximity switches; 3,pneumatic components-service unit, pressure regulation valve, solenoid valve; 4,slider vice for piston; 5,force transducer; 6,additional weights; 7,test ball; 8,impact counter) [91]

3.1.8.1 Hertzian Contact Stress

In 1882, Hertz [88] introduced a contact theory between a sphere and elastic half-space in contact with each other (shown in Figure.3.3), in order to predict the maximum stress induced. His understanding of the term hardness was that it is the contact pressure needed to initiate plastic yielding in a solid.

The assumptions of the contact theory are as follows:

- Both contacting surface are smooth and frictionless
- The size of the contact area is negligible compared to the spherical object radius
- The strain is small and is within the elastic limits of the contacting materials

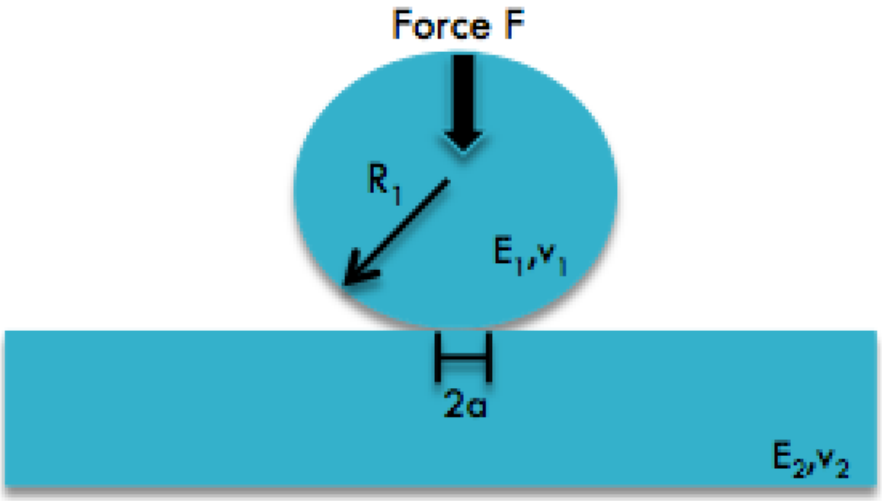

Figure. 3.3 Schematic of a sphere in contact with an elastic half-space

Summary of the parameters deduced from the Hertzian contact theory are shown in Table. 3.1 (Note that for a sphere contact with an elastic half-space, R_2 approaches ∞)

Table. 3.1 Summary of the parameters deduced from the Hertzian contact theory

Parameters	Contact area radius, a Applied Force, F Elastic modulus, $E_1 E_2$ Poisson's ratio, $v_1 v_2$ Contact radii, $R_1 R_2$
Contact area radius	$a = \sqrt[3]{\frac{3FR}{4E^*}}$
Relative radius of curvature, R	$\frac{1}{R} = \frac{1}{R_1} + \frac{1}{R_2}$
Reduced modulus, E^*	$\frac{1}{E^*} = \frac{1 - v_1^2}{E_1} + \frac{1 - v_2^2}{E_2}$
Maximum pressure, p_0	$p_0 = \frac{3F}{2\pi a}$
Mean pressure, p_m	$p_m = \frac{2p_0}{3}$

For simple static Hertzian (elastic) loading (shown in Figure. 3.4), a higher elastic modulus material would have a more confined stress field area than a lower modulus material. This in turn means that, for an impacting sphere with the same energy, higher elastic modulus material would experience a higher maximum pressure. The initial point where yielding starts is known to be sub-surface (where shear stresses are at a maximum).

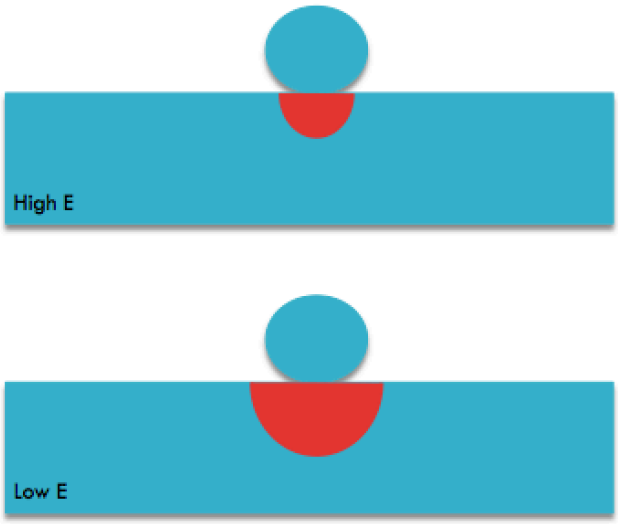

Figure. 3.4. Schematic diagram of Hertzian contact stress field of materials with different elastic moduli

3.1.7.2 Validity of using an Impact test as a substitute for Water Droplet Erosion testing

Due to the absence of Water Droplet Erosion equipment in the laboratory, an alternative coating evaluation technique was needed to create similar wear mechanisms. The Impact testing machine seems to provide similar conditions of low cycle fatigue, which is associated with water droplet impact.

The material properties of titanium and titanium nitride, used in the Hertzian contact stress calculations, are shown in Table. 3.2. It is interesting to compare whether the pressure generated in single water droplet impact is comparable with the contact stress in the impact-testing machine. The Hertzian contact pressure generated in these coating materials from the impact testing machine using a 6mm diameter spherical tungsten carbide ball at loads of between 100 and 400N) are shown in Tables 3.3 and 3.4. A calculation of the water hammer pressure is shown in Table. 3.5, based on assumptions that the density and velocity of the wave in the liquid droplet are 1000kg/m^3 and 1468 ms^{-1} respectively.

Table. 3.2 Elastic Modulus of the Ball and coating (TiN or Ti) properties

	Tungsten carbide ball (WC)	**Titanium (Ti)**	**Titanium nitride (TiN)**
Elastic modulus (GPa)	600	115	400

Table. 3.3 Hertzian contact stresses for a 6mm Tungsten carbide ball onto a titanium metallic coating for various loading force

Force (N)	**Max Hertzian contact pressure (GPa)**	**Mean Hertzian contact pressure (GPa)**
100	3.31	2.21
150	3.79	2.53
200	4.17	2.78
250	4.50	3.00
300	4.78	3.18
350	5.03	3.35
400	5.26	3.51

Table. 3.4 Hertzian contact stresses for a 6mm Tungsten carbide ball onto a titanium nitride ceramic coating for various loading force

Force (N)	**Maximum Hertzian contact pressure (GPa)**	**Mean Hertzian contact pressure (GPa)**
100	5.84	3.89
150	6.68	4.46
200	7.36	4.90
250	7.92	5.28
300	8.42	5.61
350	8.87	5.91
400	9.27	6.18

Table. 3.5 Water hammer pressure and Maximum (edge) pressure of a water droplet impact onto a surface

Impact velocity (ms^{-1})	**Water Hammer Pressure (GPa)**	**Maximum (edge) water hammer pressure generated (GPa)**
100	0.1484	0.45
150	0.2226	0.68
200	0.2968	0.90
250	0.371	1.13
300	0.4452	1.35
350	0.5194	1.58
400	0.5936	1.80
450	0.6678	2.03
500	0.742	2.25

From the calculation, the estimated Hertzian contact pressure and the maximum (edge) water hammer pressure are comparable (i.e. in the same order of magnitude). However, the (maximum or mean) Hertzian contact pressure in the impact at even the lowest possible load seems to be higher than the water hammer pressure (for the estimated impact velocity range). Therefore, the applied force selected for impact testing was not more than 150N, in order to have a comparable induced pressure with water droplet impact in the supersonic velocity range. But note that of course, the 'real' contact pressure in the ball-on-plate test will drop to just below the yield strength of the substrate (as the crater enlarges initially through plastic yielding).

The failure mechanism and the strain rate induced may be completely different. The reason primarily being the major difference between the duration of the impact impulse, for Water Droplet Erosion (WDE) being in the order of nanoseconds [92] and Solid Particle erosion (SPE) in the order of microseconds [12]. As a result, materials experiencing WDE will suffer immensely higher strain-rate compared to SPE. Moreover, the lateral jetting (known to put the surface under high transient tensile stresses and creating another mode of failure) in water droplet erosion cannot be recreated by other impact testing equipment.

In conclusion, the validity of ball-on-plate impact testing is questionable to mimic the materials response under WDE. That the material under impact testing will experience different strain rates (plus the absence of lateral jetting) suggests that the material response would be completely different. The only thing the impact testing might be adequate to simulate is the pressure induced and the repetitive impact aspects for fatigue analysis.

3.1.8 Water Droplet Erosion (WDE) Testing

The Water Droplet Erosion testing in this PhD study was carried out by the National Physical Laboratory (NPL). The WDE rig contains a rotor which is 1m in diameter (0.5 m in radius) at the centre of the chamber. Two samples can be placed on the rotor during each test. Before testing commences, the chamber must be evacuate air (vacuum).. A 100 μm nozzle is used as a water inlet and the estimated water droplet size of 300μm, however further verification is needed with a high-speed camera. The speed of the water droplet impact is approximated to around 300m/s. The mass loss is determined by stopping the test at pre-determined intervals, removing the samples and measuring the weight using a precision mass balance (The accuracy of the mass balance is to 5 significant figures + or – 0.00001g).

3.2 Deposition rig

All coatings were deposited using a TECVAC IP-70 coating deposition system (shown in Figure.3.5). The TECVAC IP-70 is an electron-beam PVD based coating deposition machine; it has the capability of performing both thermionic triode evaporative ion plating and magnetron sputtering. However, this project only employs the triode evaporative ion-plating technique. This system utilises a focused high-power electron beam to melt and vaporise the solid target material (metals or ceramics)

The frame of the chamber is constructed using thick stainless steel plates. The chamber is divided into two sections; working chamber and plenum chamber, where the total dimension of the chamber is 70cm x 70cm x 70cm (total volume 0.343 m^3). All external chamber faces are embedded with water-cooling pipes. Also fitted with a viewing port, in order to see inside the working chamber under coating deposition, viewing ports are built-in at the right hand side of the chamber and on the chamber door.

A rotatable workpiece is suspended vertically at the centre of the working chamber, it is connected to a 15kW power supply with a pulsed bias capability; minus 0-800 Volts can be set accordingly. The electron gun, mounted in the plenum chamber, comprised of tungsten filament coil as an electron source, can be negatively biased up to 10kV. The electron beam is then deflected to the target crucible by 270 degrees via a solenoid coil electromagnet. The crucible is made from copper pipe and is water-cooled. The crucible can be positively biased up to 100V. An additional electrode as a source of thermionic electron-emission is also fitted near the crucibles of the deposition chamber. To measure the deposition temperature and the substrate temperature, two K type (nickel-chromium) thermocouples are fitted, where typical range of temperature detectable is -270 to +1260 ^oC.

Figure. 3.5 TECVAC IP-70 Twin electron beam deposition system

3.3 Preliminary Investigation of the deposition techniques for titanium based coatings

3.3.1 Electron-beam system and titanium metal slug preparation

To evaporate the titanium metal, the coating deposition chamber is fitted with an electron-beam evaporation system with water cooled copper crucibles. The electron-beam system is connected to a power supply that allows the voltage and current to be independently adjusted. Adjusting the voltage will affect the energy of the electrons while adjusting the current will affect the number of electrons emitted. The optimum voltage was found to be in the range of 5-8kV (The electron-beam voltage will be kept constant at 6.5kV in this project) and the optimum current was found to be in the range of 200-500 mA. Below 200 mA, it was established that there is insufficient power to melt the titanium metal.

Before every deposition run, an additional stage must be implemented to optimise the beam spot to cover the whole surface of the titanium slug. The surface of the titanium must be melted to form a dome-shaped evaporant slug. The current used was 600-700 mA and the melt time was for roughly 1-2 minutes. This stage also ensures that the surface of the titanium melt is free of (oxide) contamination.

3.3.2 Workpiece bias

The workpiece negative bias in a triode ion-plating system can be set to much lower values than those of diode-ion plating, due to the effect of having an additional electron emission source. It has been stated that a high workpiece current density is more important for producing high quality (dense) columnar structure coatings for a triode ion-plating system. This is because most of the particles striking the workpiece are high energy ions rather than energetic neutrals (since L/λ is small) [93].

From trial findings, once the workpiece current approaches 5.0 A at a set workpiece negative bias of 50 V, little or no coating is deposited onto the substrate. This may be due to the fact that the rate of sputtering (and re-sputtering) is too high, atoms that are deposited onto the surface of the substrate is simultaneously re-sputtered out. The optimum workpiece current found tends to be around 3-3.5 A.

3.3.3 Optical emission spectroscopy (OES) system

Optical emission spectroscopy is an established method to qualitatively measure the elemental composition in plasma assisted deposition systems, where the target material is ionised (electron get ejected). They emit characteristic light at wavelengths in the visible spectrum due to the distinct energy bands. For titanium evaporation, a blue light is observed and it was found that 521nm wavelength has the highest intensity.

The usefulness of the OES system is to assist in the repeatability of coating deposition. If all the deposition parameters are kept the same (i.e. gas pressure, substrate bias, filament bias, filament power, crucible bias), the system can be used to monitor the change in the rate of titanium evaporation (due to the effect of burrowing) and consequently the electron-gun beam power can be adjusted to correspond with the intensity of the peak.

3.3.4 Crucible bias

The benefit of the TECVAC-IP 70 is that the crucible (which the titanium slug is placed inside) can be positively biased. Without the crucible bias, the plasma generated will be concentrated above the vapour source. The introduction of a positive bias on the crucible will have an effect by which the workpiece plasma potential is raised to more negative values and will also assist with the uniformity of the coating throughout the deposition chamber, by increasing secondary electron emission from the chamber walls [46]. Initial investigation

suggests that a positively bias of 25-30V is sufficient to float the plasma potential to be more uniformly distributed throughout the chamber volume.

3.3.5 Target-substrate distance

The distance between the evaporated material and substrate is important in determining the thickness of the coating. Placing the substrate too far from the evaporant source may decrease the deposition rate dramatically. Yet placing the substrate in too close a proximity to the evaporant source will make it difficult to deposit stoichiometric titanium nitride on the substrate, considering the fact that there would be an excessive amount of ionized/neutral titanium ions compared to ionised/neutral nitrogen ions (where nitrogen needs to react with titanium to produce titanium nitride).

Investigations of the effect of target-substrate distance on the thickness were performed, where the M2 Steel substrates were placed 25cm and 35cm from the titanium target. Pure titanium was evaporated with the parameters shown in Table.3.6.

Table. 3.6 Preliminary deposition parameters

Target material	Titanium
Argon gas flow	50 ml/min
Initial substrate temperature	~200^{o}C
Final substrate temperature	~350^{o}C
Workpiece negative Bias	50 V
Crucible Positive Bias	30 V
Filament Negative Bias	100 V
Filament Current	75 A
Deposition Time	30 Minutes
Electron Gun Acceleration Voltage	6.5 kV
Electron Gun Current	450-500 mA

It was found that, for a 25cm target-substrate distance, titanium coatings deposited with a thickness of ~3μm for a deposition time of 30 minutes. However, for a 35cm target-substrate distance, only ~0.3μm thick titanium coatings were found. With just 10cm apart in target-substrate distance, it seems that the deposition rate scales off exponentially from the evaporant material. Therefore, throughout this project the target-substrate distance used will be kept constant at 25cm.

3.3.6 Variability Problems

The challenge in triode-ion plating lies in obtaining optimal properties in every run. The coatings properties which can vary are the thickness, composition/phase, preferred orientation, morphology and structure.

One of the problems found was associated with the titanium melt. The TECVAC IP70 coating unit has an oval electron beam 'footprint' (impingement area). At the start of the deposition run, the impingement area covers the whole surface of the melt. However, problems arise when the deposition run is extended for 90+ minutes. The melt beam impingement area starts to concentrate towards the middle of the melt and a 'burrowing' effect (shown in Figure.3.6) starts to occur. This narrows the target vapour flux; changing the whole plasma composition, density and energy. Consequently, the deposition run needs to be terminated. The solution to this problem is to use an electron gun equipped with a sweep mode, where the electron beam spot can be swept across the whole melt surface. The sweep mode for the electron gun has been established in the TECVAC IP-70 unit, where it has found to delay the onset of the 'burrowing' effect by approximately 60 minutes more.

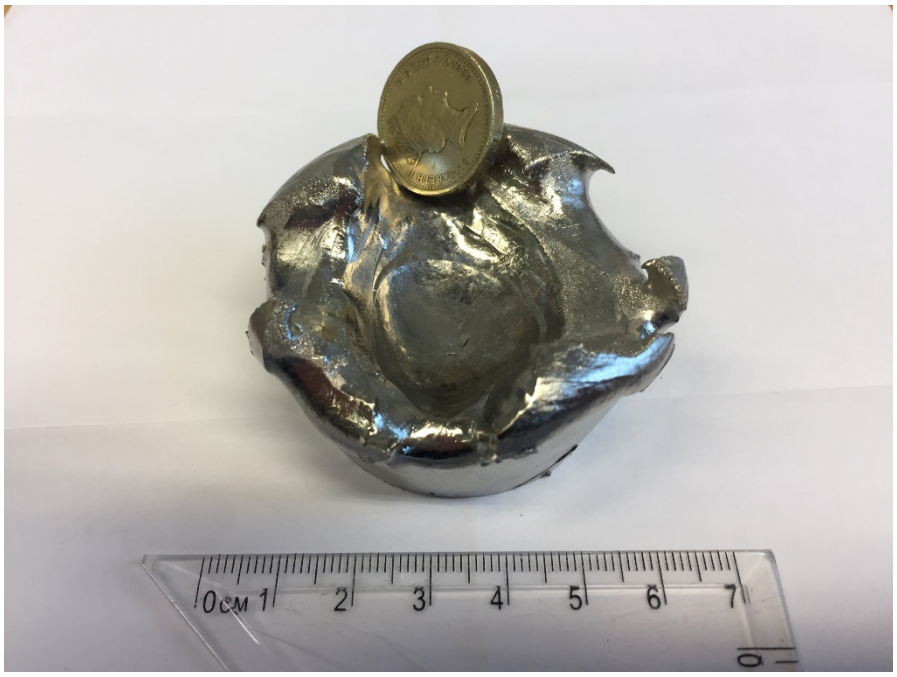

Figure. 3.6 Melt ‘burrowing’ effect of the titanium slug after 10+ deposition runs

Furthermore, regarding the introduction of nitrogen to the deposition chamber, it was found that the gas control system tends to send a spike of nitrogen into the chamber once it has been initially switched on, but falls rapidly to the set nitrogen gas flow rate. This is believed to be detrimental to the coating composition/adhesion. This ‘spike’ of nitrogen is likely to create hyper-stoichiometric TiN, which is extremely brittle. The sharp interface of the soft titanium and hyper-stoichiometric TiN is likely to cause delamination. The solution to this problem was to open the nitrogen gas flow value for 1-2 minutes before starting the coating deposition.

Likewise, controlling the deposition rate is a challenge; the rate is likely to be governed by the workpiece current (or current density). However, as you progress through a coating deposition cycle, normally the workpiece current increases even though all the parameters are fixed i.e. electron-beam system voltage/current, filament voltage/current and workpiece bias. An explanation for the increase in workpiece current may be the narrowing

of the target vapour flux (from the burrowing effect). Furthermore, the tungsten filament (additional electron source) could be the source of the gradual increase in workpiece current. This is due to the sputtering and thinning of the tungsten filament, where the grains boundaries of the tungsten filament would likely to open up with time, which produced a more faceted surface. This is likely to increase the proportion of the electrons emitted at a constant power.

3.3.7 Titanium Niobium deposition trials

The most commonly used titanium interlayer is the alpha (α) phase, which has a hexagonal closed packed (HCP) structure. However, Beta (β) titanium exhibits a body-centred cubic (BCC) structure that is more desirable due to its higher ductility (more available slip systems). β-Ti would be a more suitable candidate as an interlayer material for erosion-resistant multilayer coatings since the β-Ti phase is more likely to fail by "ductile tearing" than α-titanium under high strain-rate impact loading circumstances.

In regards to mechanical properties, β-Ti would provide a lower elastic modulus and relatively similar hardness to α-Ti. Thus, it would exhibit a higher H/E ratio than α-Ti phase, making it more resilient. An interlayer that exhibits lower elastic modulus would be expected to show superior performance in the accommodation of impact loading stresses.

Nevertheless, in practice due to the nature of titanium, it is impossible to develop the β-Ti phase at ambient temperature without adding β-stabilising elements. This sparked an interest of incorporating niobium into the titanium interlayer. Attempts were made to therefore evaporate niobium granules by the use of electron beam melting. Even though, I managed to melt niobium, no traces of niobium (via EDX technique) were found to be deposited on the substrate.

Another approach was an attempt to mix titanium and niobium granules together. Similarly, no traces of niobium were found on the substrate. The reason for this might be due to niobium having a low vapour pressure at melting temperature suitable for titanium. The textbook values of vapour pressure at different temperatures for titanium and niobium are shown in Table. 3.7. Surprisingly, at a temperature of 2600-2800 ^{o}C, the vapour pressure of titanium is 3 to 4 orders of magnitude higher than niobium. This means at this melting temperature (if the titanium and niobium are melted simultaneously), there would be 3 to 4 magnitude more (vaporised) titanium atoms than niobium atoms.

Table. 3.7 Vapour pressure of a) titanium and b) niobium at different temperatures [28]

a)

Temperature (^{o}C)	Vapour pressure (Pa)
1709	1
1898	10
2130	100
2419	1000
2791	10000
3285	100000

b)

Temperature (^{o}C)	Vapour pressure (Pa)
2669	1
2934	10
3251	100
3637	1000
4120	10000
4740	100000

3.4 Coating Deposition

3.4.1 Introduction

There have been various literature reviews on the effect of Nitrogen flow rate on the properties of titanium-based PVD coatings, with the amount of nitrogen concentration in the coating determining the phase composition and mechanical properties. The Ti-N binary equilibrium phase diagram (shown in Figure. 3.7) can reveal the relative concentration of nitrogen needed to give the desired phases, Ti, Ti_2N, TiN, being a single or a mixture of phases.

The concept of doping nitrogen into a metallic coating structure, as a means to improve the H/E ratio (increases in Hardness, but Elastic modulus stays comparatively the same), has been investigated for chromium. Rebholz et.al [94] found that up to 15at% of nitrogen can be saturated into the bcc-chromium structure, at a low deposition temperature of ~250^{o}C, under non-equilibrium conditions. Whereas in equilibrium conditions (according to the Cr-N binary phase diagram, only up to ~4.36 at% of Nitrogen, at ~1600^{o}C (and insignificant amounts at temperatures below 1000^{o}C), can be saturated into the chromium structure before ceramic phases start to form.

However, this concept has not until now been investigated for titanium. Therefore, I decided to try and explore on this matter using the triode ion-plating process. The highly non-equilibrium conditions in PVD processing arise from high-temperature of evaporated atomic species (3000-5000K) coupled with relatively low substrate temperature (450-750K), which consequently lowers the mobility of the atomic species deposited. The nitrogen concentration in structure will be mainly controlled by the reactive gas flow rate (if every other parameter used is kept constant).

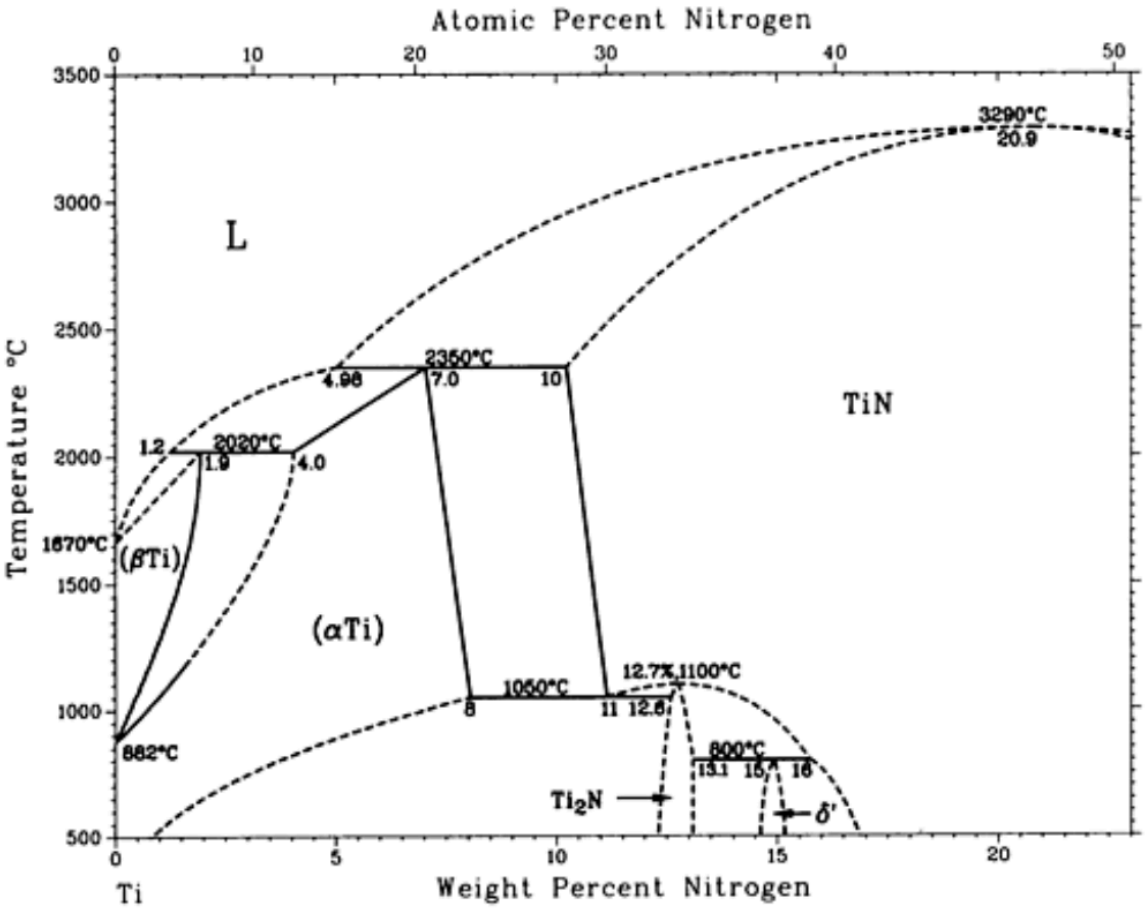

Figure. 3.7 Ti-N binary phase diagram [95]

The 'nitrogen-doped' titanium system may not be promising as the chromium system, because α-titanium has a HCP (hexagonal closed packed) structure whereas α-chromium has a BCC (body centred cubic) structure. In terms of the number of interstitial sites where nitrogen atoms can be positioned, a BCC structure has more available empty sites than a HCP structure. Hence, predictions can be made that the limit of concentration of nitrogen that can be incorporated into the α-titanium structure may be significantly less than the 15at% possible with PVD-Cr films.

As discussed previously, thicker hard coatings (~50μm) are desirable in erosion applications. Typically, monolithic TiN hard coatings are in the range of 2-7μm. Thicker coatings (>7μm) have a tendency to spall off prematurely, due to the build-up of large

residual compressive stress in the coatings - arising from the thermal mismatch between the coating and substrate. The multilayer approach seems to be the only option available to build a thicker coating in titanium-based PVD systems – by incorporating a soft metallic interlayer (being Ti, or 'nitrogen-doped' Ti) that could accommodate the residual compressive stresses.

The coatings deposited and examined in this thesis were designed to test some of the mechanical and acoustical theories discussed in section. 2.3. The fundamental mechanical properties of the coating, monolithic or multilayer, such as hardness, elastic modulus and density will be predicted and/or examined. These mechanical properties will be used to validate and prioritise the mechanical or acoustical theories.

3.4.2 Substrate Preparation

Two types of steel substrate were used for this work, M2 molybdenum tool steel and 15/5 PH precipitation-hardened martensitic stainless steel. The M2 tool steel is round-shaped coupons with a diameter of 30mm and thickness of 3mm. The M2 steel substrates were received in highly polished condition (Ra $\leq$ 0.05µm).

15/5 PH steel substrates coupons had a complex "trapezoidal prism" shape (shown in Figure. 3.8) with dimensions of 8mm x 25mm x 21.25mm x 3mm. These substrate coupons were designed specifically to fit the complex sample holder of NPL's water droplet erosion testing machine. The chemical composition ranges of M2 tool steel and 15/5 PH steel is shown in table.3.8. The mechanical and physical properties of M2 tool steel and 15/5 PH steel is shown in table.3.9.

Table.3.8 Elemental composition range of M2 tool steel and 15/5 PH stainless steel

M2 tool steel	
Elements	Weight percent (wt%)
Iron, Fe	Balance
Chromium, Cr	3.75-4.5
Nickel, Ni	Max 0.3
Manganese, Mn	0.15-0.4
Silicon, Si	0.2-0.45
Molybdenum, Mo	4.5-5.5
Tungsten, W	5.5-6.75
Vanadium, V	1.75-2.2
Carbon, C	0.78-1.05

15/5 PH stainless steel	
Elements	Weight percent (wt%)
Iron, Fe	Balance
Chromium, Cr	14-15.5
Nickel, Ni	3.5–5.5
Copper, Cu	2.5-4.5
Manganese, Mn	Max. 1
Silicon, Si	Max. 1
Molybdenum, Mo	Max. 0.5
Niobium, Nb	0.15-0.45
Carbon, C	Max.0.07

Table.3.9 Mechanical properties of M2 tool steel and 15/5 PH stainless steel. [48]

Mechanical and physical properties	M2 Tool Steel	15/5 PH stainless steel
Hardness, Rockwell C	62-65 C	35-46 C
Elastic modulus, GPa	190-210 GPa	195-200 GPa
Poisson's ratio	0.27 – 0.30	0.27-0.30

These coupons were received as machined samples. Therefore, they were subsequently ground with SiC papers from 600 mesh until 4000 mesh. Furthermore, they were polished using a 6μm diamond suspension and 1μm diamond suspension for mirror-like surface finish (Ra ≤ 0.05μm).

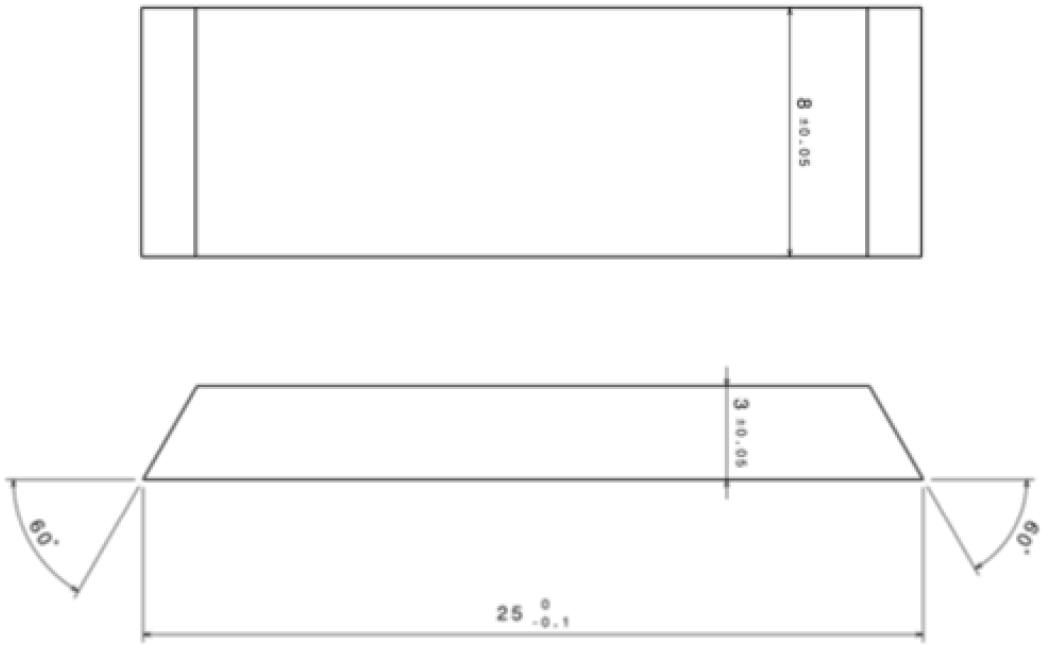

Figure. 3.8 15/5 PH steel substrate dimensions (measurements are in millimetres)

3.4.3 Deposition stages

3.4.3.1 Cleaning stage

Prior to coating deposition, all substrates were ultrasonically cleaned using acetone and isopropanol for 10 minutes each (sequentially), then immediately dried using compressed air. The substrates were held (using a bolt) in the sample holder and placed at a distance of 25cm from the source. The substrates were then radiant-heated to 250°C at a vacuum pressure of $1x10^{-5}$ mbar.

The substrates were subjected to a 10-minute sputter cleaning stage in argon at a pressure of ~$2x10^{-2}$ mbar and substrate negative bias of 800V. This was to ensure that the surface is free of any contaminants such as oxide layers or hydrocarbons, which could affect the coating/substrate adhesion. The sputter cleaning stage is followed by a 'plasma cleaning' stage. During this stage the substrate temperature is further elevated (increase atom mobility) which will aid in building up of denser structure during coating deposition [82].

3.4.3.2 Monolithic coatings

Titanium (Ti), 'nitrogen-doped' titanium (Ti(N)) and titanium nitride (TiN) monolithic coatings were investigated (as shown in Table. 3.10). The total coating thickness aimed for was approximately 6.5μm (including a pure titanium adhesive bonding layer of ~0.3μm).

Table. 3.10 Monolithic coating design architecture

Monolithic coating	Nitrogen flow rate (ml/min)
Ti	0
Ti(N)	5
Ti(N)	10
Ti(N)	15
TiN	55

All the monolithic coating depositions runs were subjected to the cleaning stage. The evaporant material used for this project consisted of a titanium slug of 99.99% purity. The standard monolithic coating deposition conditions were as follows:

- Chamber pressure (argon): 2-3x10^{-3} mbar
- Substrate Bias: -50V
- Crucible Bias: +30V
- Effective workpiece bias: -80V
- Filament bias: -100V
- Electron gun power : 6.5kVx450mA (plus or minus 50mA)
- Source-to-substrate distance : 25cm
- Deposition Time : 65 minutes

The variation to produce different composition, either Ti, Ti(N) or TiN, in each coating lies in the difference in the nitrogen gas flow rate during deposition run (presented in Table.3.4).

3.3.3.3 Multilayer coatings

Two sets of different multilayer coatings were deposited, TiN/Ti and TiN/Ti(N), with the TiN layer serving as the hard (and stiff) layer and the Ti or Ti(N) serving as the ductile (and compliant) layer. However, the Ti(N) interlayer expected to be much harder than pure Ti. The total coating thickness was held constant at approximately 10μm and the total number of layers was kept at 14 layers (i.e. 7 pairs). This included an initial bonding layer of pure Ti, which is designed to be around 0.3μm. The purpose of the bonding layer was to increase the coating adhesion to the substrate. Other than the bonding layer, individual layer thicknesses were chosen to be 0.5, 0.75 or 1μm, depending on the intended thickness ratio of hard and soft layers. The thickness ratio, defined by the ratio of the thickness of the TiN layer to the Ti or Ti(N) interlayer, would either be 1:1, 2:1, or 1:2. A summary of the multilayer coating architectures is presented in Table. 3.11

All of the multilayer deposition runs were subjected to the cleaning stages. The Multi-layered coatings deposited were over a substrate temperature range between 450 and 500°C. To control the composition of each layer, nitrogen was switched in and out at set intervals. The standard deposition conditions were the same as for the monolithic coatings (section.3.4.3.2)

Table. 3.11 Multilayer coating design architecture

Multilayer type	Total number of layers	Thickness ratio	TiN thickness (μm)	Ti/Ti(N) interlayer thickness (μm)
TiN/Ti	14	1:1	0.75	0.75
TiN/Ti	14	2:1	1.00	0.50
TiN/Ti	14	1:2	0.50	1.00
TiN/Ti(N)	14	1:1	0.75	0.75
TiN/Ti(N)	14	2:1	1.00	0.50
TiN/Ti(N)	14	1:2	0.50	1.00

Initial multilayer coating trial runs demonstrated that the Ti and TiN layers have different deposition rates – at a constant e.b. gun power, the titanium deposition rate seems to be 15-20% higher than that of TiN. This effect is not clearly understood; however, it is probably to do with the increase in the workpiece current density (once the Nitrogen is switched off) and atoms/species surface mobility. At the current parameters, the deposition rate for titanium was ~0.12μm/min and for TiN ~0.10μm/min. This meant that, to deposit a one-micron layer of titanium or titanium nitride, the required time was 8 minutes 20 seconds or 10 minutes respectively. Thus it would take roughly 2 hours to deposit a multilayer that is ~10-11μm thick, depending on the bilayer ratio, shown in table. 3.5.

Regarding the beam-footprint shape on the titanium melt, as discussed earlier, the beam-footprint seems to have an oval-shape, which covers the whole surface area of the melt. However, as the deposition time progresses, the beam-footprint contracts and is more concentrated to a smaller area. This ultimately changes the lateral evaporant flux distribution,

making it more directional to the workpiece. Once this happens, the counts on the Optical Emission Spectrometer (OES) change as well (lowering the counts). Therefore, in order to maintain the counts reading on the OES to the expected level, you would need increase the e.b. gun power or the filament current.

As the deposition run time is extended compared to a single layer, the melt-burrowing problem is more severe than production of monolithic coating layers. Additionally, the encountered problem was more severe when using melts that have been previously topped-up with titanium granules/rods many times (10 or more), and may have been contaminated by oxygen, nitrogen, tungsten and other impurities found in the chamber.

Chapter 4 PVD Monolithic and Multilayer Coating Characterization

4.1 SEM, EDX and FIB cross-section thickness analysis

Scanning Electron Microscopy (SEM) cross-sectional analyse were performed on all of the coated samples. The thicknesses of monolithic (shown in Table. 4.1) and multilayer (shown in Table. 4.2) coatings have some variability; however, all the coating thicknesses were within the intended range.

Table. 4.1 Monolithic coatings thickness with their corresponding nitrogen flow rate

Nitrogen Flow (ml/min)	Thickness (µm)
0	6.8
5	6.4
10	6.5
15	6.2
55	6.2

The monolithic coating thickness varied between 6.2 and 6.8 µm, although the deposition time (65 minutes) and other deposition parameters were constant. The coating thickness appears to have an inversely proportional relationship with the nitrogen flow rate, such that increasing nitrogen flow rate decreases the net deposition rate. This phenomenon is not clearly understood but may be due to the sudden increase in workpiece current density (once the Nitrogen is switched off) - nitrogen molecular species (N_2*) have multiple vibrational sub-states, which can 'quench' the plasma, which affects the energy of the atoms/ionised, species, and/or thinning of the tungsten wire filament.

Attempts at semi-quantitative measurement of the composition of all the samples were completed using Energy Dispersive X-ray spectroscopy (EDX). However, it is difficult to detect the concentration of nitrogen in titanium because the footprint of the major nitrogen peaks is nearly identical to that of the titanium peaks; such overlapping in footprint can lead to misidentification of the elements peaks. This led to the inability to accurately measure the concentration of each element in this system.

Table. 4.2 Summary the designed multilayer coatings in terms of their layer thickness ratio, designed total coating thickness, and actual total thickness obtained. Note that the ratios in brackets represent the TiN and Ti or Ti(N) layer thickness ratio.

Coating	**Total coating thickness (µm)**	
	Design	**Actual**
TiN/Ti (1:1)	10	9.4
TiN/Ti (2:1)	10.2	10.5
TiN/Ti (1:2)	10.2	9.6
TiN/Ti(N) (1:1)	10	8.4
TiN/Ti(N) (2:1)	10.2	9.1
TiN/Ti(N) (1:2)	10.2	9.4

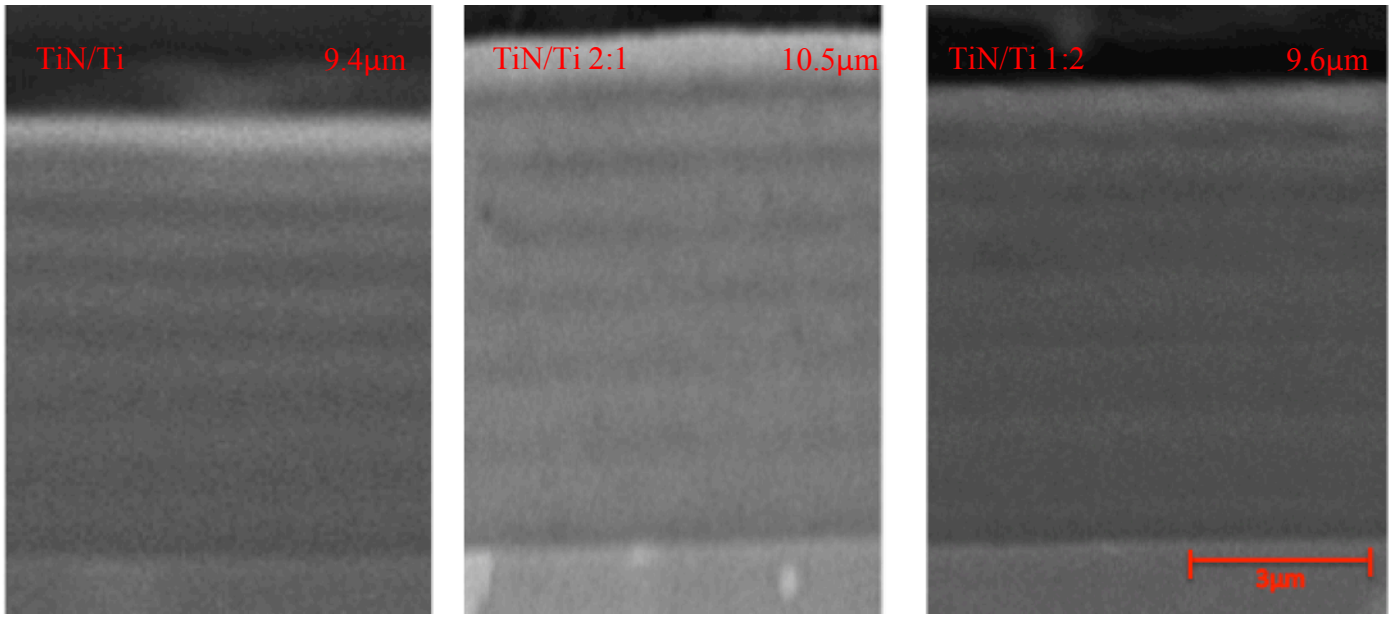

Figure. 4.1 SEM cross-sectional images of TiN/Ti multilayer coatings with their corresponding thickness

The SEM cross-section imaging (Figure.4.1) of the TiN/Ti multilayer group revealed that the coating exhibited a dense structure but since the SEM displayed a poor resolution, a definitive conclusion on whether or not it exhibited a columnar structure cannot be made. The TiN/Ti(1:1), TiN/Ti(2:1) and TiN/Ti(1:2) coatings have total thicknesses of 9.4, 10.5 and 9.6 µm, respectively. The contrast in the layers revealed different compositions. As illustrated in Figure. 4.2, titanium nitride appears brighter, whereas the titanium interlayers are represented by the darker layers. They appear to have the expected TiN and Ti layer thickness ratio of either 1:1, 2:1 or 1:2.

Figure 4.2 below illustrates the SEM cross-section of the TiN/Ti(N) multilayer group, with TiN/Ti(N) (1:1), TiN/Ti(N) (2:1) and TiN/Ti(N) (1:2) coating thicknesses of 8.4, 9.1 and 9.4 µm, respectively. They also appear to have the expected TiN and Ti(N) layer thickness ratio of either 1:1, 2:1 or 1:2.

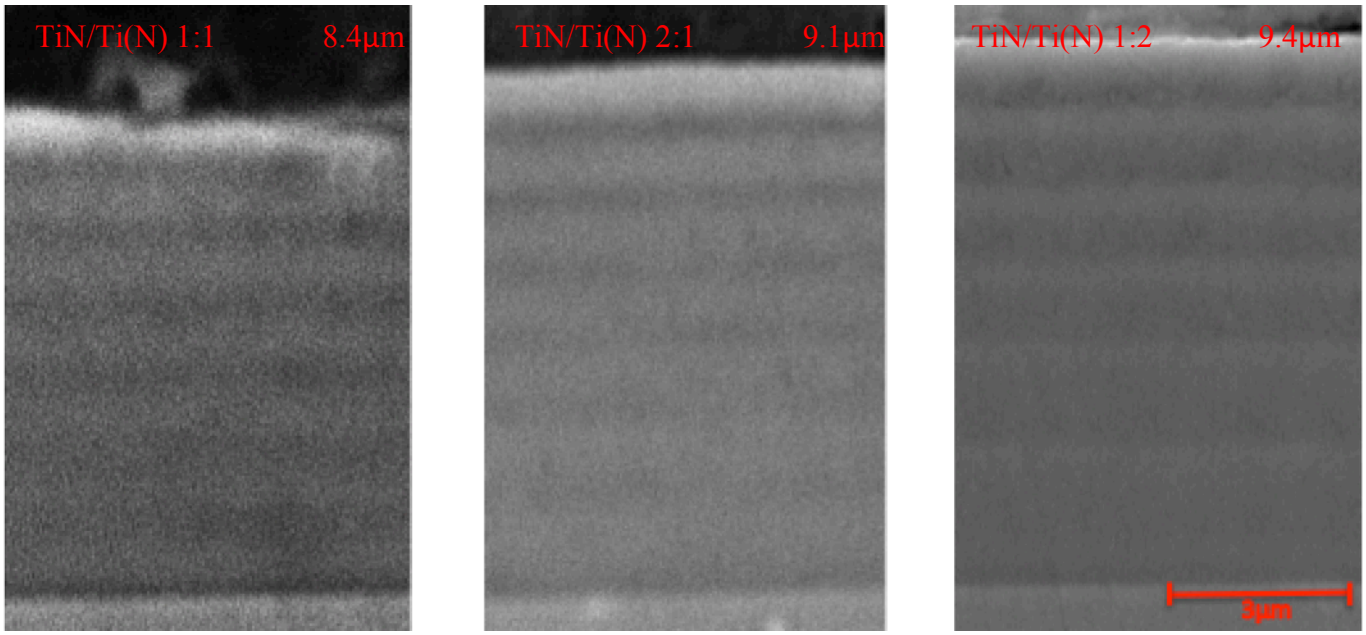

Figure. 4.2 SEM cross-sectional images of TiN/Ti(N) multilayered coatings with their corresponding thicknesses

The variation in the thickness of the layers (and of the total coating thickness) is due to the difficulty in controlling the deposition process. The extended deposition time of the multilayer coatings (2 hours) makes it problematic to control the deposition conditions, as discussed in section.3.2.6, due to the "burrowing" effect of the titanium slug and the gradual increase in substrate current density (due to the sputter thinning of tungsten filament, which leads to increased thermionic electron emission).

In comparing the TiN/Ti and TiN/Ti(N) multilayer total coating thickness as a whole, the TiN/Ti multilayer group appears to be thicker than the TiN/Ti(N) group. The difference in the nitrogen flow rate during the metal interlayer deposition is likely to be responsible for this. As seen in the deposition of the monolithic coatings, increasing the nitrogen flow rate reduces the net deposition rate of the coating.

A challenge in achieving total thickness measurements may lie in the samples' cross-sectional preparation, where the samples were mounted in Bakelite. Preparation of the sample in this way normally leaves a gap between the sample and the mount. When observed under

the SEM, there is an edge rounding effect that makes the image blurred and inaccurate for determining the thickness of the coating. Furthermore, the mounted samples were subjected to manual grinding and polishing methods. Errors may occur due to the uncontrollable pressure exerted. The best solution may be to mount two samples together 'face-to-face' (to minimise the edge rounding effect). An improved way to measure the thickness of the coating may be by using non-destructive methods, such as X-ray fluorescence methods where thicknesses of up to about 15µm are possible to evaluate [96].

Another cross-section thickness analysis technique, Focused Ion Beam (FIB) combined with SEM, were performed on all of the coating samples to confirm the TiN/Ti and the TiN/Ti and the TiN/Ti(N) coating thickness ratio results.

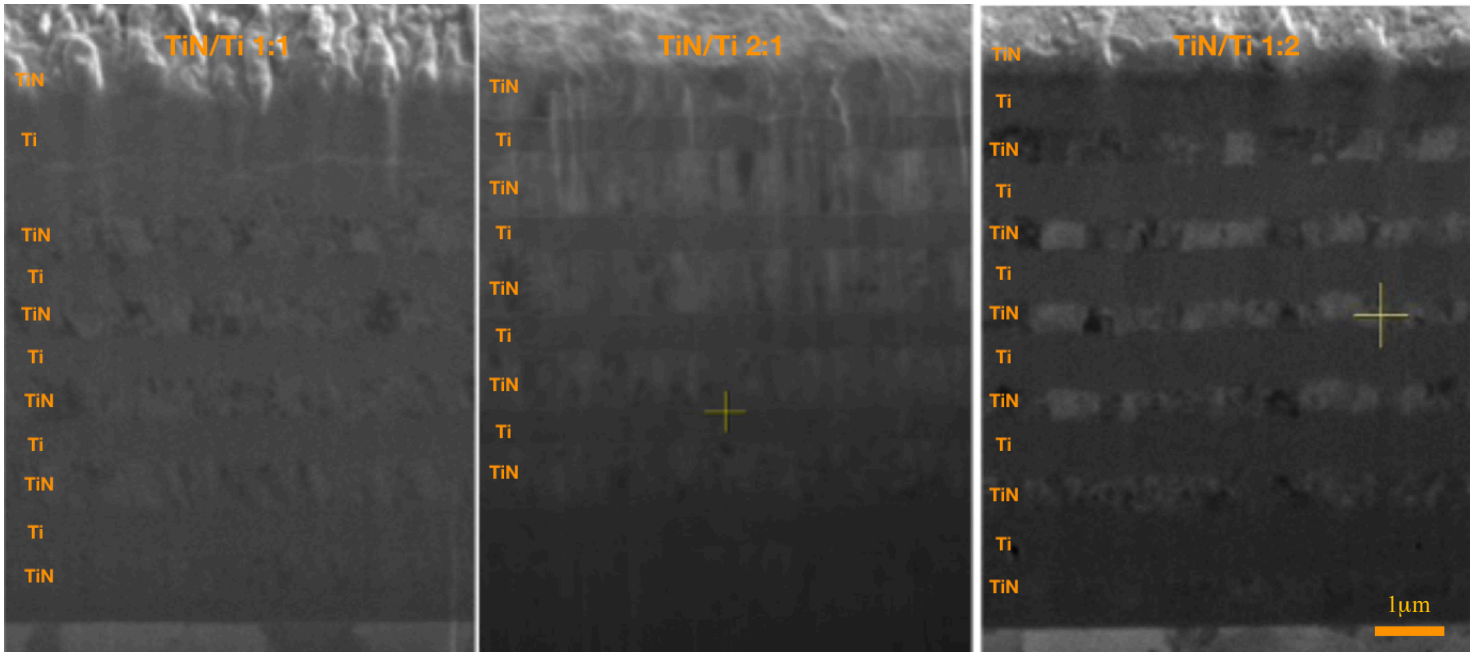

Figure. 4.3 FIB SEM cross-sectional images of TiN/Ti multilayer coatings (TiN layers are bright and Ti layers are dark)

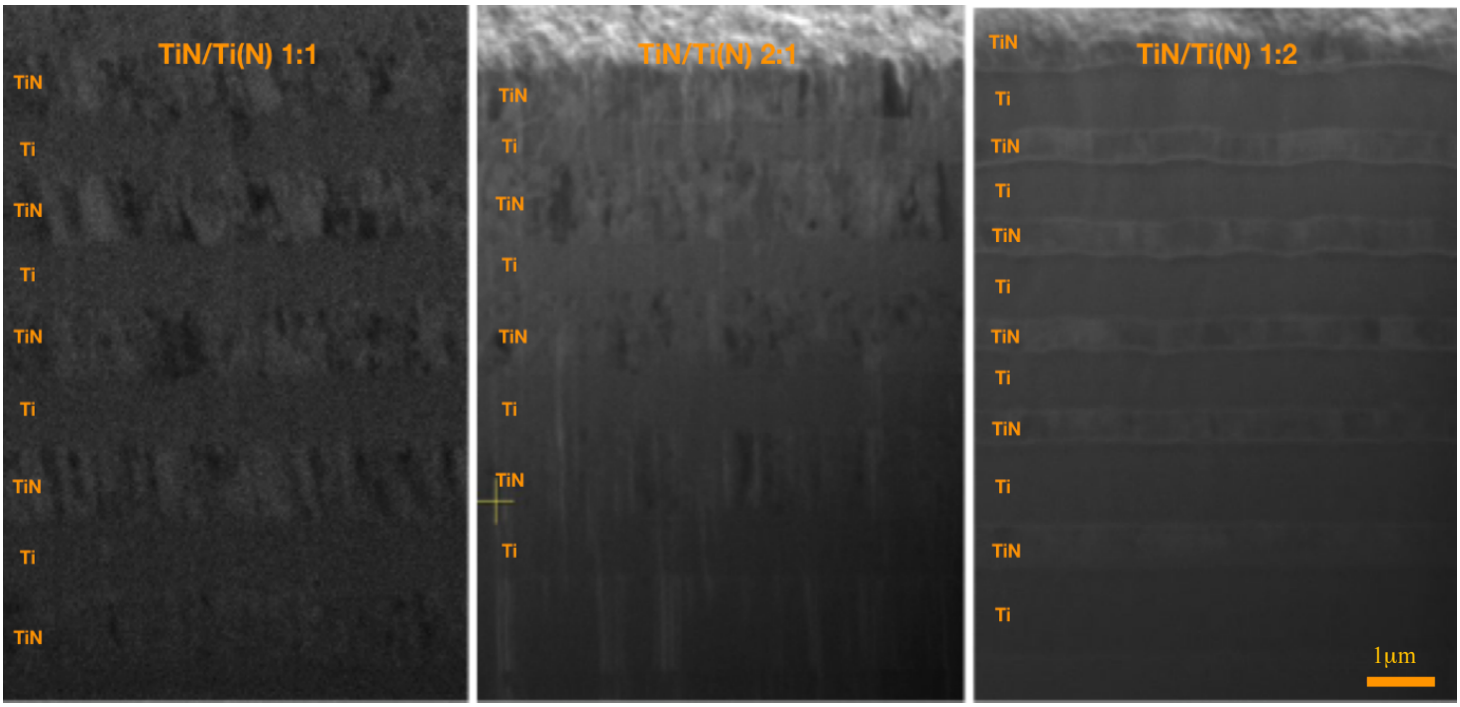

Figure. 4.4 FIB SEM cross-sectional images of TiN/Ti(N) multilayer coatings (TiN layers are bright and Ti(N) layers are dark)

Figure. 4.3 and 4.4 illustrated that titanium nitride appears brighter, whereas the titanium interlayers are represented by the darker layers. The TiN/Ti or TiN/Ti(N) thickness ratio appears to be as their designated ratios, either 1:1, 2:1 or 1:2. Furthermore, Definitive conclusion can be made that the TiN layers exhibit a coarse structure (compared to the Ti or Ti(N) layer, which may suggest that it has a columnar structure), however the Ti or Ti(N) layers appears to be dense.

4.2 Transmission electron microscopy (TEM) analysis

The TiN/Ti (2:1) coating were chosen for TEM analysis to further investigate the layer structure and phase composition of the coatings. Selected Areas Electron Diffraction (SAED) patterns, together with the bright field (BF) and dark field (DF) transmission images were collected.

Figure. 4.5 displays the bright field TEM imaging of the TiN/Ti 2:1 coating, the SAED pattern corresponding to selected layers of TiN and Ti in the undamaged region and the SAED pattern of the whole sample. The SAED pattern confirms the presence of the TiN and Ti layers. The layers being either TiN or Ti, seem to have a columnar structure. According to the Thornton structure-zone model [82, 97], the coating structure is dominated by homologous temperature; i.e. the ratio function of substrate temperature (T) to melting temperature of the coating material (Tm). The TiN layers show evidence of having the same characteristics as the Zone-T morphology, whereas Ti layers appear to have a denser columnar structure, as expected in Zone-2 type morphology. This is expected since the melting temperature (T_m) of TiN is higher than Ti (2930^{o}C [98] compared to 1667^{o}C [99], respectively). The TEM image confirms the thickness ratio of 2:1 for TiN and Ti layers, as shown in the SEM cross-sectional analysis (section.4.1)

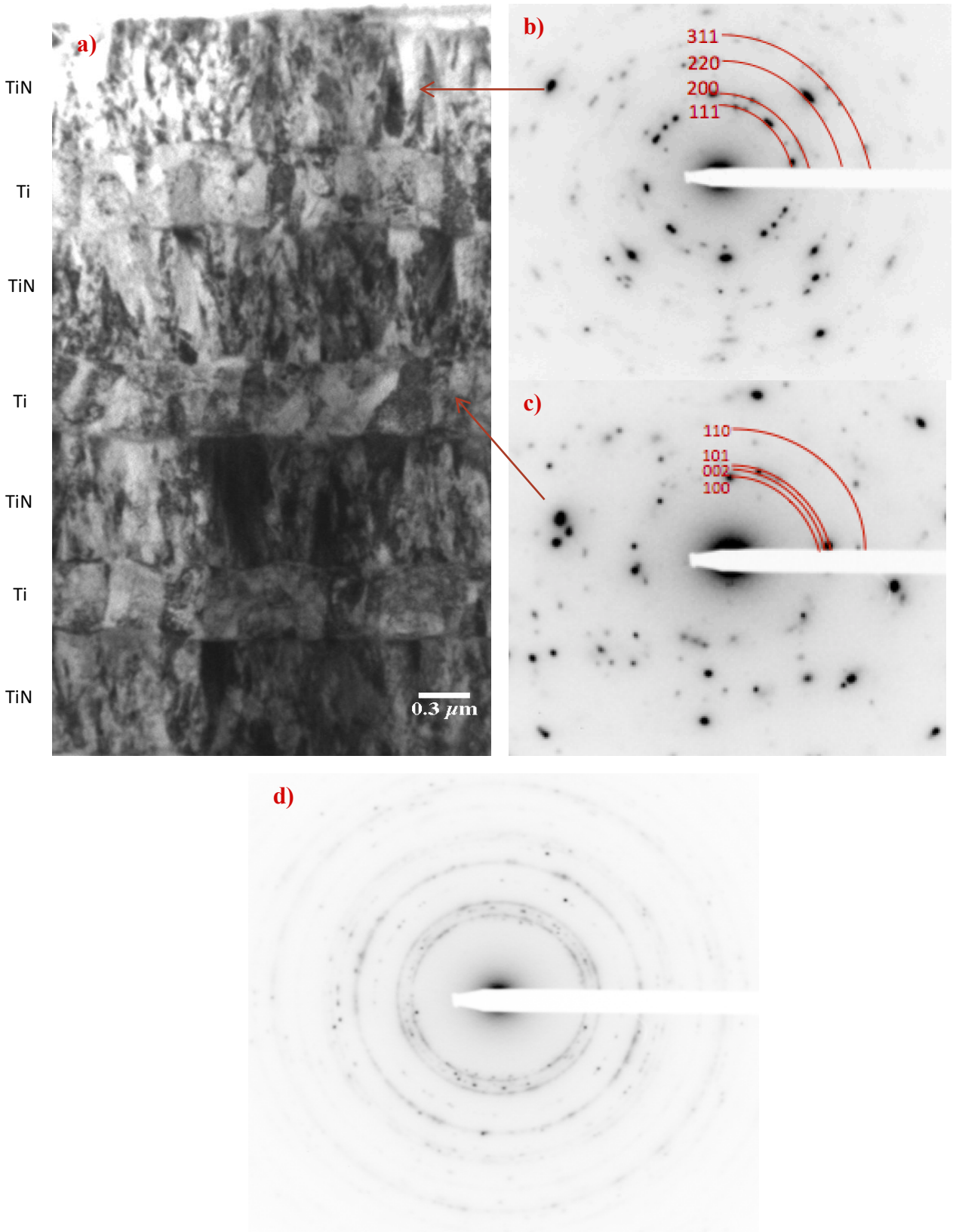

Figure. 4.5 Plane-section BF images and SAED pattern a) BF image at low magnification; b) SAED pattern of the 1st layer (corresponding to TIN); c) SAED pattern of the 4th layer (corresponing to Ti); d) SAED pattern of the whole sample.

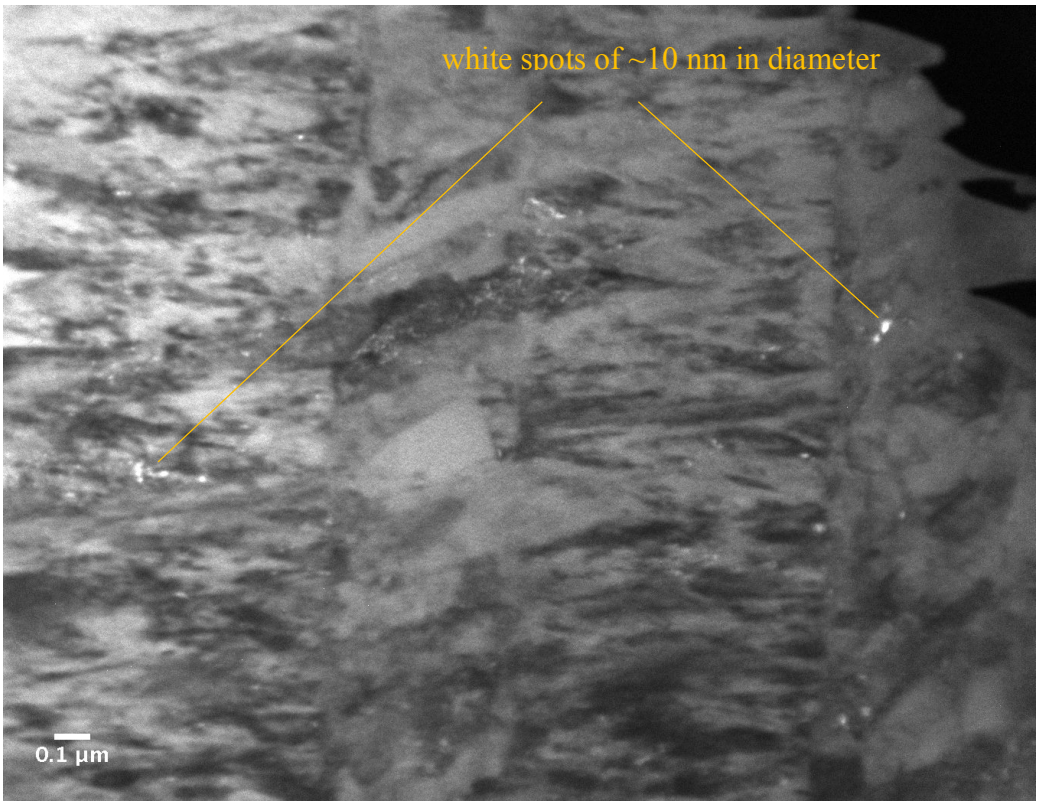

Figure. 4.6 High magnification DF imaging reveals white spot contamination throughout the structure

Higher magnification in the DF imaging (shown in Figure. 4.6) reveals that there appear to be small particles of nanometric dimensions (white spots ~10 nm in diameter) embedded in the whole coating structure, both in the TiN and Ti layers. Fancey [46] stated that tungsten contamination is likely to be significant in coatings if the deposition time is over 90 minutes (for our multilayers, deposition time is ~120 minutes). The source of the tungsten contaminant is from the sputtering of the thermionic discharge filament. Moreover, Fancey [46] also described that the grains boundaries of the tungsten filament open up with time, which produces a more faceted surface. This is likely to increase the proportion of the electrons emitted at a constant power. The effects of tungsten contamination in the structure on the wear performance is unknown.

4.3 XRD analysis

When titanium is being evaporated, increasing the nitrogen gas flow rate from 0-55 ml/min affects the crystallographic phases, in a way that generally corresponds to the Ti-N equilibrium phase diagram. Note that XRD analyses were only performed on monolithic coatings

The XRD patterns of the monolithic coatings (shown in Figure.4.7) that were deposited from 0-15ml/min flow rate, exhibit a hexagonal closed packed (HCP) structure with (100), (002), (101) and (110) peaks observed. With increasing nitrogen flow rate from 0-15ml/min, preferred orientation of the coating changes from (002) plane to a strong (110) texture. The explanation for the change in preferred orientation to a strong (110) plane is possibly due to the changing energy of the bombarding species – or maybe nitrogen is accumulating at the grain boundaries of the growing film with increasing nitrogen flow rate, which may also change the growth direction. Introduction of neutral molecular nitrogen gas to the system is responsible for lowering the energy of the plasma discharge. Reduction in system energy is likely due to energy input in the dissociation, ionisation, or excitation of nitrogen molecules. This in turn weakens the kinetic energy of the bombarding ions/atoms [100, 101].

Coatings deposited at 0-15 ml/min nitrogen flow rate show no sign of the Ti_2N lower nitride phase being present. However, the peaks are shifted towards a lower diffraction angle which probably correspond to the effects of crystal lattice expansion due to interstitial nitrogen incorporation within the α-Ti lattice.

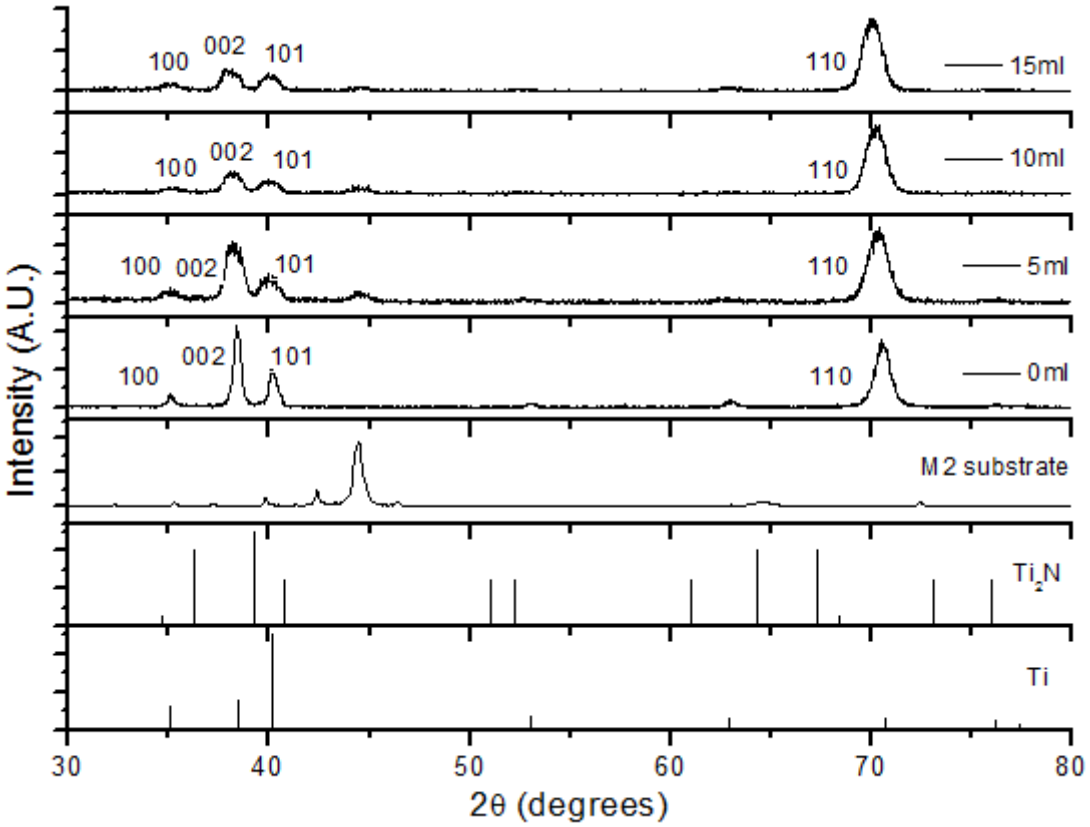

Figure. 4.7 XRD spectra for titanium coatings with varying nitrogen flow rate (0-15ml/min)

The XRD spectra (Shown in Figure. 4.8) illustrate that the monolithic coating deposited at 55ml/min nitrogen flow rate demonstrate a face centred cubic (FCC) structure with (111), (200), (220), (311) and (222) peaks observed, matching perfectly with the reference XRD spectrum of TiN. Thus, a definitive conclusion can be established that the coating with 55 min/ml nitrogen flow rate contains exclusively the TiN ceramic phase.

Rickerby et al. [102] suggests that, when depositing TiN coating onto HSS steel substrate under PVD (non-equilibrium) conditions, it is possible to yield strongly textured growth in the direction of the (200) plane. Under 'equilibrium' conditions, the growth direction in the (111) plane is most preferred in order to minimise the energy in the system. Kobayashi and Doi [103] further elaborated that the sputtering process of TiN on cemented carbide substrates also influences the preferential growth plane, the preferential growth

direction changes from (200) to (111) and finally to (220) with, increasing substrate bias. The XRD spectra show that titanium nitride ceramic coatings (at the chosen nitrogen flow rate of 55 ml/min) have a slight preferred growth texture in the (200) direction. This may not be desirable, since TiN coatings with strong growth direction in the (111) plane are claimed to yield a smoother surface finish than growth in the (200) plane [104]. Sundgren [105] suggested that TiN coatings with the growth direction in the (111) are more desirable than the (200) direction for wear resistance applications.

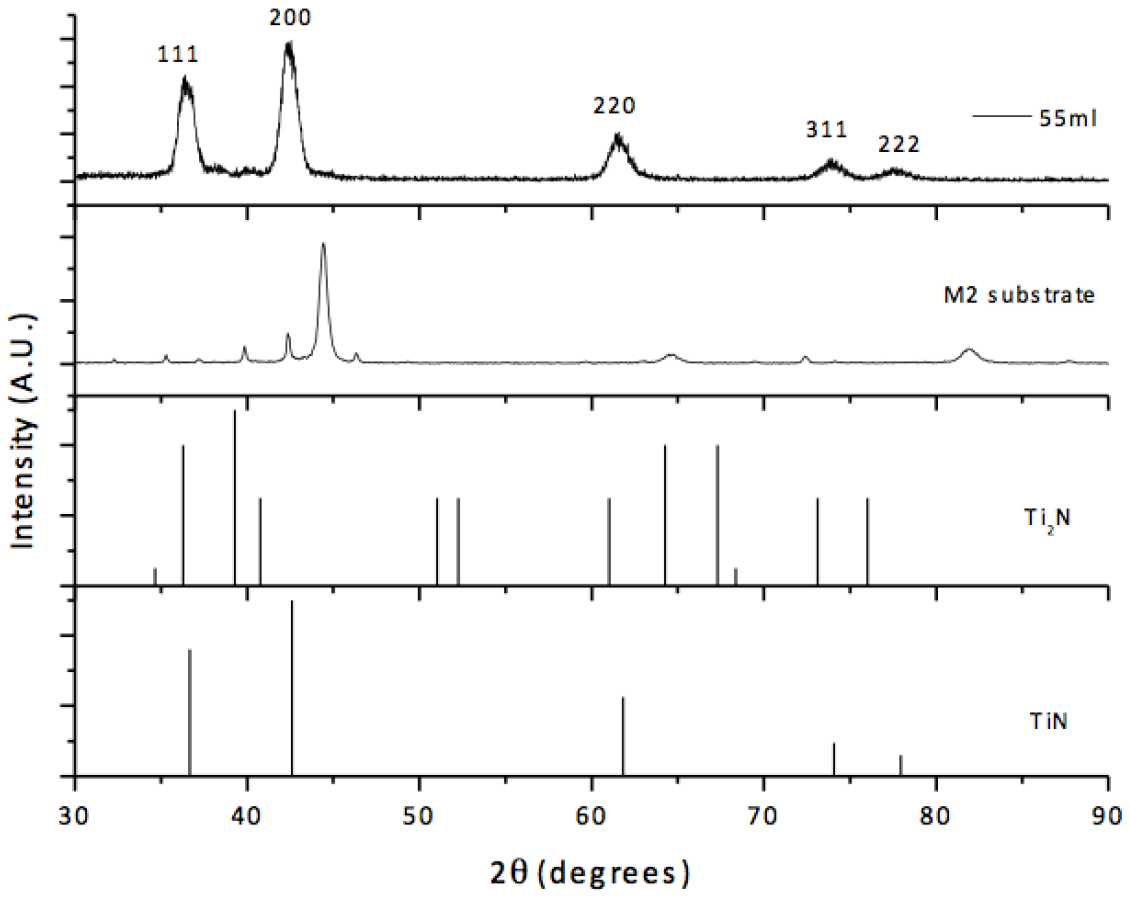

Figure. 4.8 XRD spectra of the titanium-based coating with 55 ml/min nitrogen flow rate

4.4 Mechanical properties

Nano-indentation is now a commonly-used method to measure the hardness and modulus of coatings. Each coated sample was subjected to 16 indents, with the maximum indentation depth being less than 1/10 of the coating total thickness as suggested by Oliver and Pharr [89], to eliminate the substrate influence. However, if the substrate is not a hardened tool steel (e.g. soft ductile metal) or an elastomer, the maximum indentation depth must be less than 1/25 of the coating total thickness in order to obtain the mechanical properties of the coating without substrate effects [106].

Hardness and elastic modulus data for the monolithic titanium-based coatings are presented in Figure. 4.9 and Figure.4.10 respectively. The coatings deposited at 0 ml/min nitrogen flow rate has a hardness and modulus of 4.8GPa and 118GPa. Increasing the nitrogen flow rate to up to 15ml/min results in a significant increase in hardness from 4.8GPa to 10.3GPa but only a slight increase in the modulus, 118GPa to 148GPa. The near monotonic increase in modulus suggests that nitrides probably are not being formed. The nitride coating deposited at the highest nitrogen flow rate (55ml/min) exhibits, as expected, the highest hardness and modulus, 16.5GPa and 318GPa, respectively, confirming that the phase present is TiN. The hardness enhancement from 0 ml/min to 15ml/min nitrogen flow rate is perhaps attributed to the doping of nitrogen into the titanium structure or possibly to the formation of nanocrystalline Ti_2N ceramic precipitates (which would explain the moderate increase in modulus). The Ti_2N phase is a much harder phase than the α-Ti. Nevertheless, as observed by XRD spectra, the results of increasing the nitrogen flow rate from 0-15 ml/min shows no sign of Ti_2N crystallographic peaks. However, if the Ti_2N particles were very small nanocrystalites (≤2nm in diameter), XRD analysis would not be able to pick up the associated crystallographic peaks.

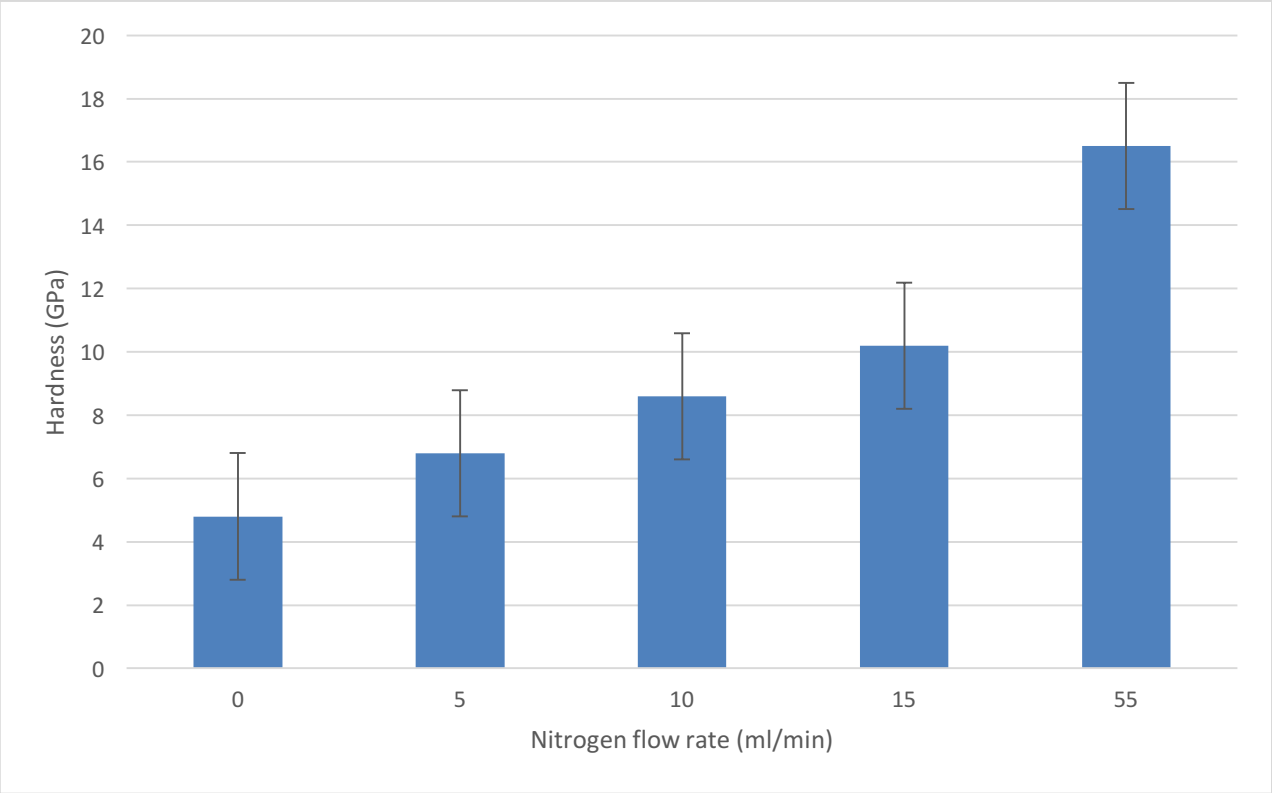

Figure. 4.9 Hardness of monolithic titanium-based coatings

The coating deposited at 55ml/min nitrogen flow rate has a hardness of 16.5GPa and modulus of 318GPa. This coating has the highest hardness and elastic modulus; this is due to the presence of the TiN phase, as confirmed by the XRD spectrum in Figure 4.8.

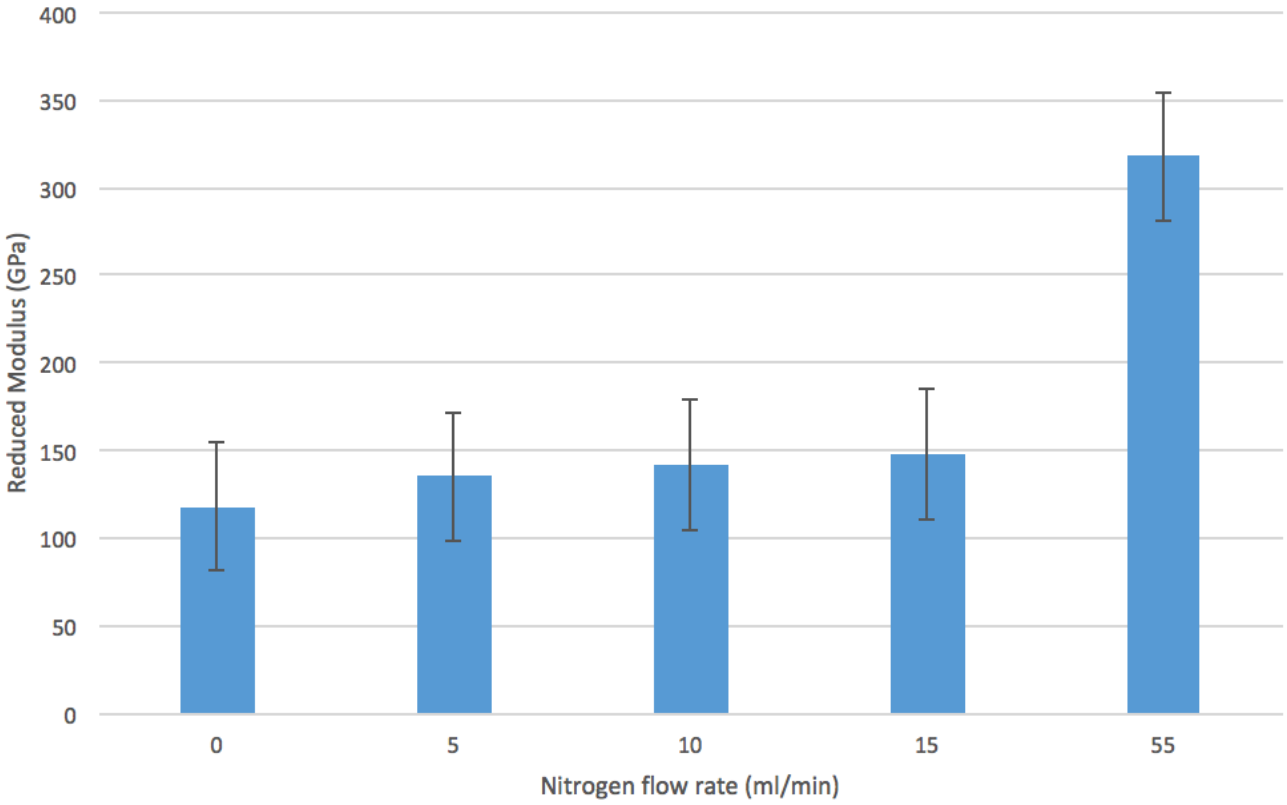

Figure.4.10 Elastic modulus of monolithic titanium-based coatings

Leyland and Matthews [47, 87] proposed that (from a tribomechanical perspective) there is often a strong correlation between the H/E or H^2/E ratio of the coating and wear resistance, where higher H/E or H^2/E ratio translates to better wear resistance. Figure. 4.11 and 4.12 shows the H/E and H^2/E data for the monolithic coatings. The increase in nitrogen flow rate from 0 to 15 ml/min yields a gradual small increase in H/E ratio from 0.041 to 0.069 and an associated increase of H^2/E ratio from 0.200 to 0.699. However, an increase in nitrogen flow rate to 55 ml/min shows a sudden drop of H/E ratio to 0.052, however the H^2/E ratio shows an increase to 0.851. According to the H/E and H^2/E ratio data, the H/E ratio indicates that the monolithic titanium coating at deposited 15ml/min nitrogen flow rate will exhibit the best wear resistance, whereas H^2/E ratio indicate that monolithic titanium coating at deposited at 55ml/min nitrogen flow rate will exhibit the best wear resistance. However,

both ratio (H/E and H^2/E) suggested that monolithic pure titanium coating (0 ml/min nitrogen flow rate) will exhibit the worst wear performance.

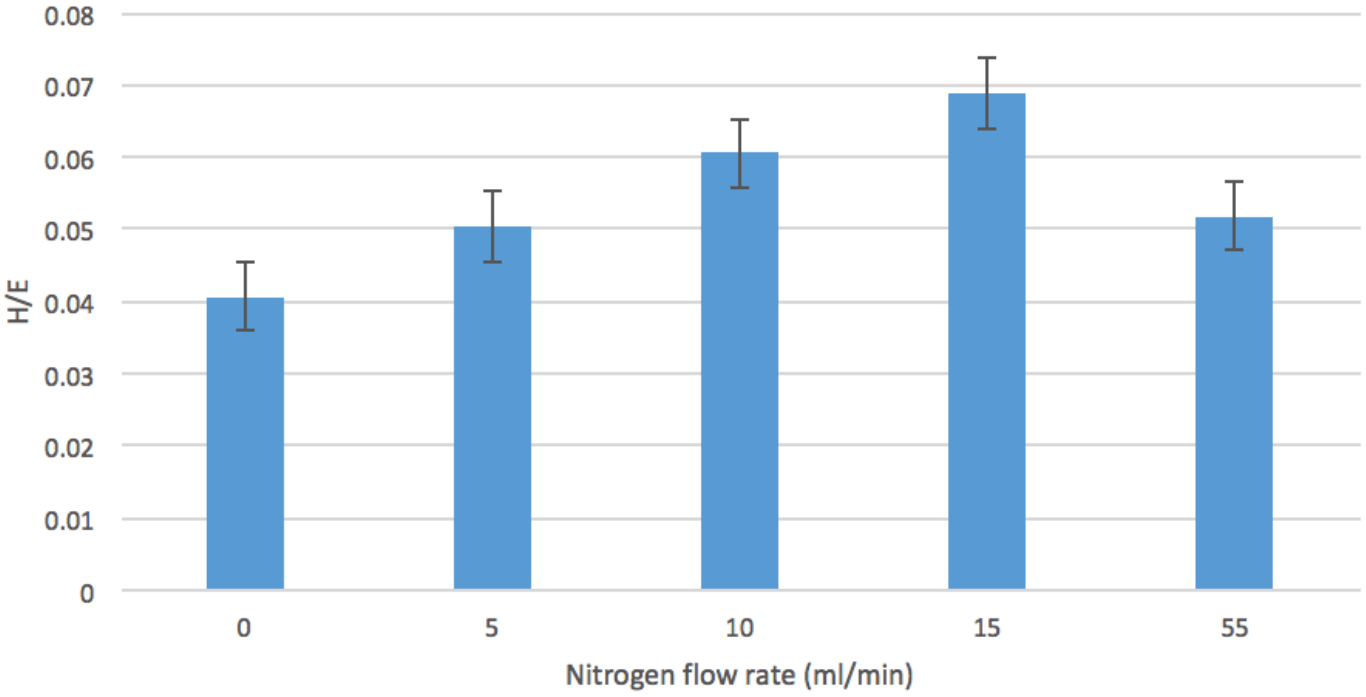

Figure. 4.11 The H/E ratio of the monolithic coating

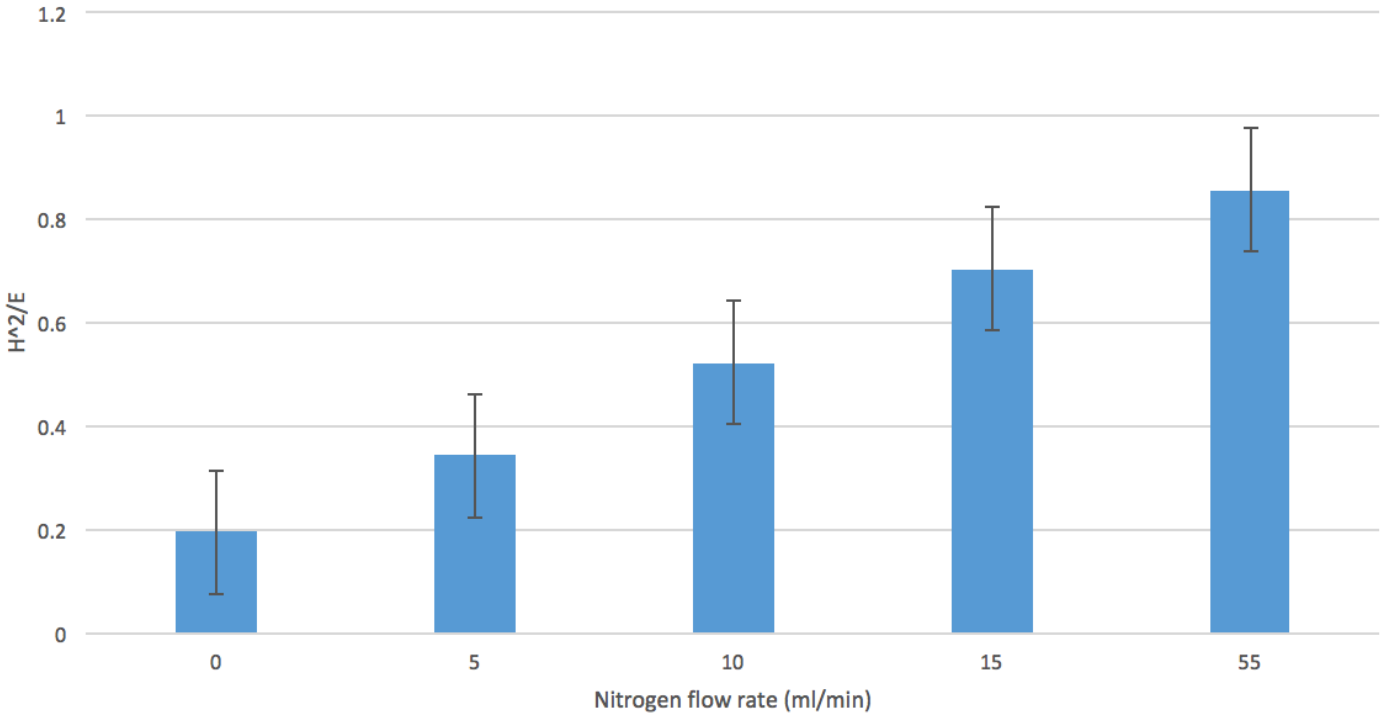

Figure. 4.12 The H^2/E ratio of the monolithic coating

4.5 Surface roughness

The performance of a component subjected to water droplet erosion has been reported to be directly correlated with the roughness of the surface. Rougher surfaces worsens the onset of material/component erosions' resistance [107] . The surface roughness was measured using a stylus profilometer. Randomly selected areas of the coating were subjected to 5 line scans (of 3000μm) on the surface. Results are shown in table. 4.3

Table. 4.3 The samples surface roughness

Material/Coating	**Averaged Surface roughness, Ra, (μm)**
Polished, uncoated M2 Tool Steel substrate	0.010
0 ml/min	0.025
5 ml/min	0.028
10 ml/min	0.035
15 ml/min	0.030
55 ml/min	0.023
TiN/Ti (1:1)	0.061
TiN/Ti (2:1)	0.043
TiN/Ti (1:2)	0.015
TiN/Ti(N) (1:1)	0.031
TiN/Ti(N) (2:1)	0.028
TiN/Ti(N) (1:2)	0.026

The result shows that the uncoated polished substrate exhibits (not surprisingly) the lowest surface roughness of 0.010μm Ra, signifying that deposition of a coating onto a sample increases the surface roughness, but by varying degrees. The coatings with the highest and lowest average surface roughness of 0.061 μm and 0.015 μm are TiN/Ti 1:1 and TiN/Ti 1:2, respectively.

Interestingly, comparing the whole of the multilayer coatings with both Ti and Ti(N) interlayers, the multilayer coating with Ti(N) interlayer appears to exbihit smoother surface (lower Ra) roughness. Furthermore, increasing the interlayer (both Ti and Ti(N) thickness in the multilayer coatings appears to minimise the coating surface roughness. The cause of this effect is not investigated in this thesis work.

The deviations in surface roughness in the surface of all the coated samples seem to be small and the surface roughness are in the order of ($\sim 10^{-2}$μm). Therefore, the effects of surface roughness on the erosion performance could be negligible.

Chapter 5 Solid and Liquid particle impact tests

5.1 Ball-on-plate impact tests

The ball-on-plate impact wear resistance of both monolithic and multilayer coatings was evaluated. All coatings were subjected to 1000, 5000, 10000, 20000 and 50000 impact cycles. The counterface used was a 6mm WC-6%Co ball and the applied load was 150N. As mentioned previously, the decision to use a relatively low impact load was made to try and match the water hammer pressure of water droplet erosion, where the speed of impact is however often much higher, sometimes up to 300-400m/s. The initial Hertzian contact pressure at 150N loading is approximated to be 3.8-6.7 GPa. A contact pressure of this magnitude is expected to cause plastic deformation in both the coating and the substrate, creating a concave depression during the first few impacts. However, there would be a gradual drop in the pressure; this is because with increasing number of impacts, the crater diameter increases. Thus increasing the contact area between the ball and the material. This reduces the effective pressure exerted on the surface of the material. Once the pressure drops below the compressive yield strength of the material, the deformation mode changes from plastic to elastic. The predominant deformation mode continues to be elastic and the fatigue wear is examined until the delamination of the coating.

Knotek et. al [90] and Bouzakis and Siganos [108] suggested that adhesive and cohesive failures were found in their experiments. Bantle et. al [91] elaborated that three failure zones can be observed (shown in Figure. 5.1) in the impact area: a central zone with cohesive failure, an intermediate zone with cohesive and adhesive failure, a peripheral zone consisting of circular cracks and piling up of the material. The presence of the intermediate zone is due to the build-up of shear stresses that arise from the plastic strain during the ball impact. Studies show that there is good correlation with the number of impacts and the volume of the crater.

The substrate also plays a role in the coating failure. For a low roughness substrate coated with a thin hard film, the failure is initiated primarily by a high-cycle fatigue mechanism. For a high roughness substrate coated by a thin hard film, the failure is initiated by fracture of asperities on the surface. which consequently lowers the coating wear performance [108].

Moreover, the elastic modulus mismatch between the coating and substrate may influence the impact wear performance of a coating. High elastic modulus mismatch between the coating and substrate promotes adhesive failure along the coating/substrate interface, due to difference in the deflections (bending stress) between the coating and the substrate. Increasing the thickness of the coating (probably to the millimetre range) can help to eliminate this effect, however coatings (less than 10μm thick) examined in this research will likely experience this elastic mismatch.

Consequently, referring back to the H/E ratio as a mechanical property wear performance indicator, not only a high H/E ratio is desired, but I suggest that matching the elastic modulus to that of the substrate is probably equally as important as having high hardness (for stress shielding) –particularly in impact wear. This is in contrast to what Hassani et al. [79] modelled on how to build a coating to resist particulate erosion (where his coating layering architecture recommended a high modulus mismatch at the coating-substrate interface), but (as with many such models) did not validate with practical experiments.

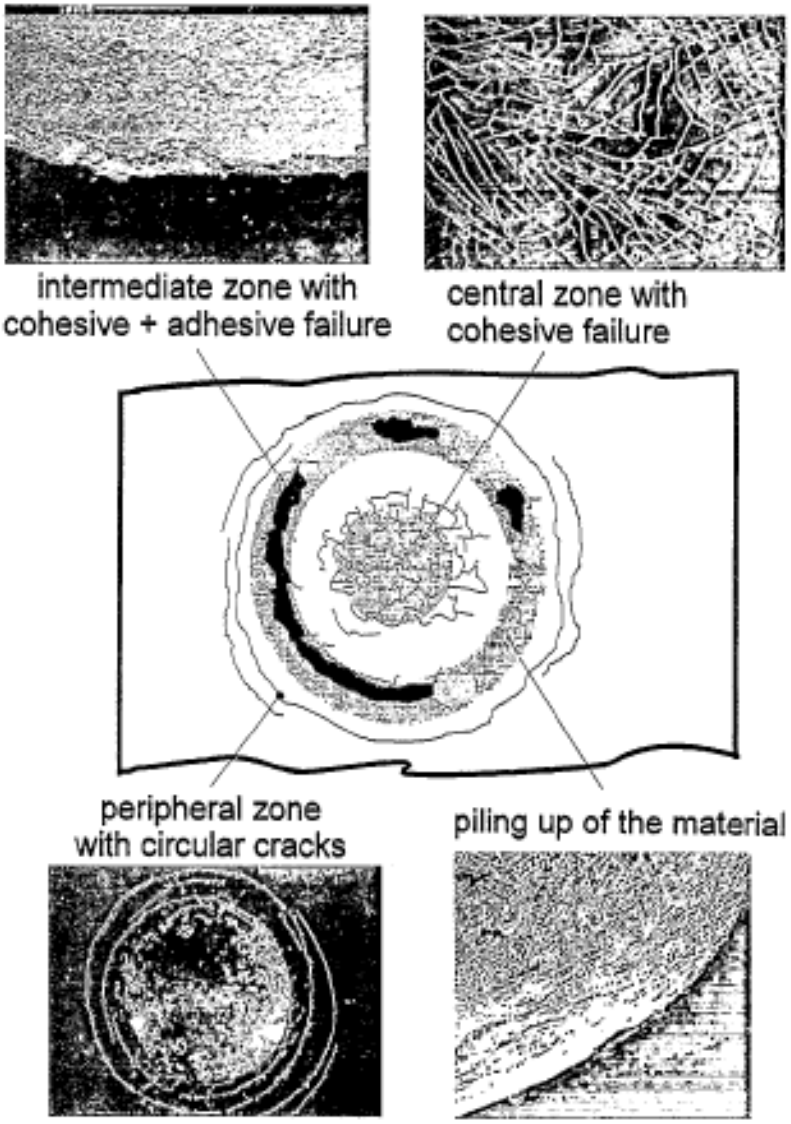

Figure. 5.1 A model of coating degradation under impact loading, showing different failure zones [91].

5.5.1 Monolithic coatings

Figure 5.2 and 5.3 illustrate (respectively) the maximum wear depth and the wear volume of the monolithic titanium coatings. The results clearly show that applying a protective coating on the substrate surface immensely increases impact wear performance. However, it is difficult to say unequivocally which monolithic titanium coating performed best under the impact test conditions applied. Regarding the mechanical properties of the monolithic coatings (shown in section. 4.4), with increasing nitrogen flow rate from 0 to 15 ml/min, hardness was reported to increase over two-fold, whilst the elastic modulus only increased by approximately 25%. Nevertheless, the impact wear results clearly show that significantly increasing the hardness does not have any strong influence on the coating impact wear performance; this implies that hardness has minimal influence in impact wear conditions – and that resilience (i.e. high H/E) and and/or toughness (i.e. low E, high ductility) are probably more significant factors.

The monolithic coating that performed the worst was the TiN ceramic coating. The significant increase in hardness to ~16.5GPa, does not provide any benefit to the impact wear performance of the coating.

Regarding the H/E and H^2/E ratio results of the coatings in section 4.4, the particulate impact wear performance appears to correlate better to the H/E ratio than the H^2/E ratio (Smart [49] suggest that H^2/E would be a better indicator for cavitation erosion wear resistance). This may signify that reducing the elastic modulus is equally or even more important than increasing the hardness for materials subjected to impact wear. Conclusively, the H/E ratio may be used as a prerequisite indicator in selecting a material for a coating to resist particulate impact wear.

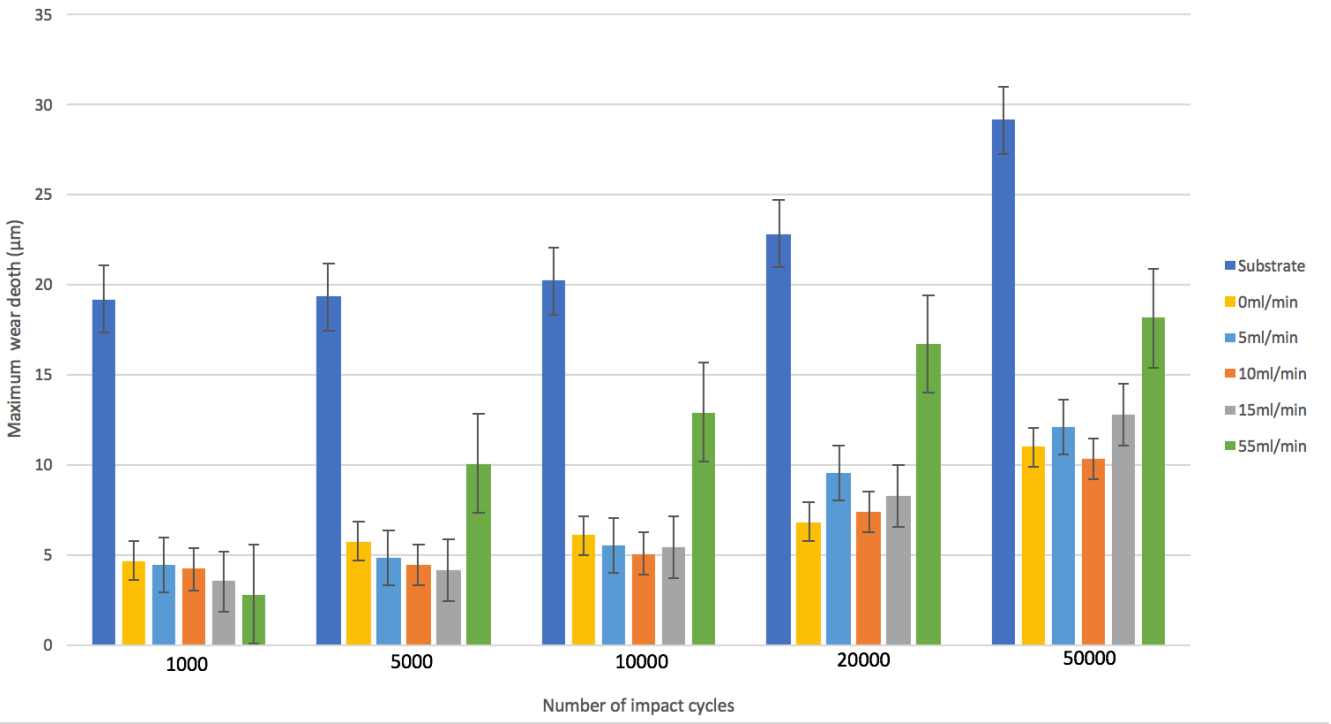

Figure. 5.2 Wear depths of monolithic coatings under impact testing, with increasing number of impact cycles.

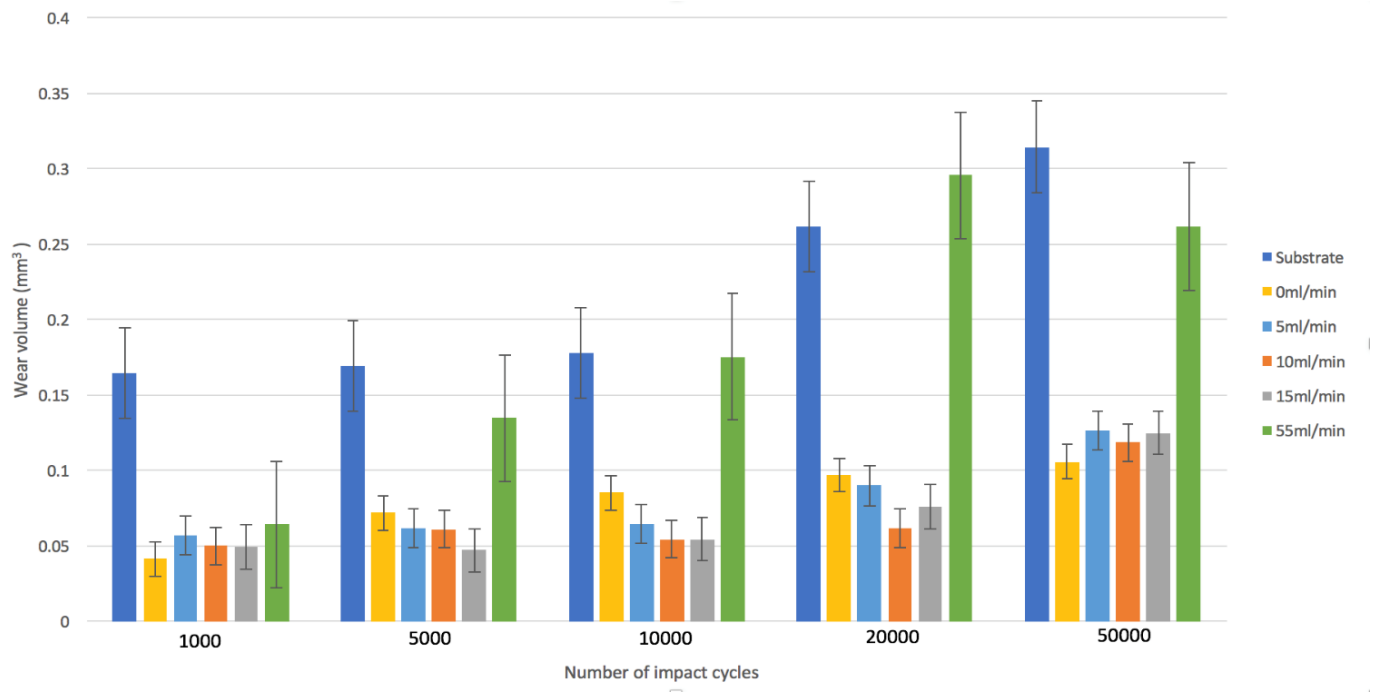

Figure. 5.3 Evolution of the wear volume of monolithic coatings after impact testing.

All of the titanium based coatings with nitrogen flow rate from 0 to 15 ml/min appear to have completely failed after 20000 impact cycles (and this is reflected in, particularly, the statistically significant increase in crater wear volume between 20000 and 50000 cycles). Cracks are normally observed at the pheriphery areas of the damaged crater, these pheripheral cracks would likely to multiply in number and size to form a network under increasing impact cycles. It is inconclusive as to whether the coating has failed due to cohesive or adhesive failure. However, observations that the coating did not fail earlier at 1000, 5000 or 10000 impact cycles suggest that there is good adhesion between the coating and the substrate.

The crater size and shape of the monolithic titanium nitride coating with 55ml/min flow rate upon impact testing at 20000 impact cycles is shown in Figure. 5.5. The smooth fracture surface at the crater periphery, usually seen with brittle material fracture, implies that when cracks are formed, only a small level of applied stress is needed to drive the growth of the cracks; this is due to little/no plastic zone at the crack tip in brittle materials (High E).

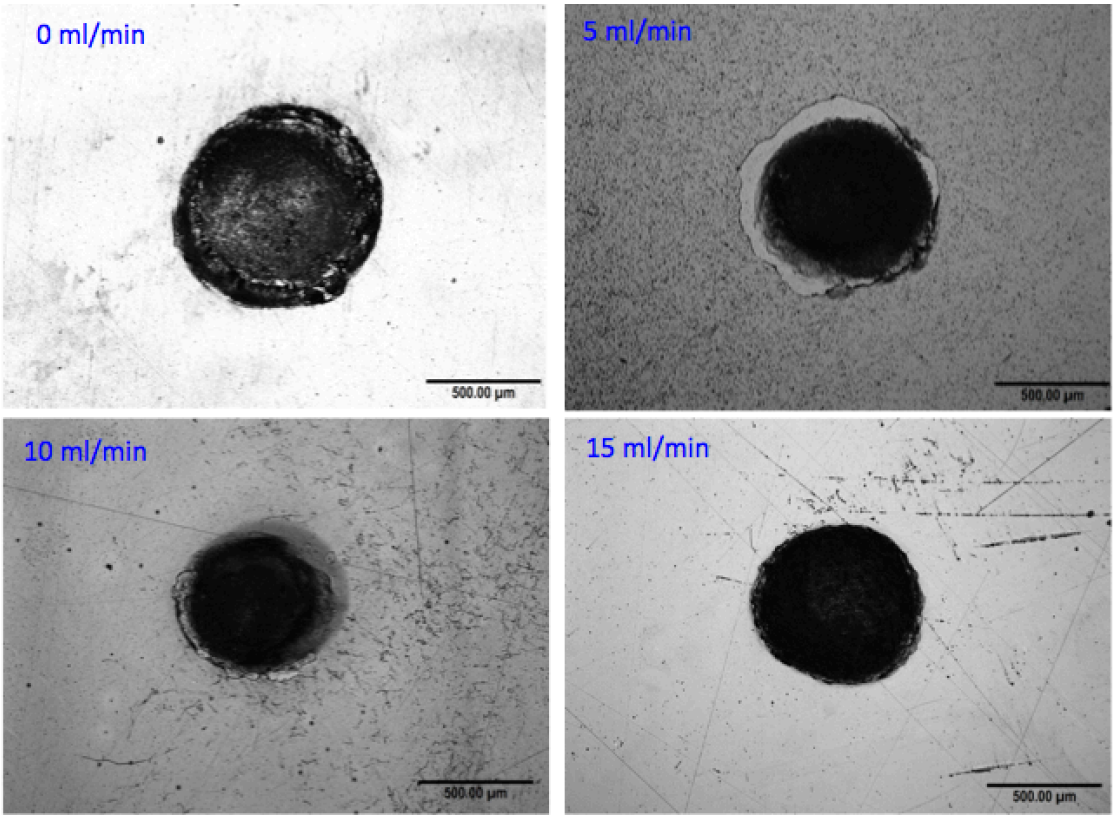

Figure. 5.4 Optical micrographs of the monolithic coatings with different, increasing nitrogen flow rates (0-15 ml/min), each after 20000 impact cycles.

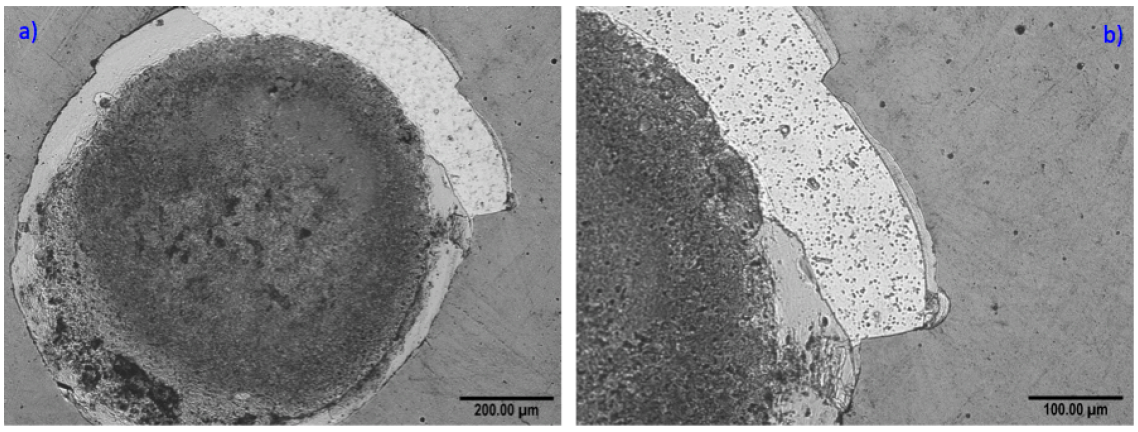

Figure. 5.5 Shows the damage crater of the TiN coating after 20000 impacts a) at low magnification b) at higher magnification, the substrate is exposes which is signifies by the smooth surface at the crater pheriphery

5.5.2 Multilayer coatings

The maximum wear depth and the wear volume of the multilayer coatings are shown in Figures. 5.6 and 5.7, respectively. In comparing the coated samples with the uncoated substrates, having a protective coating again clearly prolongs resistance to impact damage The TiN/Ti 1:1 coating exhibits the best impact wear resistance compared with all other multilayer coatings investigated; at 50000 impact cycles, only the TiN/Ti 1:1 coating shows insignificant change in both the maximum wear depth and volume, whist the other multilayer coatings exhibit significant increases in maximum wear depth and volume with increasing number of impact cycles.

Figure. 5.8 presents an optical micrograph of the TiN/Ti multilayer coatings group at 50000 impact cycles. From the observations, it is clear that the only coating that is still partially intact is the TiN/Ti 1:1 coating whilst TiN/Ti 2:1 and TiN/Ti 1:2 have completely spalled off. Referring to the evolution of the maximum impact depth, the results suggest that TiN/Ti 2:1 and TiN/Ti 1:2 coatings may have spalled off around at 10000 and 20000 impact cycles respectively. The delamination on the edge of the contact area and the intermediate zone of TiN/Ti 1:1 coating suggests that these regions fail under adhesive-cohesive failure, at the area of highest strain. These results concur well with Bantle and Matthews [91] observations of thin film coatings under impact conditions.

Also, it can be seen that TiN/Ti 2:1 coating exhibits a high number of cracks, probably due to insufficient toughness, around the impact area pheriphery; which is typically seen in the failure of a thin brittle coating [91]. Predictions can be made that the TiN/Ti 2:1 coating would have failed from crack propagation through the coating thickness, along with adhesive-cohesive failure of the substrate, leading to sudden removal of coating material.

The TiN/Ti 1:2 coating shows no cracks around the impact contact pheriphery at 50000 impact cycles. However, at 1000 impact cycles (shown in Figure.5.9), TiN/Ti 1:2 shows severe material pile up around the edge of the impact crater (which is not seen in other coatings). This suggest that the coating is excessively ductile, owing to the high volume of the soft titanium interlayer, which compromises the load-bearing capability of the coating.

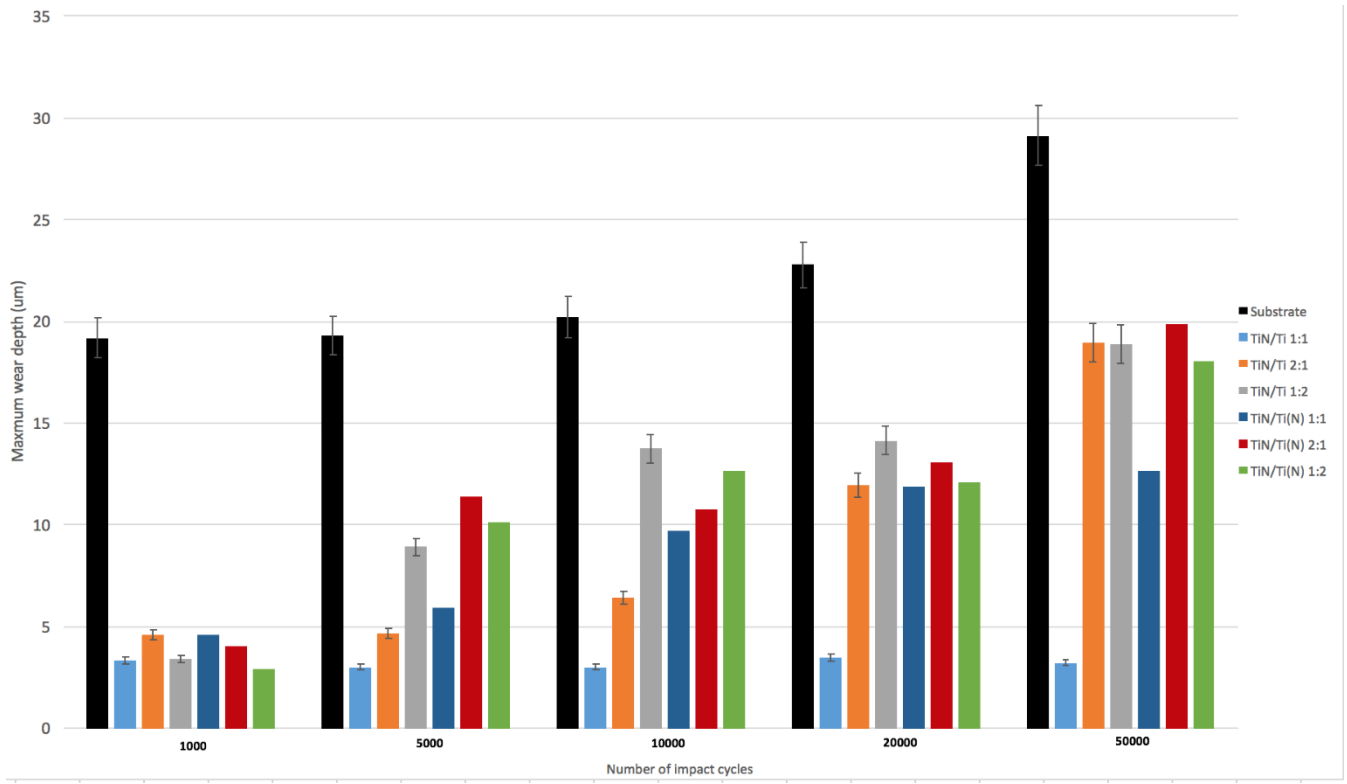

Figure. 5.6 Wear depths of multilayer coatings under impact testing, with increasing number of impact cycles

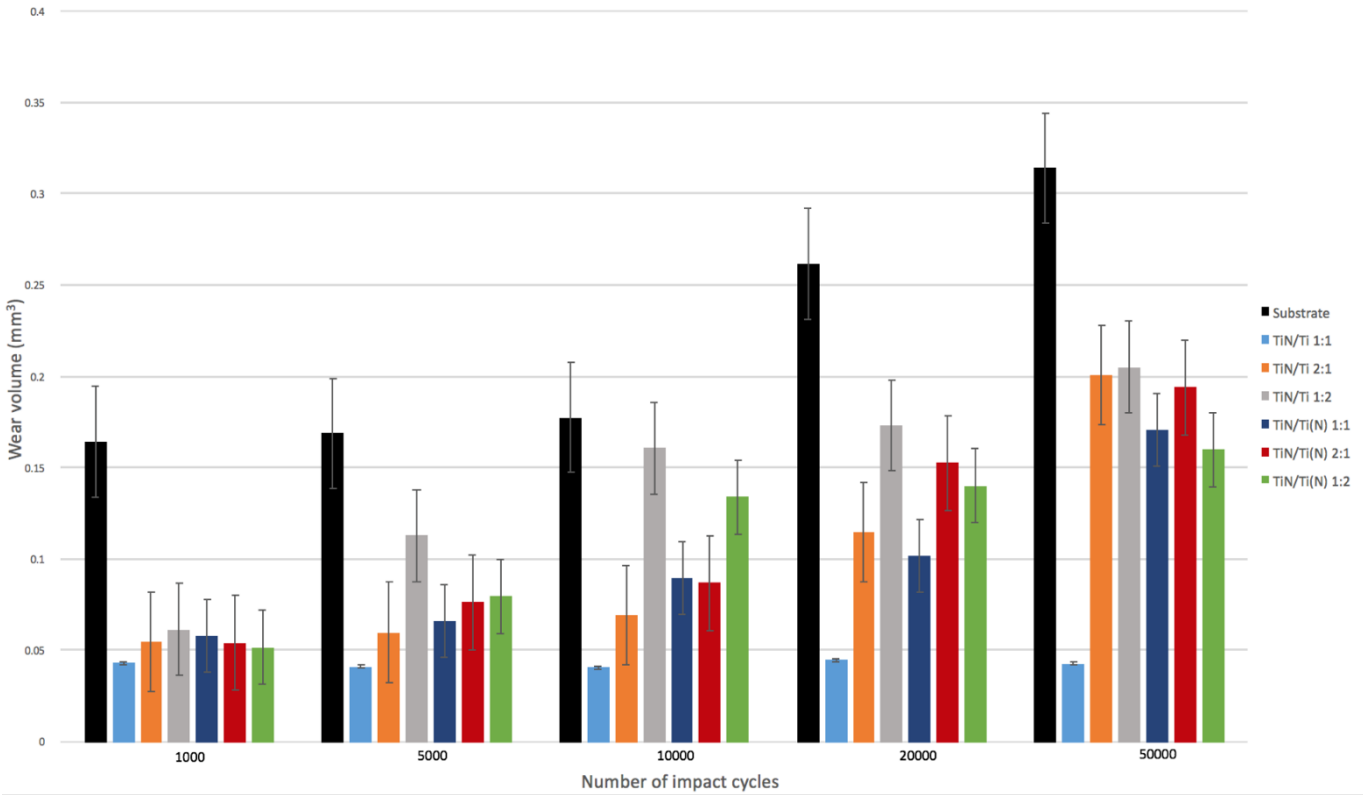

Figure. 5.7 Evolution of the volume of the multilayer coatings after impact testing

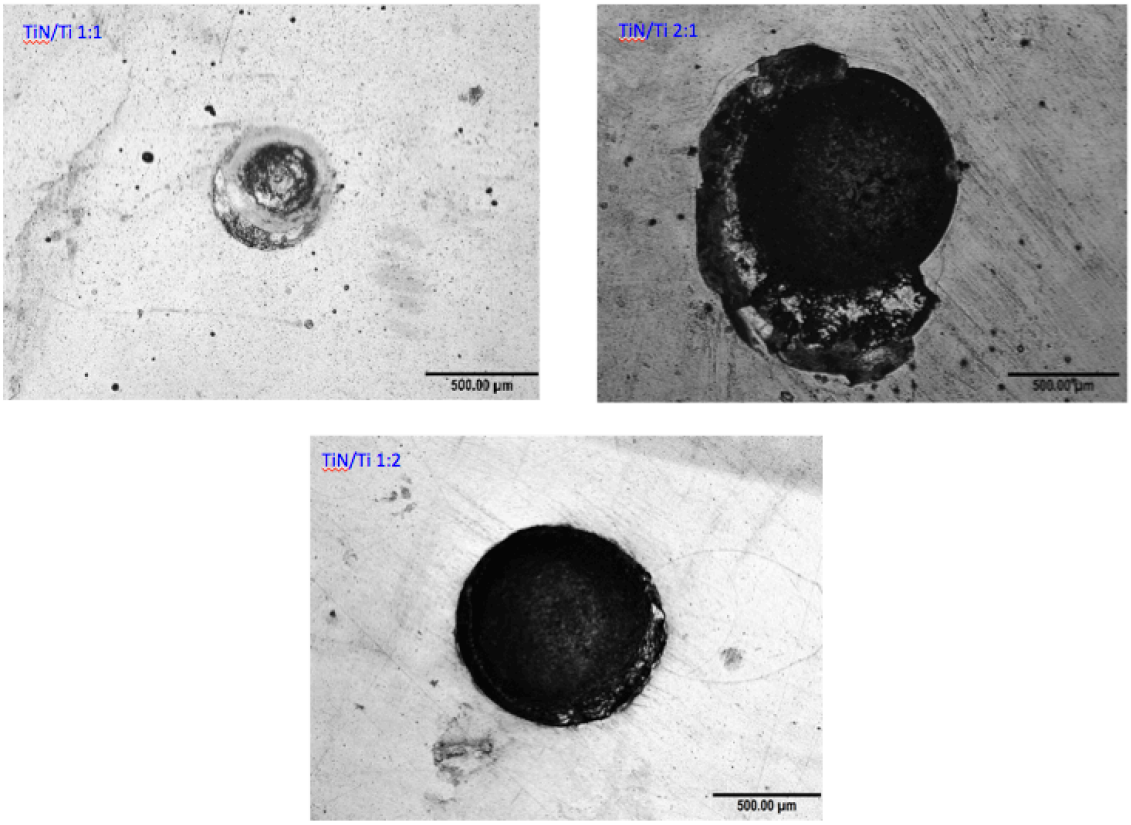

Figure. 5.8 Optical micrograph of the TiN/Ti multilayers coatings at 50000 impact cycles

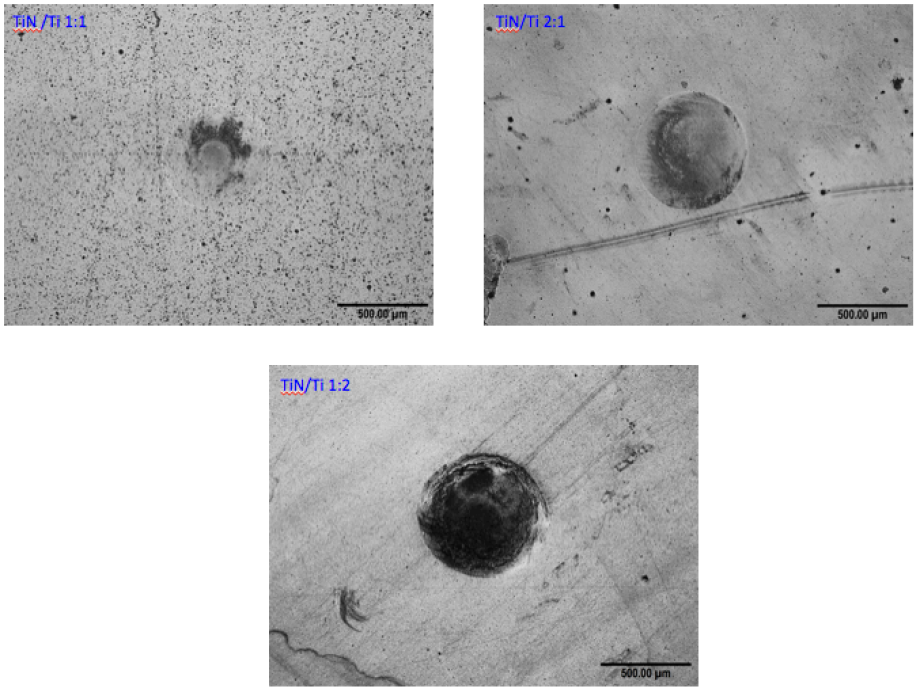

Figure. 5.9 Optical micrographs of the TiN/Ti multilayer coatings with different layer-pair ratios at 1000 impact cycles.

Regarding the impact wear performance of the TiN/Ti(N) multilayer coatings group, once again, the coating with the thickness ratio of 1:1 was superior in impact wear resistance. The TiN/Ti(N) 2:1 and TiN/Ti(N) 1:2 both performed significantly worse.

In comparing the two groups of TiN/Ti and TiN/Ti(N) multilayer coatings, the TiN/Ti(N) layers show inferior impact wear performance. The effect on ductility of nitrogen doping the titanium interlayer was possibly responsible for worsening of the impact wear performance. The Ti(N) interlayer is thought to significantly increase the hardness with minimal increase in Elastic modulus. This would increase the H/E ratio significantly which might be beneficial to the impact wear resistance according to Leyland [47]. However, the worsening of the performance suggests that under impact loading conditions, for a multilayer coating system, it is of more importance to lower elastic modulus of interlayering material than increases its hardness. Also, if the contact pressures involved will, in any case, exceed the yield strength of the materials involved, it seems that ductile layers (which can yield in shear, to accommodate strains in the harder layers) are also a requirement, but there is a need for a balance between layer ductility and overall coating load support.

5.2 Water Droplet Erosion (WDE) testing

The water droplet erosion tests were performed by the National Physical Laboratory (NPL). The speed of the water droplet impact is set to 300m/s and an estimated water droplet size of 300μm. The mass loss is determined by stopping the test at pre-determined intervals, removing the samples and measuring the weight using a precision mass balance (The accuracy of the mass balance is to 5 significant figures + or – 0.00001g).

Selected monolithic and multilayer coatings of Ti(N) and TiN, TiN/Ti 1:1, TiN/Ti 2:1, TiN/Ti 1:2 and TiN/Ti(N) 2:1 were subjected to the water droplet erosion testing. Due to the lengthy experimental time, not all coatings could be tested (and multiple repeats were also not possible).

Figure. 5.10 presents the total mass loss of the samples with respect to the number of droplet impacts. The coatings that performed best under water droplet erosion were the TiN/Ti 2:1 multilayer and the Ti(N) monolithic coating. Conversely, the coatings that performed equally badly were the TiN/Ti 1:1 and the TiN/Ti 1:2 multilayer coating. These results clearly indicate (when considering the previous solid particle impact tests) that the coating architecture is equally as important as material selection in building a water droplet erosion resistant coating.

As the coated samples were tested at different numbers of water droplet impacts, it would be better to compare the length of the incubation stage, where the mass loss remains insignificant (shown in Figure.5.11). Coatings that exhibit a longer incubation stage generally tend to have significantly better water droplet erosion resistance.

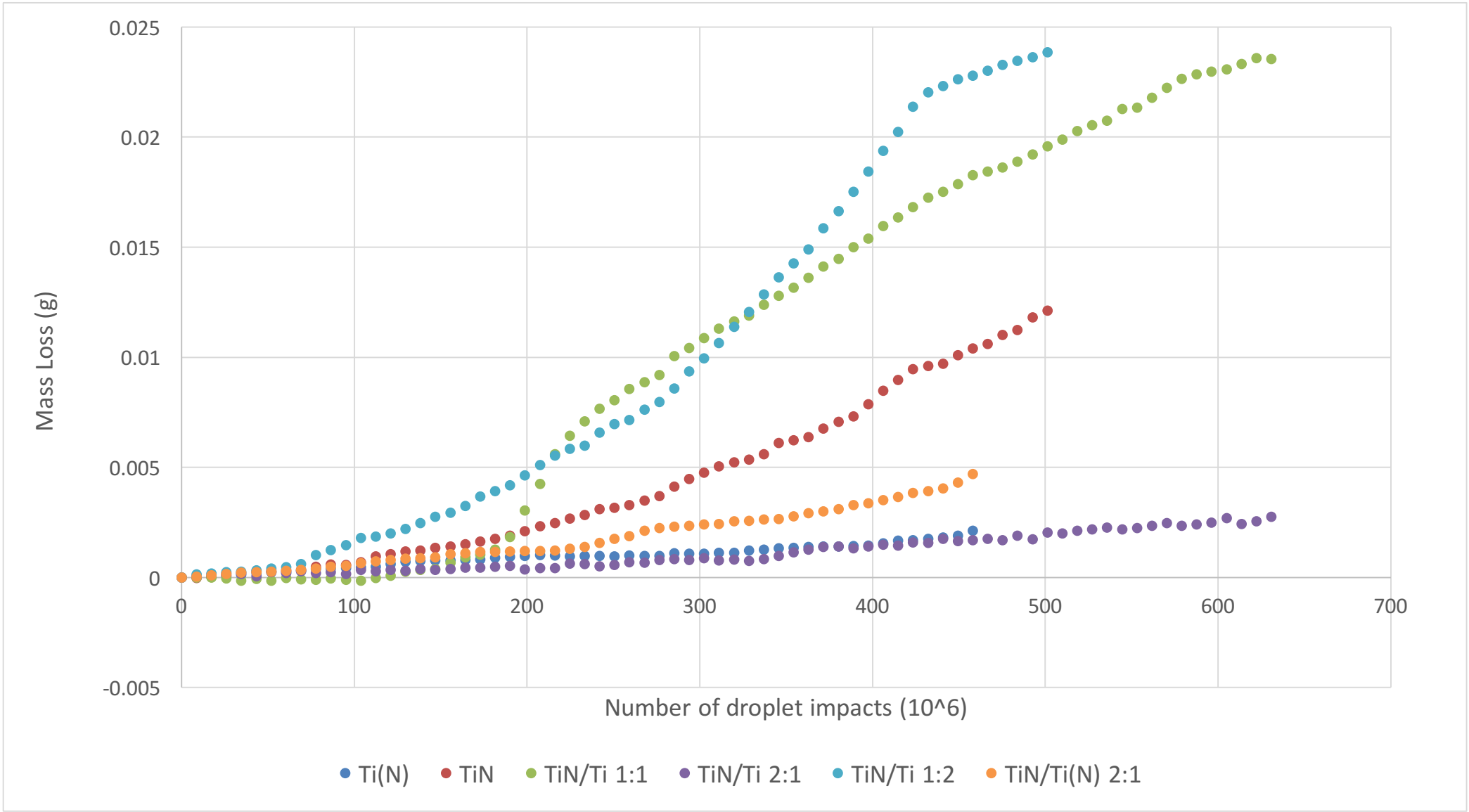

Figure. 5.10 Full data of coating total mass loss with respect to the number of droplet impacts

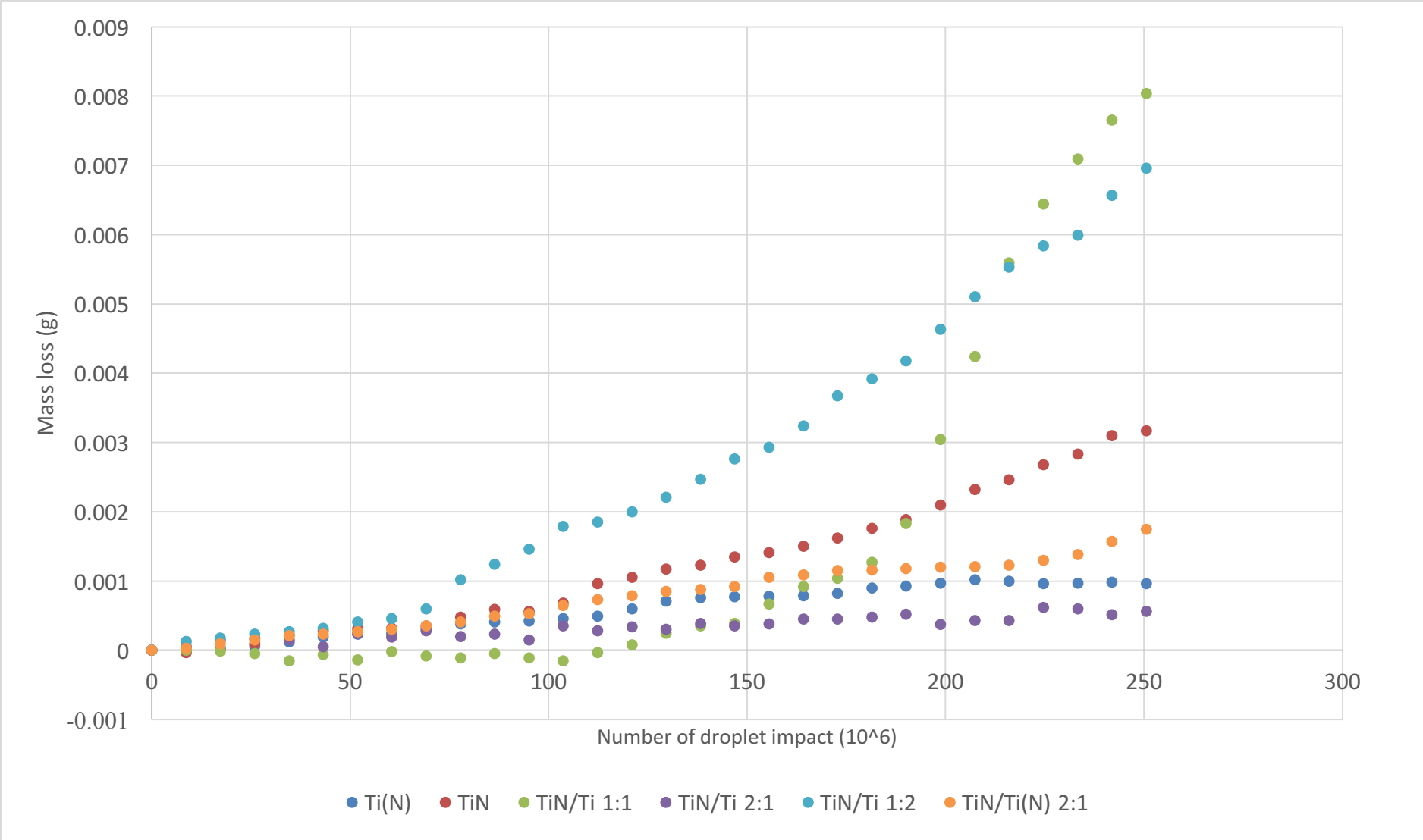

Figure. 5.11 Early stages of water droplet erosion coatings total mass loss with respect to the number of droplet impacts

The Ti(N), TiN/Ti 2:1 and TiN/Ti(N) 2:1 coatings appear to still be in the incubation stage (first stage of erosion) after 400 x10^6 droplet impacts. The coating with the shortest incubation stage is the TiN/Ti 1:2 coating (50x10^6 droplet impacts) followed by TiN/Ti 1:1 coating (180x10^6 droplet impacts) and lastly by the TiN monolithic coating (280x10^6 droplet impacts). The length of each coating incubation period and the stages of erosion are summarized in Table. 5.1

Table. 5.1 Different multilayer coating stages of erosion and approximated length of incubation periods

Coating	Stages of erosion (referring to section 2.2.5)	Approximated length of incubation period (number of droplet 10^6)
Ti(N)	Incubation stage	N/A
TiN	Deceleration stage	280
TiN/Ti 1:1	Acceleration stage	180
TiN/Ti 2:1	Incubation stage	N/A
TiN/Ti 1:2	Deceleration stage	50
TiN/Ti(N) 2:1	Incubation stage	N/A

In comparing the Ti(N) and TiN monolithic coatings, the main reason that the Ti(N) performed better than the TiN is due to the high elastic modulus of the TiN coating, which makes it much more brittle (and less resilient) than the Ti(N) coating. This suggests that even though the ability to laterally dissipate acoustic stress waves is better in the TiN coatings, due

to exhibiting higher stress wave velocity because of significantly higher elastic modulus (and slightly higher density); the mechanical considerations of load bearing capacity (i.e. toughness and resilience) must first be satisfied.

For the TiN/Ti multilayer coating group, the TiN/Ti 2:1 multilayer was superior in this category. My assessments of why the TiN/Ti 2:1 exhibits better water droplet erosion resistance than its counterparts, TiN/Ti 1:1 and the TiN/Ti 1:2, are as follows:

- In terms of mechanical considerations, the TiN/Ti 2:1 coating probably has the highest 'composite' resilience, due to containing the highest volume fraction of (hard/stiff) TiN in its multilayer coating system.
- In terms of the acoustic consideration of longitudinal stress waves, since the compressive wave velocities of TiN and Ti are $9800ms^{-1}$ and $5050ms^{-1}$ respectively (i.e. with virtually a 2:1 ratio of difference in acoustic wave velocity), the TiN/Ti 2:1 coating will also help to create standing waves, owing to the matching of the propagated and reflected wave fronts. The coating architecture will help to diminish the phenomenon of tensile reflected waves that constructively interfere with the surface waves; which is likely to be mainly responsible for the relatively poor water droplet erosion performance seen in the other coatings.

In comparing the whole of the multilayer coatings with both Ti and Ti(N) interlayers, the multilayer coating with Ti(N) interlayer appears to have a worse water droplet erosion performance at the earlier stages of erosion. although this is not conclusive since both of the coatings are deemed to still be in the incubation stage. If the test was extended, there is a possibility that the multilayer coating with Ti(N) interlayer may outlast a multilayer coating with a Ti interlayer.

Basing my arguments on the current experimental results, having a Ti(N) interlayer (compared with a pure titanium) worsens the water droplet erosion performance. This is perhaps due to the Ti(N) having a higher elastic modulus than a pure Ti interlayer. This ultimately stiffens the multilayer system and is probably responsible in reducing the overall toughness. Furthermore, in terms of the acoustical considerations, a Ti(N) interlayer conceivably possesses a higher acoustic impedance (due to higher elastic modulus and most likely slight increase in density) than a pure Ti interlayer. This would result in lower acoustic impedance mismatch between the metallic/ceramic layers, which is not desirable since it lowers the ability of the multilayer to attenuate the propagating acoustic compressive stress wave front.

According to Figure. 5.11, unpredictably the TiN/Ti 1:1 showed a slight mass gain in the early stage of water droplet erosion. The cause of the mass gained seems to be oxidation of both the TiN and Ti layers. This also suggest that, for multiple supersonic velocity water droplet erosion, droplet collapse can induce 'flash' temperatures exceeding 350^{o}C (temperature at which ceramic TiN coating oxidizes in cutting tool abrasion). This will therefore make the requirements for selection of coatings in this field even more challenging.

Characterization of the erosion damage was performed both qualitative and quantitatively. The optical micrographs in Figure.5.12 reveal the appearance of the erosion track in multiple-impact WDE (similar wear tracks are seen by Kamkar et.al. [109] in testing of uncoated Ti-6Al-4V. Large deep (and shallow) craters can be seen along the wear tracks).

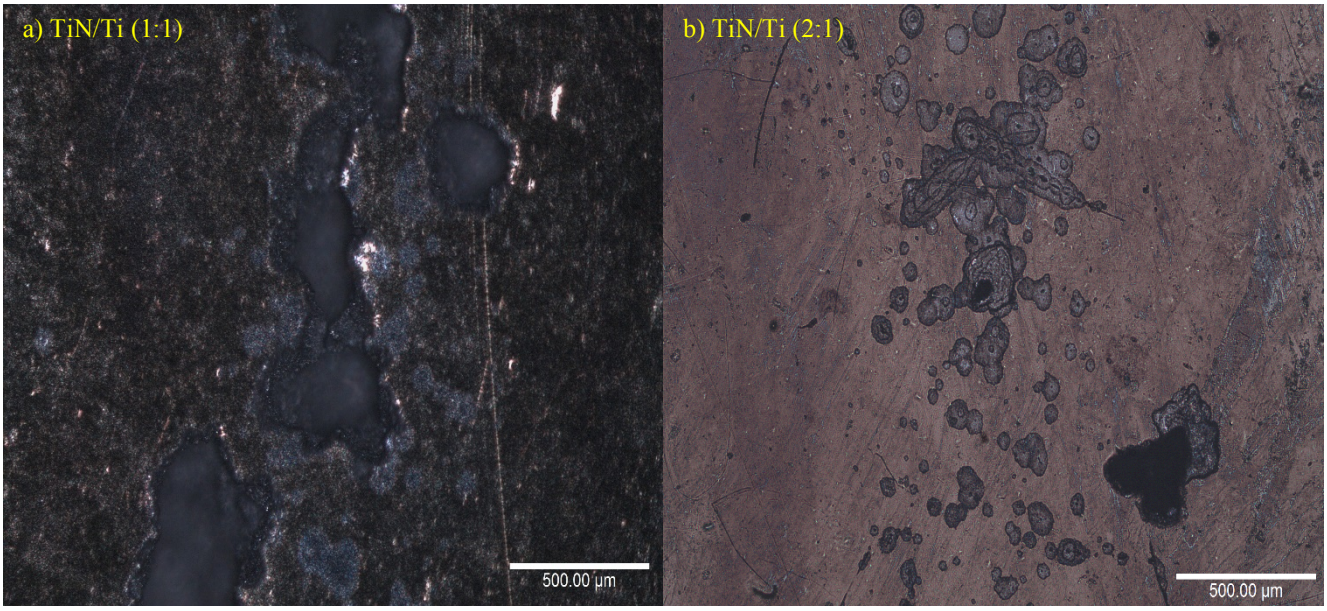

Figure. 5.12 Shows the water droplet erosion wear tracks of a) TiN/Ti 1:1 and b) TiN/Ti 2:1 multilayer coatings

The SEM was performed to reveal the details of the surface morphology of the damage done to the surface of the coatings in water droplet erosion. Firstly, The TiN monolithic coating was examined (as shown in Figure. 5.13). Figure 5.13 a) reveals that substrate fracture morphology is rough, which coincides well with behavior of ductile tearing. The coating fracture morphology appears to be smooth (observed around the edge crater), which often seen in fracturing of brittle material.

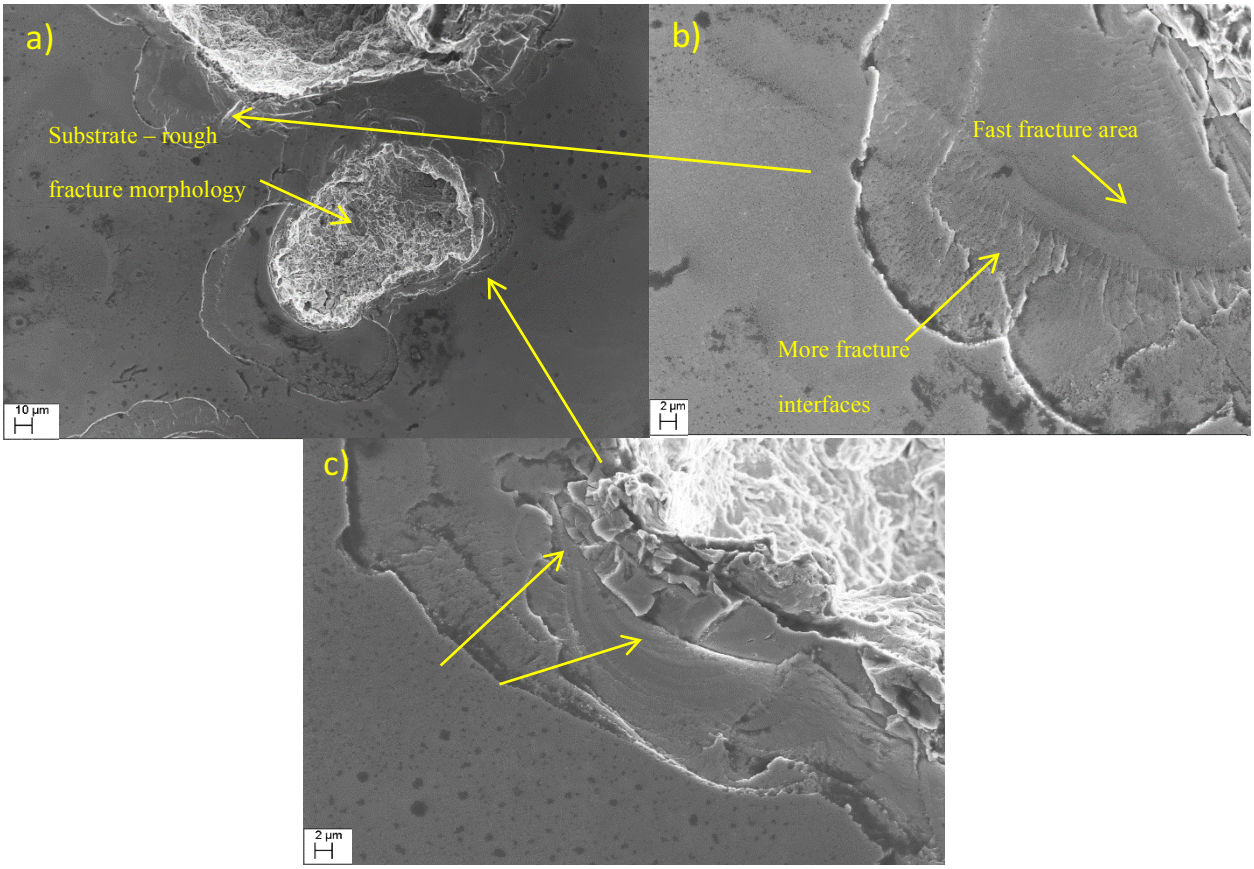

Figure. 5.13 SEM micrograph of monolithic TiN coatings; a) wear crater at low b) and c) edge of the impact crater at higher magnification

Figure 5.13 b) shows area of fast fracture near the edge of the impact crater then after that there appears to be an area of multiplication of fracture interfaces. Additionally, Figure 5.13 c) shows a ripple-like damage morphology at the edge of the impact crater. The cause of these (ripple-like) craters is probable firstly due to the high induced impact pressure and stress waves propagation when a water droplet impact onto the coating surface. This high pressure will likely to cause surface depressions (and asperities).

Various sizes of ripple-like or 'meteor-impact likes' crater are the main damaged morphology observed in the multilayer coatings, shown in Figure. 5.14. Furthermore, it appears that the multilayer coating failed progressive layer by layer detachment. This would be advantageous, since this will delay the substrate from being fully exposed to the impinging

water droplet. The detachment of the layers probably occurs when cracks coalesce with each other. This agrees well with Holleck's proposed multilayer strengthening mechanism [62], where crack propagation across the hard/stiff layer is discontinued and gets deflected once it reaches the soft/ductile interlayer.

However, small craters of ~1-10 μm diameter appear to have a different failure mechanism, this is where ejection of the whole multilayer coating is observed, this is shown in Figure. 5.15. The ejection of the coating may be due to defects at the coating/substrate interface, making this localized zone weaken. Another argument is that very small droplet sizes (possibly, of the crater size 1-10μm) may be more damaging than larger droplets. Smaller droplets would have a shorter impact impulse duration and this may increase the strain-rate experienced by the coating.

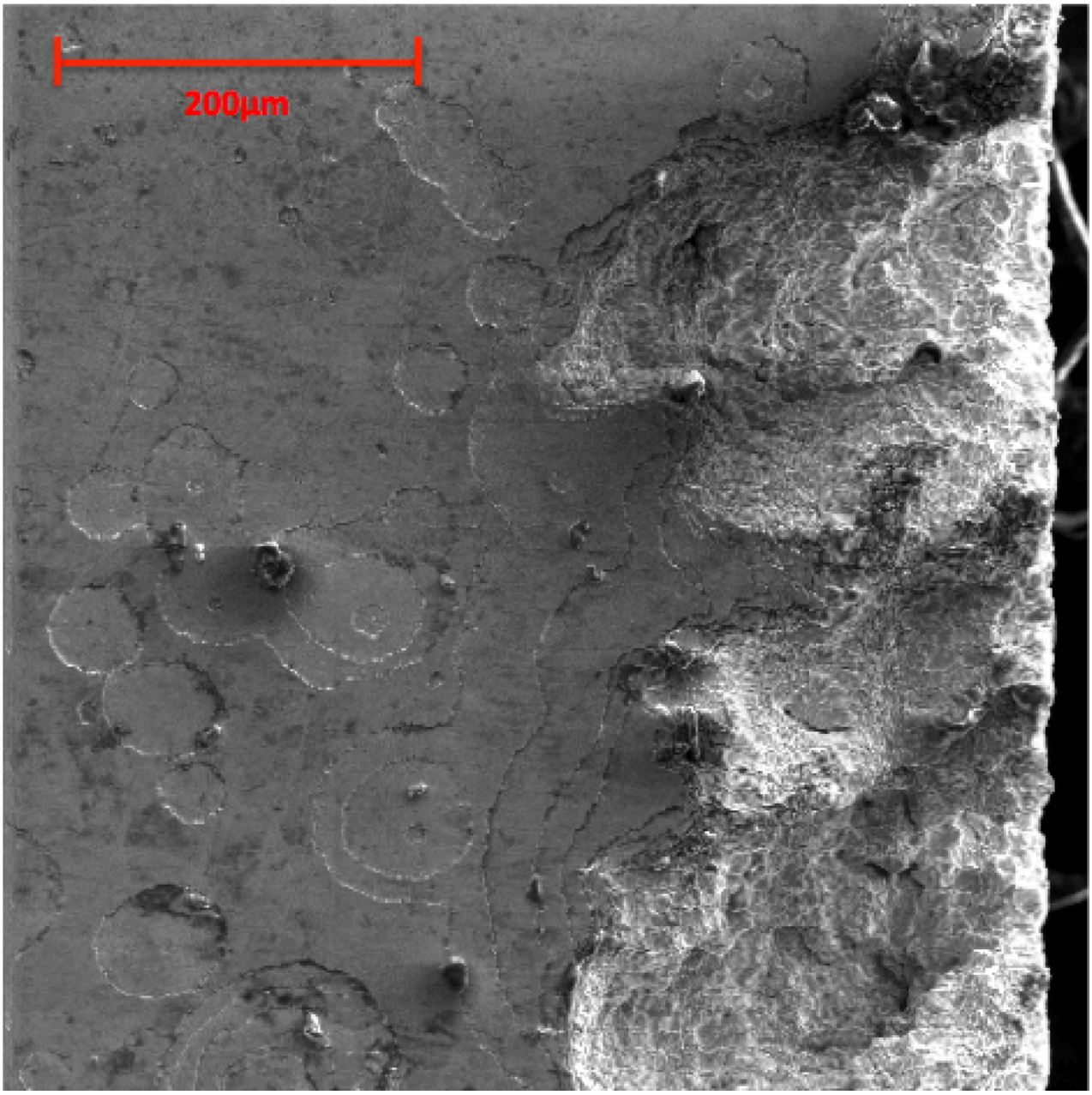

Figure. 5.14 Multilayer coating ripple-like or meteor-impact like craters of various sizes.

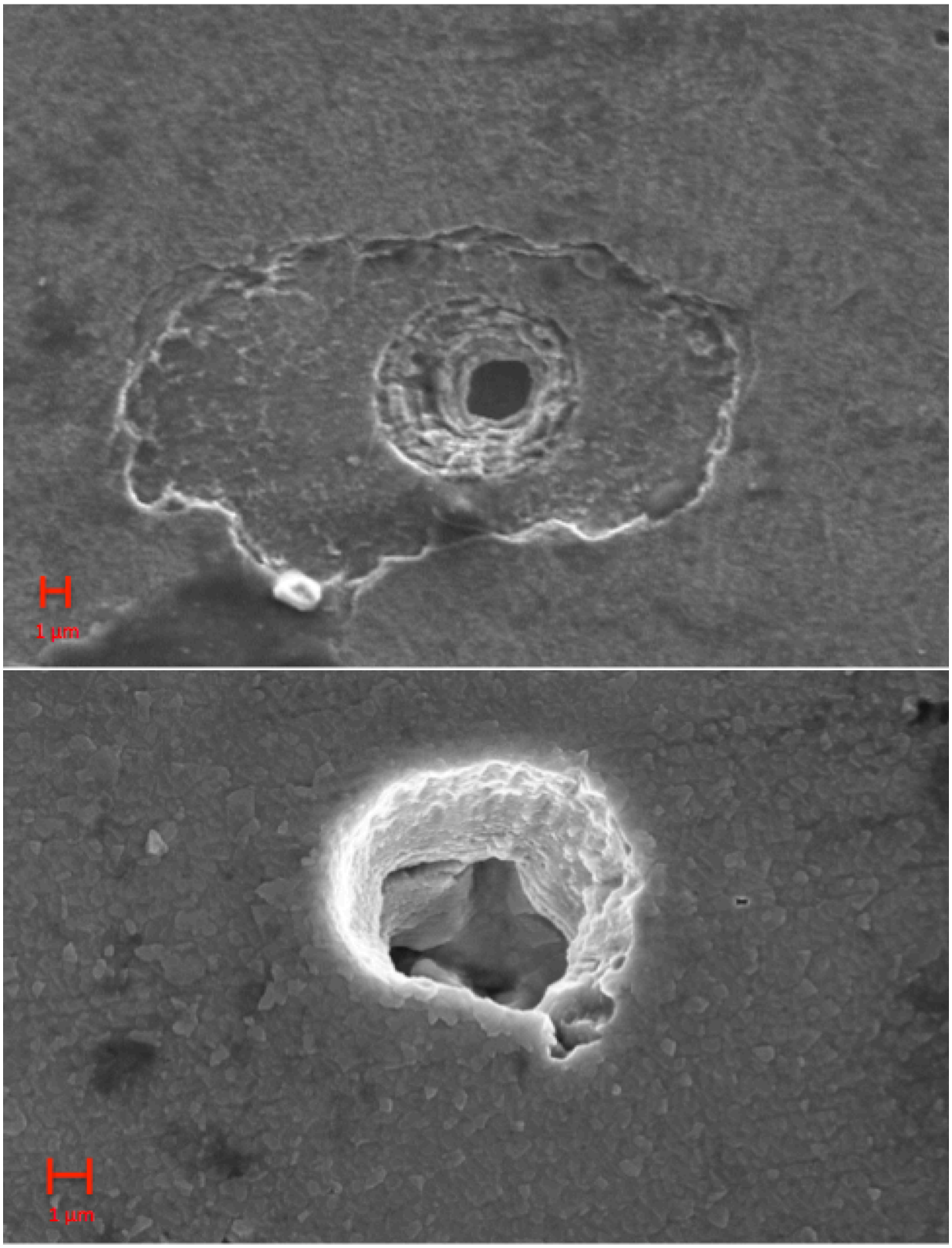

Figure. 5.15 Small crater ejection of coating with the approximated diameter of crater size a) 6µm and b) 2µm

Qualitative EDX measurements were performed on the surface of the TiN/Ti 2:1 multilayer coatings which were subjected to water droplet erosion to investigate the occurrence of oxidation. The results shown in Figure.5.16 indicate that oxidation happens in both the TiN and Ti layers. This may imply that the 'flash' temperature upon water droplet impingement at supersonic speed exceeds 350^{o}C (temperature at which ceramic TiN coatings oxidize in cutting tool abrasion). This confirms that mass gain seen in the early (incubation) stages of water droplet erosion is likely to be due to the formation of oxides on the surface.

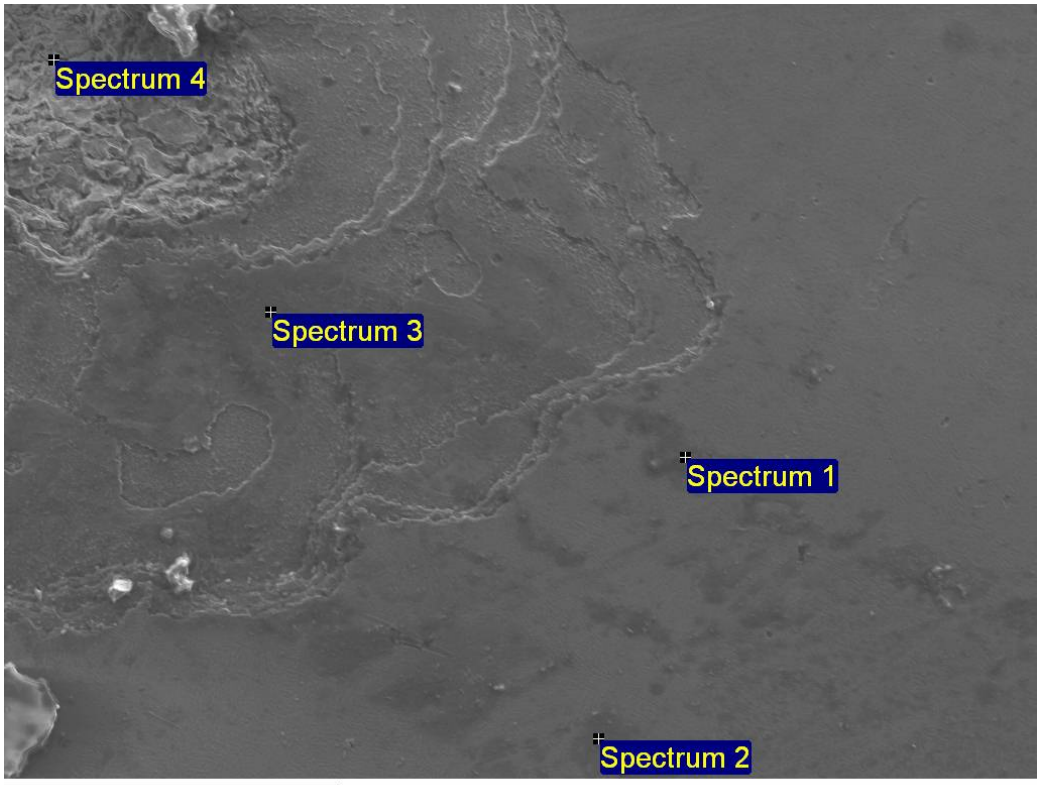

Spectrum	In stats.	N	O	Ti	Fe
Spectrum 1	Yes	6.92	41.79	51.29	
Spectrum 2	Yes	20.29	30.63	49.08	
Spectrum 3	Yes	-5.83	47.89	57.94	
Spectrum 4	Yes				100.00

Figure. 5.16 Qualitative EDX of the TiN/Ti 2:1 multilayer coating subjected to water droplet erosion

The selected TiN/Ti multilayer coatings, with thickness ratios of 1:1 and 2:1, exposed to ~630 x 10^6 water droplet impact (advance stage of erosion) were chosen for TEM analysis (Shown in Figures. 5.17 and 5.18, respectively). To further investigate the damage under water droplet erosion, damaged regions (inside the wear tracks) were analyzed. Selected Area Electron Diffraction (SAED) patterns, together with bright field (BF) and dark field (DF) transmission images were collected.

The TEM analysis of the damaged region reveals insights on the failure mechanisms of the TiN/Ti 1:1 and 2:1 multilayer coatings under water droplet erosion, shown in Figure 5.17 and 5.18, respectively. The higher number of cracks observed in the TiN/Ti 1:1 coating is due to the advanced stages of erosion (deceleration), where TiN/Ti 2:1 coating is apparently, still in the earlier stages of erosion (incubation).

The fact that cracks are only mainly concentrated in the TiN layers (and not in the Ti layers), coincides with the proposed mechanisms of fatigue-crack propagation in brittle and ductile solids, where crack initiation and growth rate in brittle solids are more sensitive to the applied loading than in ductile solids. However, in the advanced stages of erosion (shown in Figure.5.17) of the TiN/Ti 1:1 multilayer coating, cracks from the TiN layers appear to have propagated in the soft Ti interlayers as well

Interestingly, in the TiN/Ti 2:1 multilayer coating (Figure 5.18), the propagation of cracks in the TiN layers seems to be terminated once it reaches the soft Ti interlayers. This may confirm the multilayer strengthening mechanism theory proposed by Holleck [62], where the soft interlayer material acts as a site of stress dissipation and blunts the crack tip. Furthermore, Figures. 5.17 and 5.18 shows crack propagation appears to be perpendicular to the coating surface and along the columnar structure

Moreover, particularly with the HCP crystal structure, twinning deformation is commonly observed [110-112]. There is also a strong correlation between the degree of twinning deformations and the magnitude of the applied stress, high stress promotes more twinning of the grains [113, 114]. In the SAED pattern shown in Figure.5.19, a large column structure at the 6^{th} layer (corresponding to a Ti layer), reveals the occurrence of twinning deformation. Surprisingly, twinning is not observed in any other regions of the sample. The reason for this may lie in that the sample taken is very small and localized μm), other areas may exhibit higher density of twinning deformation.

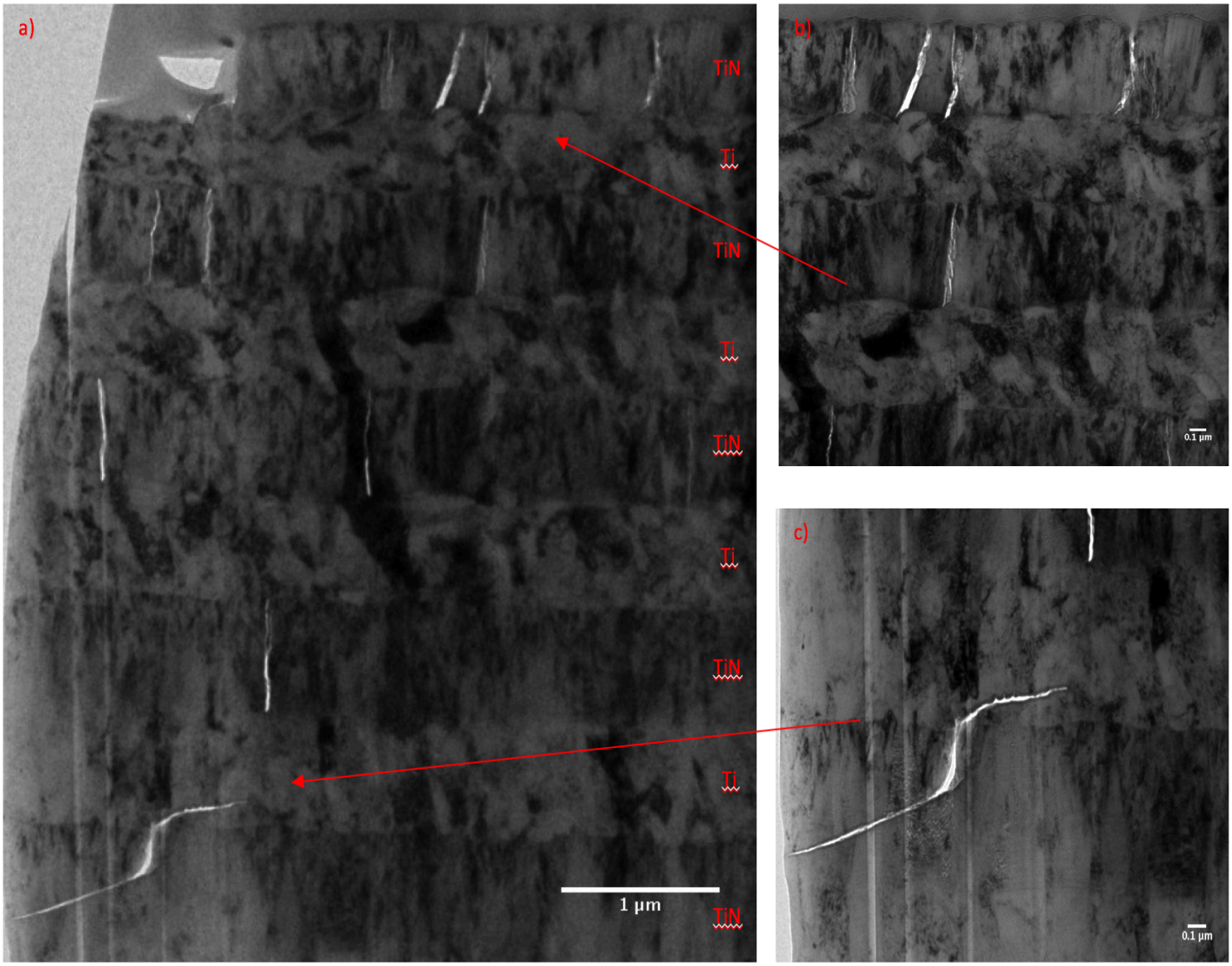

Figure. 5.17 TEM imaging of the advanced stages of erosion in the TiN/Ti 1:1 coating a) Cross-sectional BF imaging at low magnification; b) BF imaging of cracks in the first few layers at high magnification; c) BF imaging of a crack propagating through the TiN hard layer and the soft Ti interlayer at high magnification

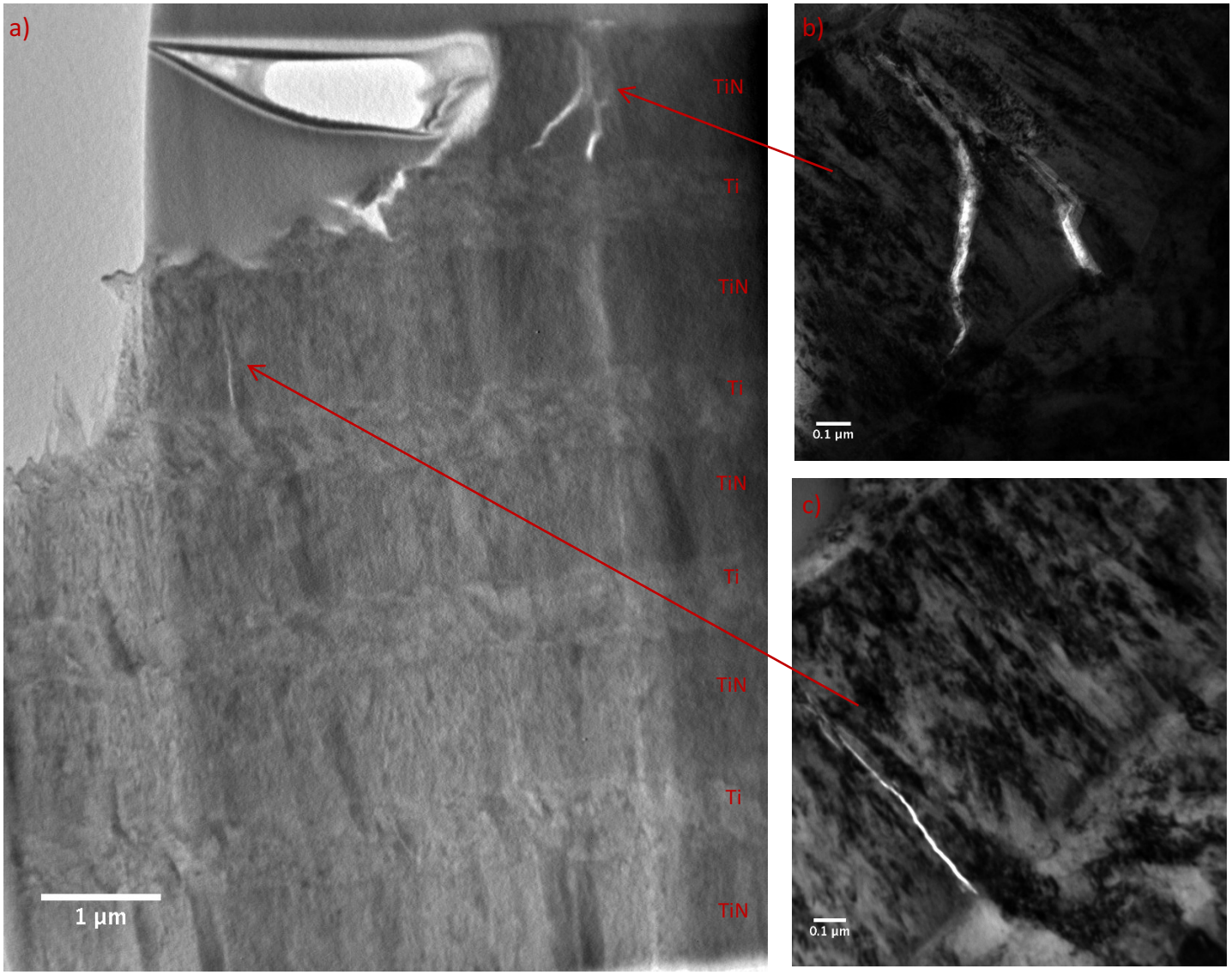

Figure. 5.18 TEM imaging in the earlier stages of erosion in the TiN/Ti 2:1 coating a) cross-sectional BF imaging at low magnification; b) BF imaging of cracks in the 1st layer (TiN) at high magnification; c) BF imaging of a crack at the 3rd (TiN) layer at high magnification

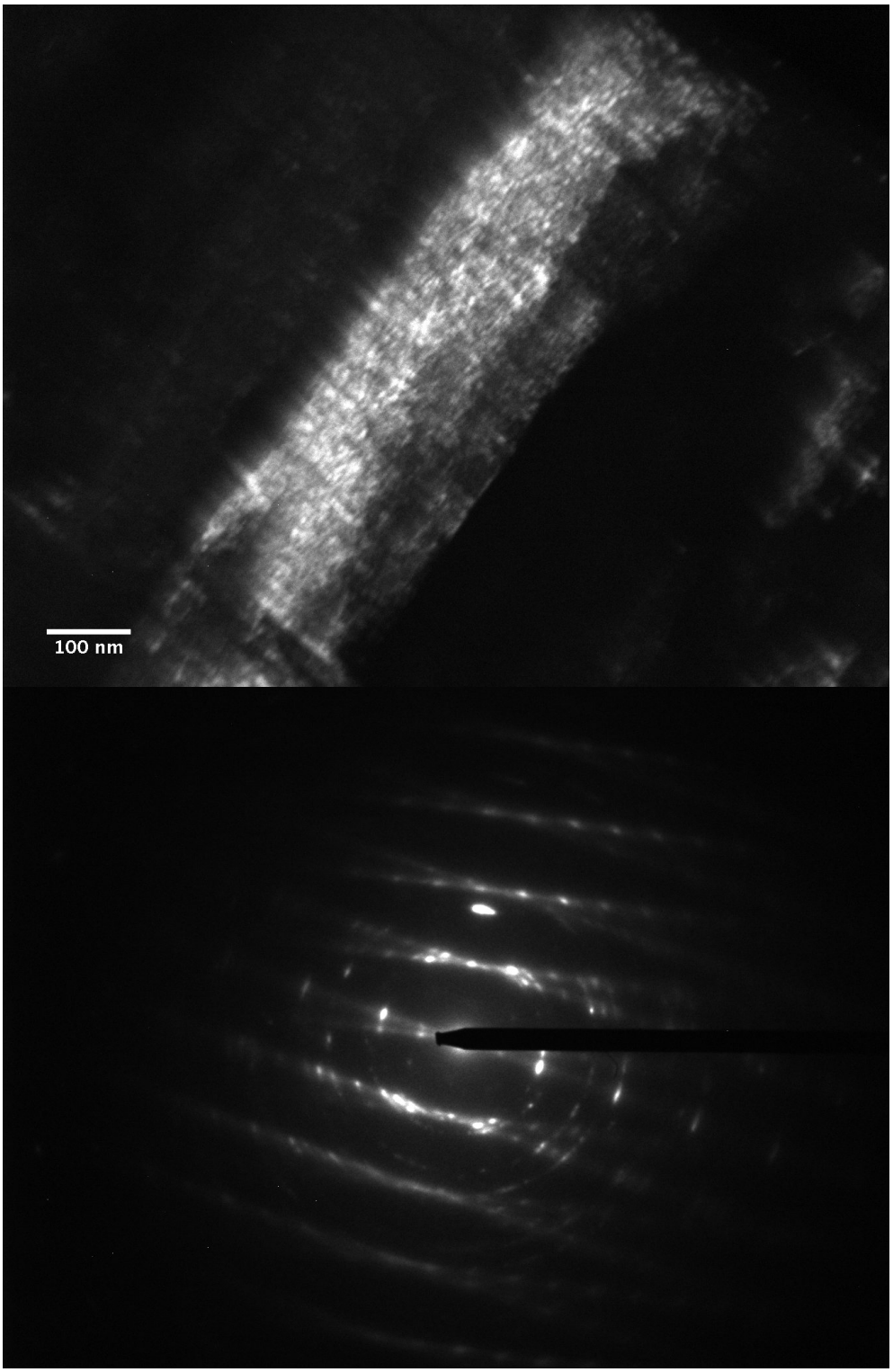

Figure. 5.19 a) DF imaging shows a large column in the 6th (Ti) layer in the TiN/Ti 2:1 multilayer coating, with b) its corresponding SAED pattern.

Chapter 6 Summary and Conclusions

6.1 Ball-on-Plate (solid particle impact) test summary

The TiN/Ti 1:1 coating was clearly superior to all other coatings in the ball-on-plate impact wear. Ti(N) with 0-15 ml of nitrogen flow rate shows no significant improvements to the impact performance compared with to a pure Ti coating. A monolithic TiN ceramic coating exhibits the worst impact wear performance, attributed to its brittle nature and high elastic modulas compared to the M2 steel substrate.

Amongst the multilayer coatings, both the TiN/Ti and TiN/Ti(N), the coatings with a thickness ratio of 1:1 appear to exhibit the best impact wear resistance. The thickness ratio of 1:1 maybe best in the combination of strength and toughness, wheres 2:1 ratio sacrifices toughness and 1:2 ratio sacrifices strength.

Substituting the Ti interlayer with a Ti(N) interlayer apparantly worsens the impact wear performance. Hardness for the Ti(N) interlayer is predicted to increase over two-fold, whilst the elastic modulus will only increase by approximately 25% compared to a Ti interlayer. this implies that hardness has minimal influence in impact wear conditions – and that resilience (i.e. high H/E) and or toughness (i.e. low E, high ductility) are probably more significant factors. Moreover, it may be suggested that selecting an even lower elastic modulus than Ti for an interlayering material maybe provide enhancement to the impact wear resistance. Furthermore, the ball-on-plate impact wear performance appears to correlate better to the H/E ratio than the H^2/E ratio.

6.2 Water Droplet Erosion WDE (liquid particle impact) test summary

From the experimental results it is inconclusive whether the titanium-based monolithic or multilayer coatings would perform better in water droplet erosion. The nitrogen-doped Ti(N) performed equally as well as the TiN/Ti 2:1 and both TiN/Ti 1:1 and TiN/Ti 1:2 coatings performed poorly.

The reason the TiN/Ti 2:1 multilayer coating performed better than the other multilayers may be attributed to a more optimal combination of strength and toughness in the mechanical considerations. Furthermore, the TiN/Ti 2:1 multilayer coating satisfies the acoustical considerations in terms of minimisation of constructive interference of reflected longitudinal waves with surface (Rayleigh) waves, by attenuating the longitudinal wave component.

Monolithic TiN performed poorly due to the brittle nature of the coating. As confirmed by SEM micrographs, brittle (smooth) fracture morphology and cracks are observed around the edges of the impact craters.

TiN/Ti multilayer coatings appear to performed better than the TiN/Ti(N) coatings. This is probably due the Ti(N) having higher elastic modulus (and lower ductility) than a pure Ti interlayer. This ultimately stiffen the multilayer system and is probably responsible for reducing the overall toughness. Furthermore, in terms of acoustical considerations, a Ti(N) interlayer probably possesses a higher acoustic impedance (due to higher elastic modulus, and most likely slight increase in density) than a pure Ti interlayer. This would result in reduced acoustic impedance mismatch among the metallic and ceramic layers, which is not desirable -since it lowers the ability of the multilayer to attenuate the propagating longitudinal stress waves.

EDX analysis suggests that there is a possibility that even TiN oxidizes under water droplet erosion. This suggests that the 'flash' temperature exceeds 350^{o}C. Information on the 'working temperature' of the samples under water droplet erosion is not available.

TEM micrographs of the damaged areas of the multilayer coatings after water droplet erosion reveal that, in the early stage of erosion, cracks are observed mainly in the TiN layers, which are brittle. Coated samples in the advance stages of erosion show that cracks are able to grow and eventually will propagate into the soft Ti interlayers.

6.3 Conclusions

This thesis illustrates the versatility of the trode ion-plating PVD technique and its capability to produce thick Ti, Ti(N) and TiN monolithic coatings and TiN/Ti , TiN/Ti(N) multilayer coatings with reliable controllability in terms of chemical composition and designated layer thickness. The high deposition rate of the electron-beam triode ion-plating technique is also commercially viable.

This thesis has critically reviewed existing literature in various scientific fields and has tried to point out (and also bridge) some of the knowledge gaps within the field of water droplet erosion. Many models and theories has been proposed on how to build coatings to resist water droplet erosion. However, quite basic assumptions are usually made in all of these models and theories which do not usually incorporate both the mechanical (stresses/strains) and acoustical (stress waves) considerations. Furthermore, most proposed models and theories are not validated experimentally, which brings into question their validity. The fact that the mechanical and acoustical aspects are not concurrently considered in the models and theories proposed so far may be due to the complex interaction between a liquid water droplet and a solid material surface, where modelling techniques to consider both components are not yet available.

According to the results of this work, there is a definite distinction between the coating requirements for solid particle impact tests and liquid particle water droplet erosion. A TiN/Ti 1:1 multilayer coating performed the best under the repetitive ball-on-plate impact test; however, for water droplet erosion testing, monolithic Ti(N) and a TiN/Ti 2:1 multilayer performed equally as well. Furthermore, substituting Ti with Ti(N) interlayers in the multilayer coating worsens both the solid particle impact test and liquid droplet erosion test performance. The fact that Ti(N) worsens the wear performance suggests that it would be beneficial to find an alternative interlayer which can exhibit lower elastic modulus, as well as

higher hardness. Additionally, comparison of the experimental results confirms that a solid particle test cannot serve as an alternative to water droplet erosion testing (strain rates are too low and the impulses during which the energy is transferred are too long).

There is continuing debate as to whether a multilayer or a monolithic coating performs better in erosion applications. Experimental data gathered in this thesis on the subject of water droplet erosion has provided clues for the design aspects to consider in building the 'right' coating architecture to resist water droplet erosion (WDE). The multilayer coating approach of alternating layers of hard/stiff and soft/complaint material seems to be the way forward in building protective WDE coatings. As shown in this thesis work, the propagation of cracks in the hard/stiff (TiN) layer seems to be terminated once it reaches the soft/complaint (Ti) interlayers. This may also confirm the multilayer strengthening mechanism theory proposed by Holleck [62], where the soft interlayer material acts as a site of stress dissipation and blunts the crack tip. Furthermore, architectural design in multilayer coatings must consider the energy dissipated both mechanically (stresses/strains) and acoustically (stress waves). Choosing the 'right' architectural multilayer design will optimize the ability of the coating in both dissipation of the mechanical stresses/strains and attenuation of the acoustic stress waves, where monolithic coatings cannot offer the same design flexibility.

Furthermore, the information gathered experimentally was analyzed (with existing proposed models and theories) and interpreted to propose my own designs for both monolithic and multilayer a coatings to better resist WDE (presented in following section.6.4.1)

6.4 Recommendations for future work

- In order to understand and validate coating models to resist water droplet erosion (and because of the lack of availability of WDE testing equipment and its' time-consuming nature), appropriate modelling appears to be the alternative solution to the problem. However, even modelling conditions of water droplet erosion proves to be a challenge. This is due to the complex mechanical and acoustical interactions that occur during water droplet impact. These phenomena include the compressibility of the impinging water droplet, high generation of heat during droplet compression and collapse, high-strain rates, longitudinal and lateral short impulse times, longitudinal and lateral stress wave propagation (and their interactions) and lateral supersonic jetting after droplet collapse. Conventional computational modelling techniques such as finite element modelling (FEM) may not be an appropriate approach. Since the model needed in this application is an acousto-mechanical (liquid-solid impact) model, FEM may not be able to include all of the conditions in its model. Moreover, the fact that accuracy of FEM results relies on the quality of mesh construction (ultra-fine mesh is needed) means that a massive amount of data needs to be processed; this prohibits the practicality of such techniques, where even the most powerful computer (supercomputers) may not be capable of processing data of this magnitude. Thus, the key to produce a feasible and accurate model may lie in the recent development of modelling techniques such as Smooth Particle Applied Mechanics (SPAM), where the technique is mesh-free and involves only differential equations [115, 116].
- As the results indicate that multilayer coatings containing the Ti(N) interlayers performed worse than 'pure' α-Ti interlayers, lowering the elastic modulus (and/or increasing the ductility) of the interlayer may increase the erosion resistance of the

multilayer coating. Alloying titanium with group V and group VI elements is potentially of great interest, to produce multilayer coating systems such as (Ti,Nb)N/TiNb. Since the TiNb interlayer will exhibit the BCC crystal structure, as Niobium is a beta-stabilising element for titanium, it is therefore expected to have a much lower elastic modulus than HCP α-Ti and also show enhanced twinning effects, with low work hardening. Such a multilayer system may however only be possible to deposit using the technique of magnetron sputtering, because (as demonstrated in this thesis) the electron-beam triode ion plating system does not have enough power to co-vaporize Ti and Nb.

- As discussed previously, knowledge of the most damaging frequency ranges of acoustic waves associated with water droplet impingement onto a component under real-life applications is absent. The fact that this aspect has not been explored is due to the difficulty in implementing a suitable measurement device onto the water droplet machine itself. However, there may be a possibility to remotely sense the frequency response using thin, PVD-deposited piezoelectric coatings such as Lead Zirconate Titanate (PZT) or AlN/Al.

6.4.1 Proposed design of a protective coating for water droplet erosion

In order to design a coating for a particular wear application, one must understand the materials' physical phenomena in respect of their application. As shown from the results, coating requirements for water droplet erosion differ from solid particle applications.

The main purpose of this thesis work was to attempt to link existing (but fragmented) knowledge of different aspects of water droplet erosion and the requirements to construct a protective coating to resist it. Emphasis is given to the influence of the coating properties i.e. hardness; elastic modulus; density; Poisson's ratio in the ability to counteract different damage phenomena; extremely high contact pressure; stress wave propagation; jetting and excessive heating that occur in high-speed water droplet erosion. These occurrences make the design of the coating challenging. Despite the efforts that have been put into this field over the past 50 years, no one has solved the problem of water droplet erosion.

Designing a coating to resist water droplet erosion requires a wide field of knowledge in the mechanical and acoustical properties of materials, tailoring the properties to maximise its performance. Typically, a coating design focuses on just the mechanical properties, however, due to the phenomenon of bulk longitudinal and surface lateral stress wave propagation (and their interactions), the acoustical properties of a coating cannot be ignored in WDE.

Stress wave propagation is more important in water droplet than solid particle impact due to the differences in the impact impulse. The impact impulse is usually two to three orders of magnitude more in the solid particle impact. Thus, stress waves can be attenuated in the incident solid particle. Due to the short impact impulse (nanoseconds) in water droplet erosion, attenuation of stress waves does not occur in the water droplet and subsequently is

passed into the impacted material. Therefore, the design of a coating must serve as a means to mitigate these stress waves.

According to the results, the design of the coating to resist WDE can both be monolithic or multilayer, but multilayer coatings offer versatility in terms of wave-attenuating architectural structural features, compared to monolithic coatings. Therefore, I would like to proposed designs for both monolithic (chromium-based) and (titanium-based) multilayer coatings.

6.4.2 Monolithic coating (chromium-based)

A chromium-based coating is chosen instead of titanium-based monolithic coating because I would like to build a compositionally-graded coating. If you elect to build compositionally-graded titanium-based coating, I believe that the formation of Ti_2N ceramic phase (in large quantities – near the coating surface) would be detrimental to the wear performance, since Ti_2N is an extensively brittle phase (high E). Thus building a compositionally-graded chromium-based would be more beneficial because the Cr_2N phase does not exhibit excessively modulus – and can co-exist with either Cr(N) metallic or CrN ceramic coating phase constituents without compromising the coating structural integrity.

The proposed monolithic coating design is shown in figure.6.1. The coating is a compositionally-graded chromium-based coating. This design can be achieved by constantly increasing the nitrogen gas flow rate with respect to the deposition rate. The coating is designed so that the top part of the coating is chromium nitride (hard and elastically stiff) and the bottom part (coating-substrate interface) is pure chromium (relatively soft and compliant). The top is chosen to be CrN due to its high/moderate hardness and moderate elastic modulus. High elastic modulus is desired to dissipate the stress waves faster by means of higher speed. However, excessive elastic modulus leads to the material being very brittle and may it fail prematurely.

As discussed earlier, according to the Dundurs' parameters, compositional grading of the coating, with decreasing elastic modulus to match the substrate elastic modulus, will serve to increase interfacial toughness (adhesion). Also, the pure chromium composition towards the bottom will help to accommodate the coating/substrate interfacial loading. Furthermore, the primary acoustical consideration is satisfied, since stress waves will be attenuated faster, due to the propagation through ultimately 'dissimilar' media throughout the coating.

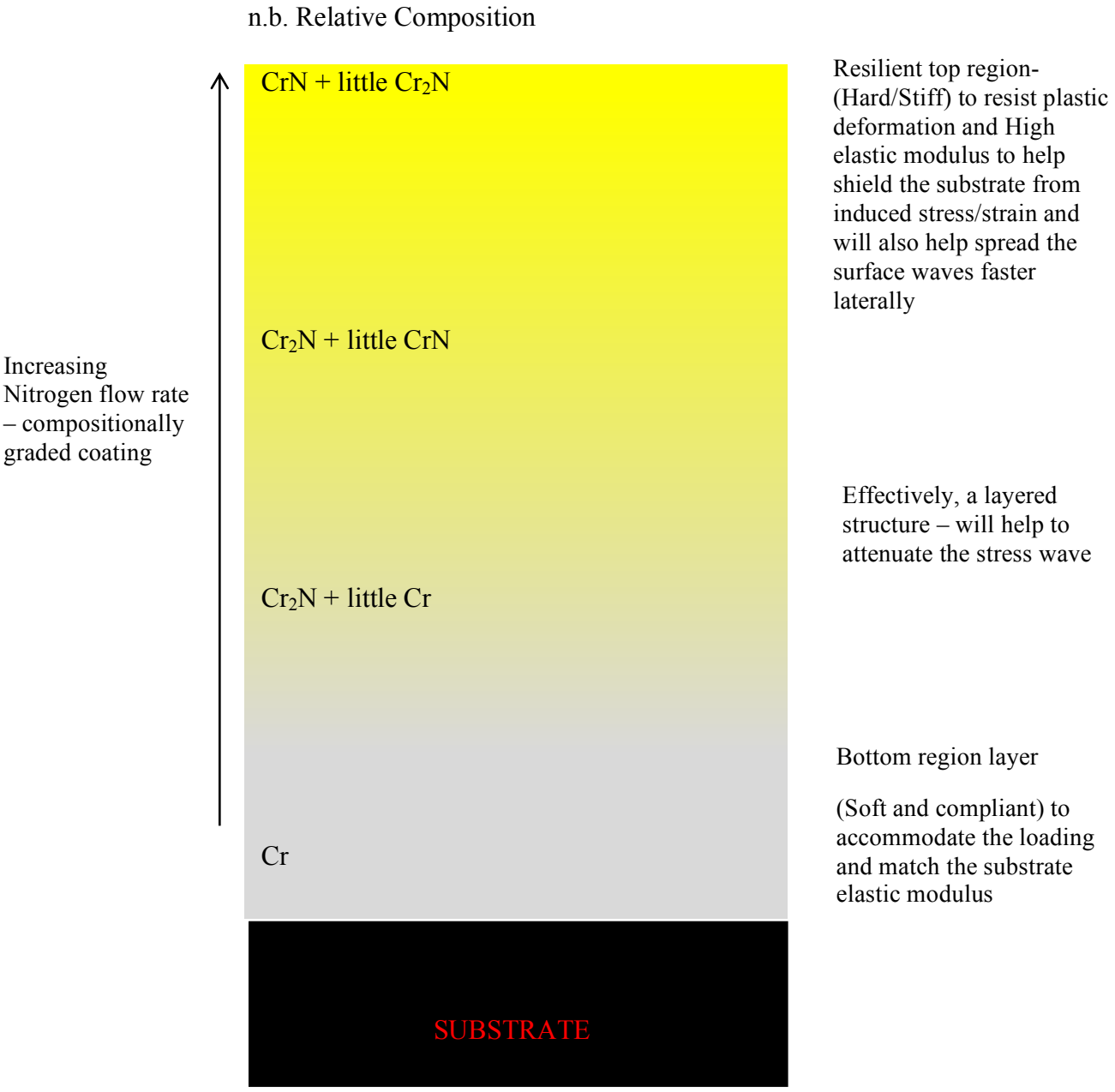

Figure. 6.1 Proposed ideal chromium-based compositional graded coating

6.4.2 Multilayer coating (TiN/Ti based)

Due to the superior water droplet erosion performance of the multilayer (TiN/Ti 2:1) coating presented in this thesis work – the proposed design of the multilayer coating will be based on this architecture (but with optimised aspects). The multilayer coating design will be much more complex (than a monolithic coating); this is shown in figure.6.3. The designed multilayer has 14 layers with a total thickness of around 20-30μm. It would have been ideal to increase the thickness to more than 100μm; however, it is not yet commercially feasible to produce such thick coatings without compromising the coating integrity (or overheating the metallic substrate). The first layer, counting upwards from the substrate, is an adhesion-promoting interlayer where optimal thickness would be in the order of 100-250nm. From the experimental results, it has been established that the TiN/Ti with the thickness ratio of 2:1 performed the best under water droplet erosion. This may suggest that water droplet erosion applications require an even higher ratio of TiN than Ti. Moreover, there is a lack of literature data and information that systematically investigates ceramic-metal or metal-metal thickness ratios in multi-layered systems.

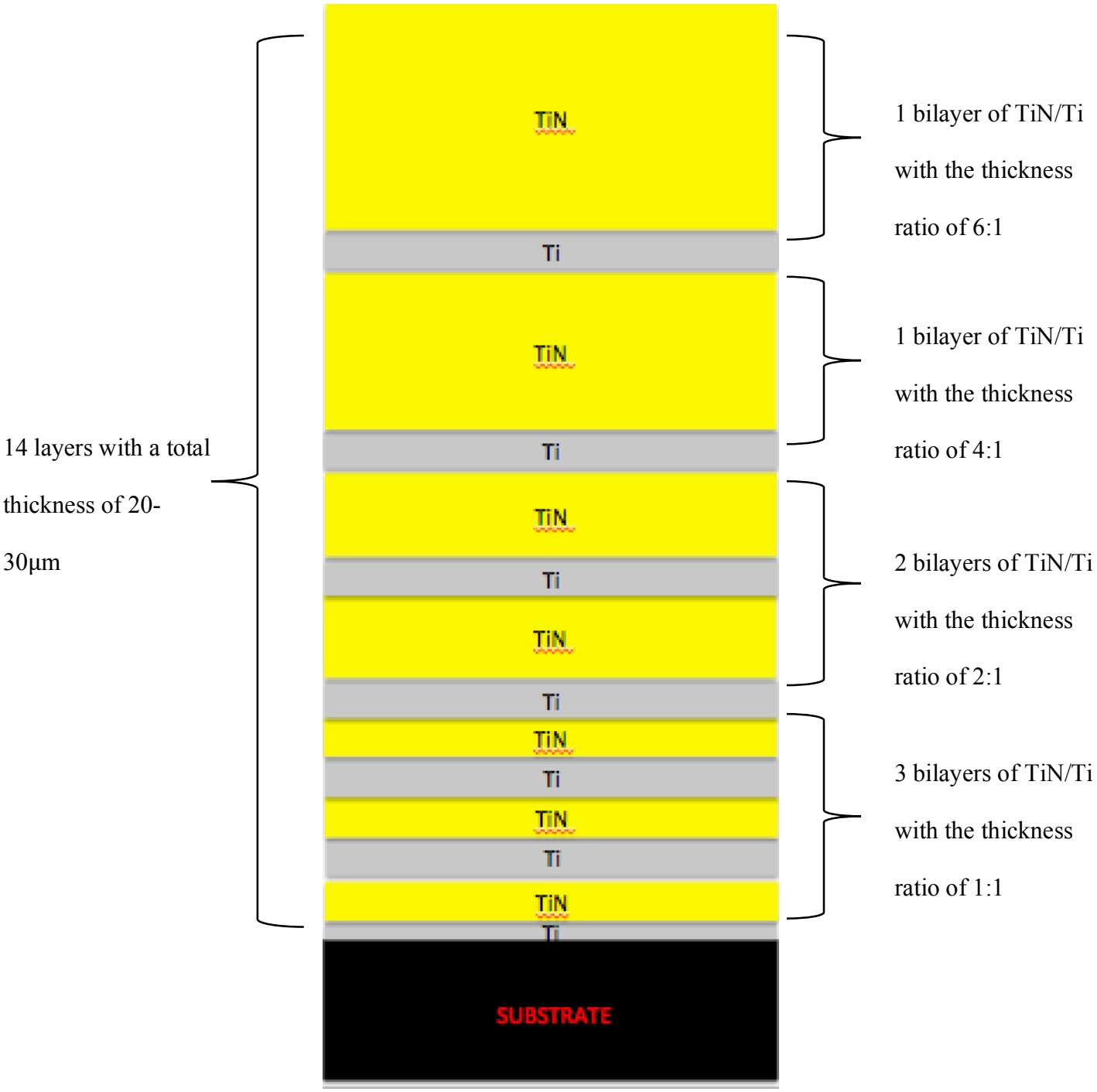

Figure. 6.2 Proposed ideal TiN/Ti multilayer coating architecture

The multilayer coating is designed at a distinct TiN/Ti bilayer thickness ratio, where the top region yields as high as a 6:1 ratio. Preceding bilayers of TiN/Ti have decreasing thickness ratios, from 4:1 to 1:1. The design of a high TiN/Ti thickness ratio towards the top region serves the purpose that ideally you want the stress/strain field to be concentrated in the hard/stiff layer, which is more resilient. However, if the hard/stiff layer is too thick, the soft/compliant interlayer may not be sufficient to accommodate the loading and might be not effective to minimise the bending stresses. Furthermore, thicker hard/stiff layers will help to shield the substrate from the induced impact stresses.

The discrete coating architecture proposed will also help to create standing waves and minimise the reflected tensile wave effects, as they are detrimental (and lead to cohesive failure in the coating) when they constructively interfere with the surface waves. In order minimise the amplitude of the incident waves, by destructive interference of the waves, (shown in figure. 6.3), The 6:1, 4:1 and 2:1 bilayer thickness ratio of TiN/Ti was selected, as a means to match the propagated and reflected (at the free surface or individual layer) wavefront, of the compressive stress waves in each layer since the compressive wave speeds of TiN and Ti are approximately $9800ms^{-1}$ and $5050ms^{-1}$, respectively. TiN/Ti thickness ratio of 3:1 or 5:1 cannot be selected because the effect of cancelling out the incident and reflected waves cannot happen. Furthermore, Higher TiN/Ti bilayer thickness ratio than 6:1 is not recommended because the layers would be more prone to delamination.

The descending TiN/Ti thickness ratio is designed to optimise both the mechanical and acoustical considerations. The mechanical consideration is optimised, as it would be advantageous to match the elastic modulus with the substrate, to boost the adhesive strength of the coating with the substrate – whilst at the same time shielding the substrate from incoming stress pulses. Additionally, this creates a region with a greater number of layers and

it will serve as a means to aid the attenuation of any longitudinal stress waves propagating through the upper region.

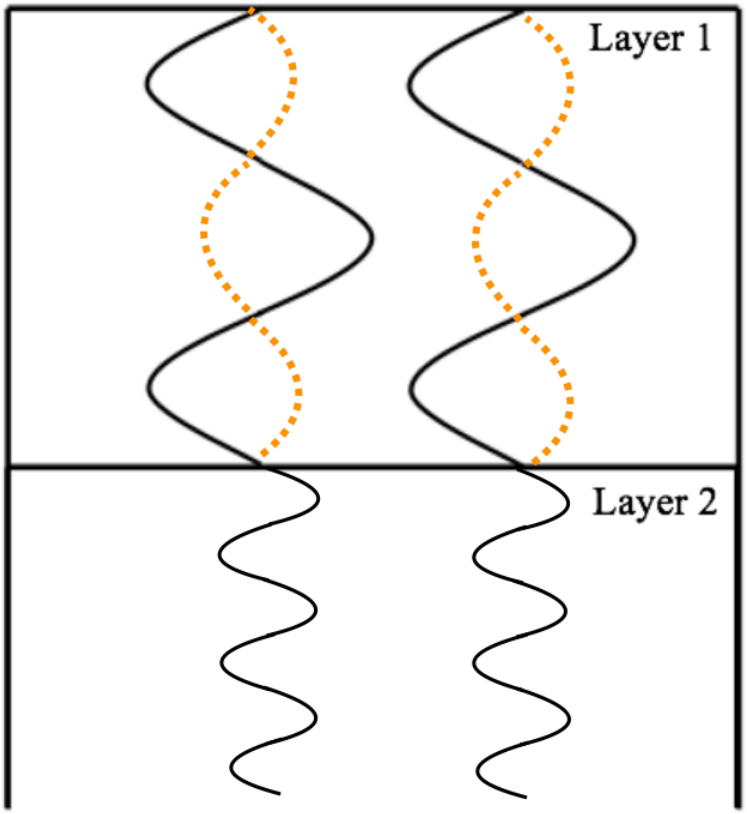

Figure. 6.3 Schematic of how the amplitude of the incident waves can be minimise, black line shows the compressive waves and dotted orange line shows the reflected tensile wave.

References

1. N.K.Mukhopadhyay, S.G.Chowdhury, G.Das, I.Chattoraj, S.K.Das, and D.K.Bhattacharya, *An investigation of the failure of low pressure steam turbine blades.* Engineering Failure Analysis, 1998. **5**(3): p. 181-193.
2. G.W.Coles, Proceedings of the Institution of Mechanical Engineers (London) 1904. **parts 3 and 4**: p. 625-635.
3. O.G.Engel, *Waterdrop collisions with solid surface.* Journal of Research of the National Bureau of Standards, 1955. **54**(5).
4. S.S.Cook, *Erosion by water hammer.* Proceedings of the Royal Society of London 1928. **119**(A): p. 481-8.
5. F.J.Heymann, *High-speed impact between a liquid drop and a solid surface.* Journal of Applied Physics, 1969.
6. H.S.Kirols, D.Kevorkov, A.Uihlein, and M.Medraj, *The effect of initial surface roughness on water droplet erosion behaviour.* Wear, 2015. **342-343**: p. 198-209.
7. G.S.Springer, *Erosion by Liquid Impact*. 1976: Scripta Publishing.
8. F.J.Heymann, *On the shock wave velocity and impact pressure in high-speed liquid impact.* ASME, 1969: p. 400-402.
9. M.C.Rochester, *The Impact of a liquid drop with a solid surface* 1977, University of Cambridge.
10. M.C.Rochester and J.H.Brunton, *Pressure distribution during drop impact.* Proceedings of the 5rd International Conference by Liquid and Solid Impact, 1979.
11. M.B.Lesser, *Analytic solutions of liquid-drop impact problems.* Proceedings of the Royal Society of London, 1981. **A**(377): p. 281-308.
12. F.P.Bowden and J.E.Field, *The brittle fracture of solids by liquid impact, by solid impact, and by shock.* Physcis and Chemistry of Solids, Cavendish Laboratory, University of Cambridge, 1964.
13. J.E.Field, *The physics of liquid impact, shock wave interactions with cavities, and the implications to shock wave lithotripsy.* Physics in medicine and biology, 1991. **36**(11).
14. M.Meyers, *Dynamic Behavior of Materials*. 1994: John Wiley.
15. J.J.Camus, *High-Speed Flow in Impact and its Effect on Solid Surfaces*. 1971, University of Cambridge.
16. J.H Brunton, J.J.C., *The flow of a liquid drop during impact.* Proceedings of the 3rd International Conference on Rain Erosion and Associated Phenomena, 1970: p. 327-352.
17. J.E. Field, M.B.L., J.P. Dear, *Studies of two-dimensional liquid-wedge impact and their relevance to liquid-drop impact problems.* Proceedings of the Royal Society of London, Series A, 1985. **401**(1821).
18. F.P.Bowden and J.H.Brunton, *The Deformation of Solids by Liquid Impact at Supersonic Speeds.* Proceedings of the Royal Society of London. Series A, Mathematical and Physical Science, 1961. **263**(1315): p. 433-450.
19. F.J.Heymann, *A survey of clues to the relationship between erosion rate and impact parameters.* Proceedings of the Second Meersburg Conference on Rain Erosion and Allied Phenomena Held on the Bondensee, Fedreal German Republic, 1967: p. 683-760.
20. G.F.Miller and H.Pursey, *On the artition of Energy between Elastic Waves in a Semi-Infinite Solid.* Proceedings of the Royal Society of London, 1955. **233**(1192): p. 55-69.

21. F.J.Sanchez-sesma, R.L.Weaver, H.Kawase, S.Matsushima, F.Luzon, and M.Campillo, *Energy Partitions among Elastic Waves for Dynamic Surface Loads in a Semi-Infinite Solid.* Bulletin of the Seismological Society of America, 2011.
22. C.Haosheng and L.Shihan, *Inelastic damages by stress wave on steel surface at the incubation stage of vibration cavitation erosion.* Wear, 2009. **266**(1-2): p. 69-75.
23. J.D.N.Cheeke, *Fundamentals and Applications of Ultrasonic waves*. 2002: CRC Press.
24. P.C.Vinh and R.W.Ogden, *On formulas for the Rayleigh wave speed.* Wave Motion, 2004. **39**.p. 191-197
25. I.B.Morozov, *An elastic acoustic impedance and the correspondence principle.* Grophysical Prospecting, 2011. **59**: p. 24-34.
26. S.Buravova, *Surface erosion under particle impact.* High Pressure Research, An International Journal, 1991. **11**(4).
27. G.P.Tilly, *Erosion caused by airbourne particles.* Wear, 1969. **14**(1).
28. E.R.Cohen, D.R.Lide, and G.L.Trigg, *AIP Physics Desk Reference*. 3 ed. 2003, New York: Springer.
29. D.Schneider and T.Schwarz, *A photoacoustic method for characterising thin film.* Surface and Coating Technology, 1996. **91**: p. 136-146.
30. M.S.Mahdipoor, D.Kevorkov, P.Jedrzejowski, and M.Medraj, *Water droplet erosion behaviour of gas nitrided Ti6Al4V.* Surface and Coating Technology, 2016. **292**: p. 78-89.
31. G.P.Thomas and J.H.Brunton, *Drop impingement erosion of metals.* Proceedings of the Royal Society of London, Series A, 1970. **314**(1519).
32. F.J.Heymann, *Liquid impingement erosion.* ASM Handbook: Friction, Lubrication, and Wear Technology 1992. **18**.
33. Jr., G.F.S., *Erosion Rate-Velocity Dependence for Materials at Supersonic Speeds.* ASTM STP, 1970. **474**: p. 323-349.
34. G.Hoff, G.Langbein, and H.Rieger, *Material Destruction Due to Liquid Impact.* ASTM STP, 1967. **408**: p. 42-69.
35. N.Ahmad, M.Casey, and H.Surken, *Experimental assessment of droplet impact erosion resistance of steam turbine blade materials.* Wear, 2009. **267**: p. 1605-1618.
36. O.G.Engel, *Pits in Metals Caused by Collision with Liquid Drops and Soft metal Spheres.* Journal of Research of the National Bureau of Standards, 1959. **62**: p. 229.
37. D.M.Mattox, *Ion plating past, present and future.* Surface and Coatings Technology, 2000. **133-144**: p. 517-521.
38. D.M.Mattox, *Fundamentals of Ion Plating.* Journal of Vacuum Science and Technology, 1973. **10**(1): p. 47.
39. R.F.Bunshah, R.Nimmagadda, W.Dunford, B.A.Movchan, A.V.Demchishin, and N.A.Chursanov, *Structure and properties of refractory compounds deposited by electron beam evaporation* Thin Solid Films 1978. **54**(1): p. 85-106.
40. G.A.Baum, *Dow Chemical Co. Report RFP-686/UC-25 Colorado, USA* 1967.
41. A.Matthews, *PH.D. Thesis, University of Salford.* 1980.
42. K.S.Fancey and A.Matthews, *Some fundamental aspects of glow discharges in plasma-assisted processes.* Surface and Coatings Technology, 1987. **33**: p. 17-29.
43. W.D.Davis and T.A.Vanderslice, *Ion Energies at the Cathode of a Glow Discharge.* Physical Review, 1963. **131(1)**: p. 219-228.
44. B.N.Chapman, *Glow discharge processes*. 1980, New York: Wiley.
45. J.Rickards, *Energies of particles at the cathode of a glow discharge.* Vacuum, 1984. **34**: p. 559-562.

46. K.S.Fancey, *An investigation into phenomena which influence the optimisation of ion plating systems, Ph.D Thesis, University of Hull.* 1989.
47. A.Leyland and A.Matthews, *On the significance of the H/E ratio in wear control: a nanocomposite coating approach to optimised tribological behaviour.* Wear, 2000. **246**: p. 1-11.
48. W.D.Callister, *Materials Science and Engineering: An Introduction.* 1940. **7**.
49. R.F.Smart, *Selection of surfacing treatments.* Tribology International, 1978: p. 97-104.
50. M.B.Peterson and W.O.Winer, *Wear Control Handbook.* 1980: ASME.
51. J.Chen and S.J.Bull, *Approaches to investigate delamination and interfacial toughness in coated systems: an overview.* Journal of Applied Physics, 2011. **44**: p. 1-19.
52. H.M.Slot, E.R.M.Gelinck, C.Rentrop, and E.V.D.Heide, *Leading edge erosion of coated wind turbine blades: Review of coating life models.* Renewable Energy, 2015. **80**: p. 837-848.
53. M.Y.Gutkin, T.Ishizaki, S.Kuramoto, I.A.Ovid'ko, and N.V.Skiba, *Giant faults in deformed Gum Metal.* International Journal of Plasticity, 2008. **24**(8): p. 1333-1359.
54. T.Furuta, S.Kuramoto, J.W.Morris, Jr.N.Nagasako, E.Withey, and D.C.Chrzan, *The mechanism of strength and deformation in Gum Metal.* Scripta Materialia 2013. **68**: p. 767-772.
55. T.Saito, T.Furuta, J.H.Hwang, S.Kuramoto, K.Nishino, N.Suzuki, R.Chen, A.Yamada, K.Ito, Y.Seno, T.Nonaka, H.Ikehata, N.Nagasako, C.Iwamoto, Y.Ikuhara, and T.Sakuma, *Multifunctional Alloys Obtained via a Dislocation-Free Plastic Deformation Mechanism.* Science, 2003. **300**(5618): p. 464-467.
56. S.Schmauder and M.Meyer, *Correlation Between Dundurs' Parameters and Elastic Constants.* Z. Metallkd, 1992. **Vol.83**: p. 524-527.
57. J.Dunders, *Effect of Elastic Constants on Stress In A Composite Under Plane Deformation.* Journal of Composite materials, 1967. **1**.
58. B.Borawski, J.Singh, J.A.Todd, and D.E.Wolfe, *Multi-layer coating design architecture for optimum particulate erosion resistance.* Wear, 2011. **271**(11-12): p. 2782-2792.
59. K.Holberg, A.Matthews, and H.Ronkainen, *Coatings tribology—contact mechanisms and surface design.* Tribology International 1998. **31**(1-3): p. 107-120.
60. S.Ramalingam and L.Zheng, *Film-substrate interface stresses and their role in the tribological performance of surface coatings.* Tribology International, 1995. **28**(3): p. 145-161.
61. A.Matthews, A.L., *Thick Ti/TiN multilayered coatings for abrasive and erosive wear resistance.* Surface and Coatings Technology, 1994. **70**: p. 19-25.
62. H.Holleck and V.Schier, *Multilayer PVD coatings for wear protection.* Surface and Coatings Technology, 1995. **76-77**: p. 328-336.
63. M.Bromark, M.Larsson, P.Hevenqvist, and S.Hogmark, *Wear of PVD Ti/TiN multi-layer coatings.* Surface and Coating Technology, 1997. **90**(3): p. 217-223.
64. G.S.Kim, S.Y.Lee, J.H.Hahn, B.Y.Lee, J.G.Han, J.H.Lee, and S.Y.Lee, *Effects of the thickness or Ti buffer layer on the mechanical properties of TiN coatings.* Surface and Coating Technology, 2003. **171**: p. 83-90.
65. P.C.Yashar and W.D.Sproul, *Nanometer scale multilayered hard coatings.* Vacuum, 1999. **55**: p. 179-190.
66. J.S.Koehler, *Attempt to Design a Strong Solid.* Physical Review B, 1970. **2**(2): p. 547-551.

67. S.L.Lehoczky, *Strength enhancement in thin-layered Al-Cu laminates.* Journal of Applied Physics, 1978. **49**(11): p. 5479.
68. E.O.Hall, *The Deformation and Ageing of Mild Steel: III Discussion of Results.* Proceedings of the Physical Society, Section B, 1951. **64**(9): p. 747-753.
69. L.H.Friedman and D.C.Chrzan, *Scaling Theory of the Hall-Petch Relation for Multilayers.* Physical Review Letters, 1998. **81**(3): p. 2715-2718.
70. P.M.Anderson and C.Li, *Hall-Petch relations for multilayered materials.* Nanostructured Materials, 1995. **5**(3).
71. B.G.Lerma, D.S.Balint, D.Dini, D.E.Eakins, and A.P.Sutton, *Attenuation of the Dynamic Yield Point of Shocked Aluminum Using Elastodynamic Simulations of Dislocation Dynamics.* Physical Review Letters, 2015. **114**(17).
72. T.Matsuda, T.Sano, K.Arakawa, and A.Hirose, *Dislocation structure produced by an ultrashort shock pulse.* Journal of Applied Physics, 2014. **116**(18).
73. M.Meyers, *Mechanism for dislocation generation in shock-wave deformation.* Scripta METALLURGICA 1978. **12**: p. 21-26.
74. R.W.Armstrong, W.Arnold, and F.J.Zerilli, *Dislocation Mechanics of Shock-Induced Plasticity.* Metallurgical and Materials Transactions A, 2007. **38**(11): p. 2605-2610.
75. M.Meyers, F.Gregori, B.Kad, M.Schneider, D.Kalantar, B.Remington, G.Ravichandran, T.Boehly, and J.Wark, *Laser-induced shock compression of monocrystalline copper: characterization and analysis.* Acta Materialia, 2003. **51**(5): p. 1211-1228.
76. E.Bringa, K.Rosolankova, R.Rudd, B.Remington, J.Wark, M.Duchaineau, D.Kalantar, J.Hawreliak, and J.Belak, *Shock deformation of face-centred-cubic metals on subnanosecond timescales.* Nature Materials, 1006. **5**.
77. B.L.Holian and P.S.Lomdahl, *Plasticity induced by shock waves in nonequilibrium molecular-dynamics simulations.* Science, 1998. **280**: p. 2085-2088.
78. A.Matthews, A.Leyland, K.Holmberg, and H.Ronkainen, *Design aspects for advanced tribological surface coatings.* Surface and Coatings Technology, 1998. **100-101**: p. 1-6.
79. S.Hassani, M.Bielawski, W.Beres, M.Balazinski, L.Martinu, and J.E.Klemberg-Sapieha, *Impact stress absorption and load spreading in multi-layered erosion-resistant coatings.* Wear, 2010. **268**: p. 770-776.
80. B.R.Lawn, K.S.Lee, H.Chai, A.Pajeres, S.Wuttiphan, I.Petterson, and X.Hu, *Damage-Resistant Brittle Coatings.* Advanced Engineering Materials, 2000. **2**(11): p. 745-748.
81. B.R.Lawn, Y.Deng, P.Miranda, A.Pajares, H.Chai, and D.K.Kim, *Overview: damage in brittle layer structures from concentrated loads.* Journal of Materials Research, 2002. **17**(12): p. 3019-3036.
82. J.A.Thornton, *High rate thick film growth* Ann Rev Mater Sci, 1977. **7**: p. 239-260.
83. Z.H.Xie, M.Hoffman, P.Munroe, A.Bendavid, and P.J.Martin, *Deformation mechanisms of TiN multilayer coatings alternated by ductile or stiff interlayers.* Acta Materialia, 2008. **56**: p. 852-861.
84. Y.M.Gupta and J.L.Ding, *Impact load spreading in layered materials and structures: concept and quantitative measure.* International Journal of Impact Engineering 2002. **27**: p. 277-291.
85. H.A.Bruck, *One-dimensional model for designing functionally graded materials to manage stress waves.* International Journal of Impact Engineering, 2002. **27**: p. 277-291.
86. P.C.Zhou and A.K.Hopkins, *Dynamic response of materials to intense impulsive loading*. 1973, Air Force Materials Laboratory: United States of America.

87. A.Leyland and A.Matthews, *Design criteria for wear-resistant nanostructured and glassy-metal coatings.* Surface and Coatings Technology, 2004. **177-178**: p. 317-324.
88. K.L.Johnson, *Contact mechanics*. 1985: Cambridge University Press.
89. W.C.Oliver and G.G.Pharr, *An improved technique for determining hardness and elastic modulus using load and displacement sensing indentation experiments.* Jornal of Materials Research, 1992. **7**: p. 1564-1583.
90. O.Knotek, B.Bosserhoff, A.Schrey, T.Leyendecker, O.Lemmer, and S.Esser, *A new technique for testing the impact load of thin films: the coating impact test.* Surface and Coatings Technology, 1992. **52**(55): p. 102-107.
91. R.Bantle and A.Matthews, *Investigation into the impact wear behavior of ceramic coatings.* Surface and Coating Technology, 1995. **74-75**: p. 857-868.
92. W.F.Adler, *Waterdrop impact modeling* Wear, 1995. **186-187**: p. 341-351.
93. A.Matthews, *PhD Thesis*. 1980, Salford University.
94. C.Rebholz, H.Ziegele, A.Leyland, and A.Matthews, *Structure, mechanical and tribological properties of nitrogen-containing chromium coatings prepared by reactive magnetron sputtering.* Surface and Coating Technology, 1999. **115**: p. 222-229.
95. H.A.Wriedt and J.L.Murray, *The N-Ti(Nitrogen-titanium) system.* ASM International, 1987: p. 176-186.
96. G.E.Totten, K.Funatani, and L.Xie, *Handbook of Metallurgical Process Design*. United States of America: Marcel Dekker.
97. J.A.Thornton, *The Microstructure of Sputter-deposited Coatings.* Journal of Vacuum Science and Technology, 1986. **4**: p. 3059-3065.
98. S.Zhang, *TiN coating of tool steels: a review* Journal of Materails Processing Technology, 1993. **39**: p. 165-177.
99. M.J.Donachie, *Titanium: A Technical Guide, 2nd Edition*. 2000: ASM International.
100. Gittis, A. and D. Dobrev, *Development of textures during the growth of silver films condensed in vacuum on glass.* Thin Solid Films, 1985. **130**(3-4): p. 335-340.
101. A.V.Eletskii and B.M.Smirnov, *Dissociation of molecules in plasma and gas: the energy.* pure and Applied Chemisty, 1985: p. 1235-1244.
102. D.S.Rickerby, G.Eckold, K.T.Scott, and I.M.Buckley-Golder, *The interrelationship between internal stress, processing parameters and microstructure of physically vapour deposited and thermally sprayed coatings.* Thin Solid Films, 1987. **154**(1-2): p. 125-141.
103. M.Kobayashi and Y.Doi, *TiN and TiC coating on cemented carbides by ion plating.* Thin Solid Films, 1978. **54**: p. 67-74.
104. J.H.Jed, Y.Noh, K.Kim, and S.Liang, *Preferred orientation of TiN films studeied by a real time synchrotron x-ray scattering.* Journal of Applied Physics, 1997. **81**.
105. J.E.Sundgren, *Structure and properties of TiN coatings.* Metallurgical and Protective Coatings, 1985. **128**: p. 21-44.
106. G.Mallikarjunachari and P.Ghosh, *Analysis of strength of response of polymer nano thin film interfaces applying nanoindentation and nanoscratch techniques.* Polymer, 2016. **90**: p. 53-66.
107. P.D.Haller, *Researches into Corrosion Caused by Cavitation (in german) - Translated to english.* Schweizerische Bauzeitung, 1933. **101**: p. 243 and 263.
108. K.D.Bouzakis and A.Siganos, *Fracture initiation mechanisms of thin hard coatings during the impact test.* Surface and Coating Technology, 2004. **185**: p. 150-159.
109. N.Kamkar, F.Bridier, P.Bocher, and P.Jedrzejowski, *Water droplet erosion mechanisms in rolled Ti-6Al-4V.* Wear, 2013. **301**(1-2): p. 442-448.

110. J.W.Christian and S.Mahajan, *Deformation Twinning.* Progress in Materials Science, 1995. **39**: p. 1-157.
111. M.A.Meyers, O.Vohringer, and V.A.Lubarda, *The onset of twinning in metals: constituive description.* Acta Materialia, 2001. **49**: p. 4025-4039.
112. R.Armstrong, I.Codd, R.M.Douthwaite, and N.J.Petch, *The plastic deformation of polycrystalline aggregates.* Philosophical Magazine, 1962. **7**(73): p. 45-58.
113. D.R.Chichili, K.T.Ramesh, and K.J.Hemker, *The high-strain-rate response of alpha-titanium: experiments, deformation mechanisms and modeling.* Acta Materialia, 1998. **46**: p. 1025-1043.
114. M.H.Yoo, *Slip, twinning, and fracture in hexagonal close-packed metals.* Metallurgical Transactions A, 1981. **12**(3): p. 409-418.
115. K.P.Travis and T.Hiddleston, *Multiscale modelling of material failure.* Molecular Simulation, 2014. **40**: p. 141-153.
116. M.B.Liu and G.R.Liu, *Smoothed Particle Hydrodynamics (SPH): an Overview and Recent Developments.* Archives of Computational Methods in Engineering, 2010. **17**(1): p. 25-76.